Coastal Erosion Assessment Using Small Unmanned Aerial Vehicles (UAVs) and Numerical Modeling:
A Case Study in the Western Region of Puerto Rico

By:

Glorimar Torres Pagán

A thesis submitted in partial fulfillment of the requirements for the degree of

MASTER OF SCIENCE
in
CIVIL ENGINEERING

UNIVERSITY OF PUERTO RICO
MAYAGÜEZ CAMPUS

2018

Approved by:

_____   _____
Jonathan Muñoz Barreto, Ph.D.   Date
President, Graduate Committee

_____   _____
Alesandra C. Morales Vélez, Ph.D.   Date
Member, Graduate Committee

_____   _____
Patricia Chardón Maldonado, Ph.D.   Date
Member, Graduate Committee

_____   _____
Kenneth Stephen Hughes, Ph.D.   Date
Representative of Graduate Studies

_____   _____
Ismael Pagán Trinidad, M.S.C.E.   Date
Chair, Department of Civil Engineering and Surveying

ABSTRACT

Coastal monitoring is fundamental to understand the morphological changes in coastal environments and the vulnerability of low-lying coasts to erosion and flooding. For this reason, this study was focused on monitoring coastal erosion in three areas distributed along the western region of Puerto Rico using small unmanned aerial vehicles (UAVs). These UAVs provided rapid-assessment and high-resolution images for shoreline monitoring from 2016 to 2018. The images served to establish a baseline aerial analysis useful to quantify the erosion rate using the Digital Shoreline Analysis System (DSAS) and computing the rate-of-change statistics of the coastal zones from multiple historic (1930 to 2010) shoreline positions. In addition, XBeach model was implemented to simulate swell events generated by Hurricane Matthew (Category 4) in 2016. The results demonstrated the synergy of low cost small UAV surveys and XBeach modeling to monitor the coastal zones and determine morphological changes in coastal environments.

RESUMEN

El monitoreo costero es fundamental para comprender los cambios morfológicos en los ambientes costeros y la vulnerabilidad de las costas bajas a la erosión e inundaciones. Por esta razón, este estudio se enfocó en monitorear la erosión costera en tres áreas distribuidas a lo largo de la región occidental de Puerto Rico usando pequeños vehículos aéreos no tripulados (UAVs). Estos UAVs proporcionaron una evaluación rápida e imágenes de alta resolución para el monitoreo costero desde el 2016 al 2018. Las imágenes sirvieron para establecer un análisis aéreo de referencia, útil para cuantificar la tasa de erosión usando el Sistema Digital de Análisis de Litoral (DSAS) y calcular la tasa de cambio estadísticas de las zonas costeras a partir de múltiples posiciones históricas (1930 al 2010) en la costa. Además, se implementó el modelo XBeach para simular los eventos de oleaje debido al huracán Matthew (Categoría 4) en 2016. Los resultados demostraron la sinergia del uso de UAVs de bajo costo y el modelaje en XBeach para monitorear las zonas costeras y determinar los cambios morfológicos en ambientes costeros.

Dedicated to the memory of my grandmother, Guillermina Salgado

Robles, who always believed in my ability to be successful in life.

This is for you, abuelita

ACKNOWLEDGEMENT

First, I thank God for all the blessings he has given me throughout my life, as well as the opportunities that have come to me. Also, I owe my deepest gratitude to my parents who have given me their unconditional love and support throughout my life, and have taught me to keep moving forward. I also want to express my warmest thanks to my brothers who supported and advised me during my university studies, and to my grandfather for supporting me and celebrating my achievements. In addition, I want to thank my boyfriend for his unconditional support, patience and advice during these years of study, and for making the difficult days more bearable.

I am deeply grateful to Professor Ismael Pagán Trinidad for his unconditional support and for giving me the opportunity to pursue graduate studies. I am also grateful to my advisor and mentor Jonathan Muñoz Barreto for allowing me to be part of his team, for believing in my potential, supporting me and guiding me during this time. I also want to express my gratitude to Professor Alesandra Morales Vélez and Patricia Chardón Maldonado for agreeing to be part of my committee and for giving me their support and advice during this time.

In addition, I would like to take this opportunity to thank all those people who in one way or another were part of this process, and who were always willing to help.

TABLE OF CONTENTS

LIST OF TABLES

LIST OF FIGURES

GLOSSARY OF TERMS

A	Wave action
Abs1d	Absorbing-generating boundary in 1D
ASTM	American Society for Testing and Materials
CARICOOS	Caribbean Coastal Ocean Observing System
c_g	Wave action propagation speed
CZMIL	Coastal Zone Mapping and Imaging Lidar
D_w, D_f, D_v	Dissipation terms for respectively waves, bottom friction and vegetation
DSM	Digital Surface Model
DTM	Digital Terrain Model
dtheta	Directional resolution
DSAS	Digital Shoreline Analysis System
EPR	End Point Rate
GNSS	Global Navigation Satellite System
GPS	Global Positioning System
HARN	High Accuracy Reference Network
JALBTCX	Joint Airborne LiDAR Bathymetry Technical Center of Expertise
LiDAR	Light Detection and Ranging
LRR	Linear Regression Rate
MAE	Mean Absolute Error
MBE	Mean Bias Error
NAD83	North American Datum of 1983
NGS	National Geodetic Survey
NOAA	National Oceanic and Atmospheric Administration
NSM	Net Shoreline Movement
OPUS	Online Positioning User Service
PRVD02	Puerto Rico Vertical Datum of 2002
R	Correlation coefficient
R^2	Coefficient of determination
RMSE	Root Mean Square Error
RTK	Real-time Kinematics
s	Standard deviation
SCE	Shoreline Change Envelope
SP	Poorly graded sand
σ	Intrinsic wave frequency
SPCS	State Plane Coordinate System
θ	Angle of incidence with respect to the x-axis
thetamax	Upper directional limit
thetamin	Lower directional limit
TLS	Terrestrial Laser Scanning
UAV	Unmanned Aerial Vehicles

USACE	United States Army Corps of Engineers
USCS	Unified Soil Classification System
ν_h	Horizontal viscosity
VRS	Virtual Reference Stations

CHAPTER 1 - INTRODUCTION

During the past years, Puerto Rico has been exposed to the direct impacts of atmospheric events, such as Hurricane Hugo in 1989, Hurricane Hortense in 1996, Hurricane Georges in 1998, and Hurricane María in 2017, and indirect impacts such as Hurricane Sandy in 2012, Hurricane Matthew in 2016, and Hurricane Irma in 2017, which increase the vulnerability of the coastal zones. Coastal erosion, for example, has been one of the biggest concerns since it can negatively impact coastal communities' ecosystems and our economy causing a significant retreat of the shoreline, coastal floods, and threats to properties and infrastructure adjacent to the shore. This phenomenon is a natural process that may occur in response to short- and long-term events, such as natural disasters, wave actions, climate changes, tides, and tsunamis. In addition, it can also be a man-made process that may occur in response to the extraction of sand, constructions adjacent to the coasts and deforestations.

In order to evaluate this effect, it is significantly important to conduct frequent monitoring to understand the morphological changes in coastal environments and the vulnerability of low-lying coasts to erosion and flooding. Previous studies have been carried out in Puerto Rico to monitor the shoreline changes using remote sensing techniques, aerial images, numerical models, published reports, maps, and field observations. Most of these methods have limitations that impede the accurate monitoring of the coasts. For example, remote sensing techniques are dependent on the pixel resolution, data availability, and cost; aerial images can be limited by the lack of high quality air cover; numerical models involve the use of assumptions and simplifications; published reports and maps are also dependent on the data availability; and field

observations can be very expensive, site specific, and difficult to obtain. Therefore, Unmanned Aerial Vehicles (UAVs) represent an alternative to monitor and assess coastal zones by providing high-resolution images at low cost that allows examine the shoreline changes in three beaches along the western region of Puerto Rico. To our knowledge, this is the first study to be conducted in Puerto Rico that uses UAVs in a systematic way to monitor coastal zones.

In addition to monitoring the coastal zones, it was also desired to perform a numerical simulation to evaluate and predict morphological changes at a specific site. The calibrated and validated results from the simulation could be used as a tool to study how the morphology of the coasts will change. For this purpose, XBeach which is a two-dimensional numerical model for wave propagation, long waves and mean flow, sediment transport and morphological changes of the near-shore area, beaches, dunes and back-barrier during storms was used to quantify the erosion rate at Cofresí Beach, during Hurricane Matthew (Category 4) in 2016. This analysis was validated using UAV high-resolution images and provided the possibility of predicting future impacts along the coast of Puerto Rico. This is also the first study in Puerto Rico to demonstrate the application of XBeach modeling to determine the morphological changes in the coastal zones.

1.1   Objectives

This project aims to explore how images obtained through UAVs, separated or combined with a numerical model, can serve as a tool to monitor coastal zones and quantify morphological changes. To accomplish this goal, the following tasks were established:

- Monitor coastal zones by the collection of aerial images using UAVs
- Create reference datasets for three beaches

2

- Provide statistical analysis and erosion rate quantification

- Develop a framework to predict erosion/accretion events at Cofresí Beach, in Rincón, Puerto Rico

CHAPTER 2 - LITERATURE REVIEW

In Puerto Rico, more than 85% of the population lives within the coastal zone (Rodriguez 2017). These zones can be exposed to natural hazards such as coastal erosion, tropical storms and hurricanes, tsunamis, earthquakes, landslides, and droughts (Diaz et al. 2014). These hazards may increase its negative effect when the vulnerability of coastal zones increases. Some of the most important factors that affect vulnerability include the continuing development of building constructions adjacent to shorelines for recreational and touristic purposes, sand extraction and removal from the beaches, poor drainage areas and maintenance of storm water management systems, and the elimination of dunes, reefs, mangroves, and other natural barriers that help reduce negative effects (Diaz et al. 2014; Scarelli et al. 2017).

Many of the beaches in Puerto Rico are eroding, causing great concern for tourism and residential development industries (Ciencia PR 2015; El Nuevo Día 2013; Rodriguez n.d.). Numerous research efforts related to coastal erosion using aerial images have been performed in Puerto Rico. For example, in 1984, ten sites that showed severe coastal erosion were studied using aerial photographs from the years 1936 to 1977. Results showed that the erosion rate on beaches is not constant over time; there are accelerations, decelerations and reversals of erosion to accretion (Morelock 1984). Another study was carried out in 1997 which documented historical shoreline behavior along the coast of Puerto Rico for the years 1936 to 1993 using aerial photos, using remote sensing techniques, published reports, maps and field observations. Results showed that shoreline changes occurred due to human activities, lack of sand deposits in the nearshore area, flood events, and variability in the wave regime (Barreto-Orta 1997). In 2000,

4

an update of the 1984 research work was conducted by studying the ten sites for changes in shoreline position between 1977 and 1999, using the same photographic technique. Results showed that certain patterns and common elements can be seen in the erosion of the shoreline in Puerto Rico; at many locations, the erosion process commences suddenly, after a period of very little or no erosion, and in some areas, the shoreline has adjusted to the altered wave and current regime and the reduced sediment supply from rivers (Morelock and Barreto-Orta 1999). Additionally, in 2007, a study of historical shoreline changes was conducted at Rincón, P.R. for the years 1936 to 2006, to expand and validate previous investigations. Shoreline positions were compiled from existing data, new ortho-photos, and Global Positioning System (GPS) field surveys. Results showed that the coast of Rincón was eroding as a result of natural and human-induced causes (Thieler et al. 2007).

Although the use of historical images seems to be the most popular method, there are a number of problems associated with the historical mapping of the coasts in Puerto Rico. This is due to the limits imposed by the complexity and diversity of the coast, as well as the nature of the available data. It is also due to the lack of high-quality air cover imagery, few accurate maps of the coast, limited ground control for photogrammetric mapping, and the highly variable geomorphology of the coast (Thieler and Danforth 1994). For these reasons, alternatives should be sought to provide better image resolution and greater availability to carry out coastal monitoring.

To efficiently monitor the coastal regions, frequent surveys are required to detect and quantify the morphological changes. These surveys may include field data collection, satellite remote sensing, and/or airborne remote sensing (Casella et al. 2016). Field data collection provides the

most precise and accurate results, but is expensive to cover large areas and a long temporal window. Satellite remote sensing provides large amount of data, but is dependent of the satellite spatial and spectral resolution, revisit time, and cost (Anderson and Gaston 2013; Matese et al. 2015). Airborne remote sensing techniques provide wide coverage and accurate topography, but they are expensive and hard to deploy aircraft regularly (Casella et al. 2015). Under the airborne remote sensing category, the unmanned aerial vehicles (UAVs) are less expensive and more flexible to operate than the manned aircraft and are in continuous development increasing their operational capabilities (Clark 2017; Unger et al. 2014). These UAVs involve the use of a ground station which is used to program missions, make in-flight adjustments, set-up dimensions of the mapping area such as the flight orientation and altitude, and receive process, and display real-time imagery (Lomax et al. 2005). Recently, several research studies have been conducted using UAVs for monitoring. A research conducted in the southwestern USA involved the use of UAVs and hyper-spectral fusion for forest monitoring. This works concluded that UAV images provide an efficient tool to monitor and classify multiple species, besides characterizing forest structure changes (Sankey et al. 2017). Another research was conducted in France involved the use of UAVs to monitor the topography of a dynamic tidal inlet using UAVs. UAV results were compared to the Global Navigation Satellite System (GNSS) and Light Detection and Ranging (LiDAR). Based on the comparison with GNSS surveys, UAV results were obtained much faster while providing much denser spatial information, although it was a slightly lesser accurate. Based on the comparison with LiDAR surveys, UAV survey was cheaper and provides finer spatial resolution (Long et al. 2016). In addition, a research was conducted in Ravenna, Italy to create and validate a Digital Surface Model (DSM) of a beach dune system using low-altitude

aerial imageries collected by a UAV and Terrestrial Laser Scanning (TLS) point clouds. DSMs elevations were compared and showed a small average distance of 0.015m. Based on the results, the UAV-based approach was demonstrated to be a straightforward one and accuracy of the vertical dataset was comparable with results obtained from TLS technology (Mancini et al. 2013). Using UAVs for coastal monitoring provides great advantages that include the relatively low hardware costs, rapid-response deployment, low operating cost, high-precision positioning, high-level of automation, high repeatability of the survey, low security risks, and high-resolution imagery (Cook 2017; Eling et al. 2013). There also some disadvantages that include the cost of the computer software to process the images and the operational distance limited by the radio link range (Gonçalves and Henriques 2015). Despite these limitations, UAVs provide an efficient and cost-effective survey tool for topographic mapping and measurements in the coastal zone (Turner et al. 2016).

In addition to the use of UAVs for monitoring, physical and numerical models have been implemented to simulate different scenarios under environmental conditions that occur along the coast. There are different hydrodynamics models such as Delft3D, SWASH, and MIKE21 as well as morphological models including UNIBEST, GENESIS and XBeach. Of these models, XBeach is considered one of the best options for coastal monitoring since it solves coupled 2D horizontal equations for wave propagation, flow, sediment transport, and bottom changes, for varying (spectral) wave and flow boundary conditions. This model also allows analyzing the evolution of coastal dunes under storm surge conditions, and it has been used to forecast the evolution of the coastline in different incident wave scenarios. For example, in 2010, XBeach, a numerical model developed by the UNESCO-IHE Institute for Water Education and Deltares

was used to evaluate the coastal erosion of Santa Rosa Island in Florida, during Hurricane Iván in 2004. Simulation predictions were compared with in-situ measurements collected using LiDAR equipment, and the results reproduced the erosion pattern capturing more than 66% of the variance recorded by in-situ measurements (McCall et al. 2010). In 2011, XBeach was also used to determine the beach erosion during storm conditions in Ostend Beach, Belgium. The model results of XBeach in 1D were compared with field measurements and with Durosta 1D model. The comparison showed that XBeach was good for predicting the storm event, and slightly better to predict the location of the erosion. However, the main advantage of XBeach for the study was the possibility to include the 2D effects (Bolle et al. 2011). In addition, in 2014, XBeach was also implemented to evaluate the morphological changes during the occurrence of Hurricane Michelle in 2001 at Varadero Beach, Cuba. Simulation results allowed the quantification of the volume of erosion, volume of accretion, sedimentary balance, and the length of the retreat of the coastline (Córdova-López 2014).

CHAPTER 3 - METHODOLOGY

This chapter presents a general overview of the methodology used during this research to monitor the coast using UAV's technologies and numerical modeling for a case study of the effects of Hurricane Matthew in Rincón, PR. This research is focused on the Puerto Rico western area; however, it could be applied on other coastal regions.

3.1   Study Area

This study was focused on monitoring coastal erosion in three areas distributed along the western region of the Puerto Rico coastline: (1) Jobos Beach at Isabela, (2) Crash Boat Beach at Aguadilla, and, (3) Cofresí Beach at Rincón (Figure 3-1). Considering the Land Use map of 2010, these three areas are categorized as beach and high-density residential. These three locations have suffered coastal erosion; as an example, Jobos Beach has been showing medium erosion events, Crash Boat Beach has been presenting low erosion and accretion events, and Cofresí Beach has been presenting severe erosion events. Jobos beach is formed by a natural beachrock which creates a protected beach ideal for aquatic activities. During winter and early spring months, since winter storms can occasionally form, the waves are higher and the beach narrower (Islands of Puerto Rico n.d.). Crash Boat occupies the site of a former military port used to rescue downed air crews from Ramey Air Force Base and still retains some remains of pier infrastructure. The waters of Crash Boat are generally flat or slightly choppy making them a great place to practice many aquatic sports. Similar to Jobos, during winter and early spring months, the waves can get quite large from time to time, but are generally very agreeable (Puerto

Rico Channel n.d.). Cofresí is located in front of the Villa Cofresi Hotel complex, built in the decade of the 1960's, and was one of the most attractive beaches on the western coast of Puerto Rico. This particular beach has no sufficient sand and beach portion between the hotel's main building and the shoreline. To mitigate this problem, the hotel administration has tried to stabilize the beach artificially building a rigid wall to protect the building from waves and erosion, especially during bad weather conditions (Scott et al. 2012).
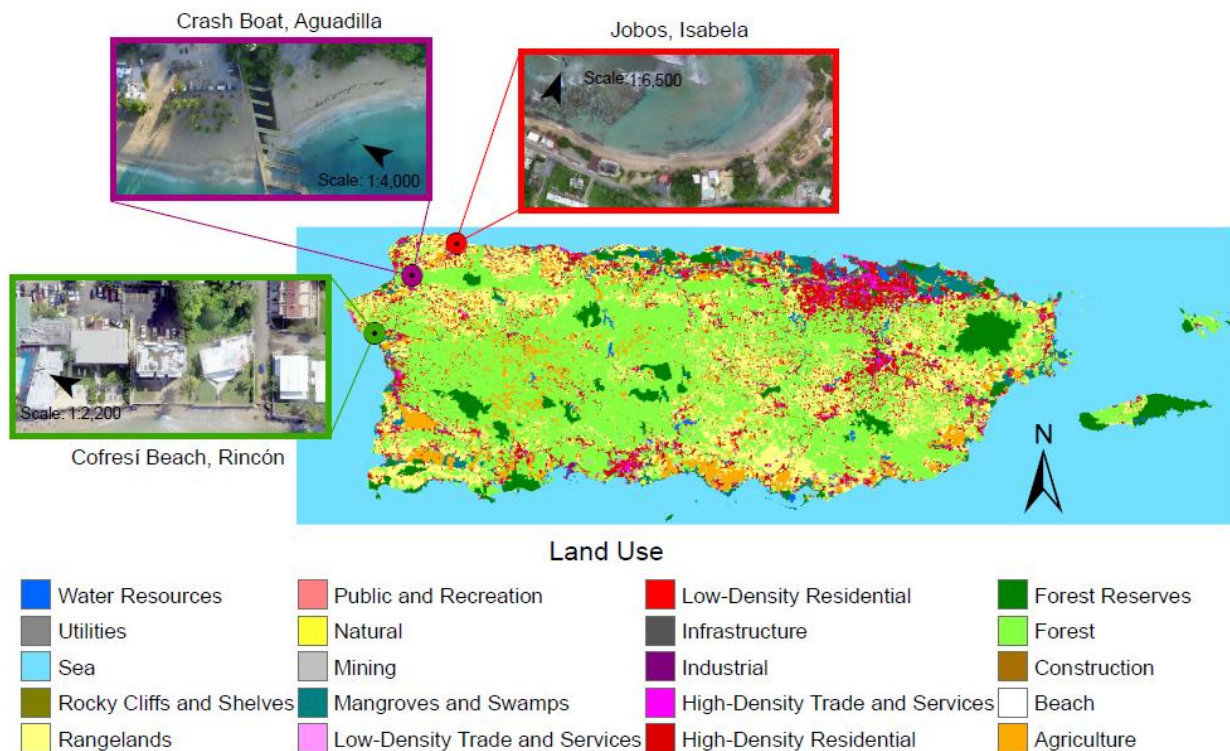
Figure 3-1. Location and Land Use map of the three areas being studied

3.2   UAV Methodology

This section will be divided into: data collection, data processing, and data analysis in order to explain the UAV methodology (Figure 3-2).

Data Collection

Deploy UAVs at CLASS Sites

Data Processing

Develop the Digital Surface Model (DSM)
Delineate the Shorelines

Data Analysis

Determine the rate of erosion with DSAS
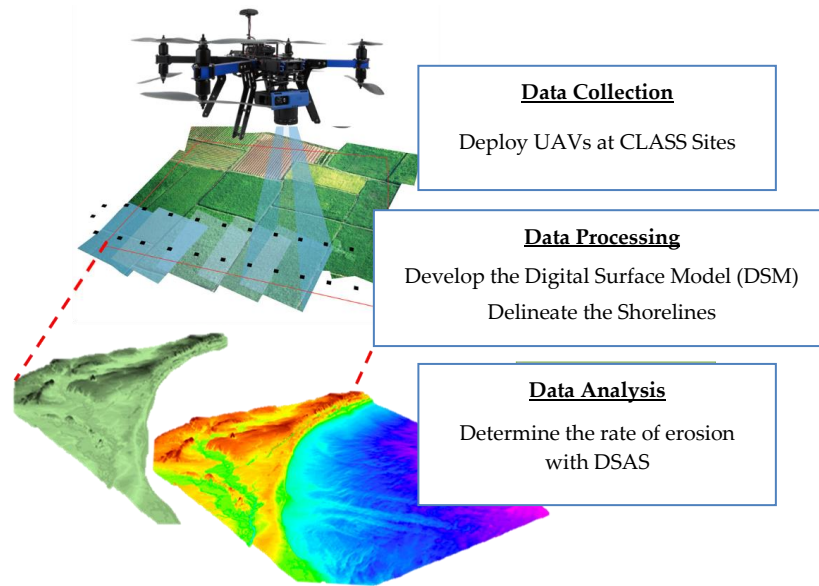
Figure 3-2. UAV Workflow

3.2.1   Data Collection

Two small UAVs based remote sensing systems (Figure 3-3) were integrated to monitor the coastal region by collecting aerial images for the years 2016 to 2018: the DJI Phantom 3 Pro (Figure 3-3a) and the DJI Matrice 100 (Figure 3-3b). The cameras used were the Zenmuse X3 RGB and Multispectral (Figure 3-3c). The first UAV provided a maximum flight time of 23 minutes and the second one of 40 minutes. Different models were used in order to compare a low-budget recreational platform with a medium-cost platform for developer users.

(a)   **(b)**   **(c)**
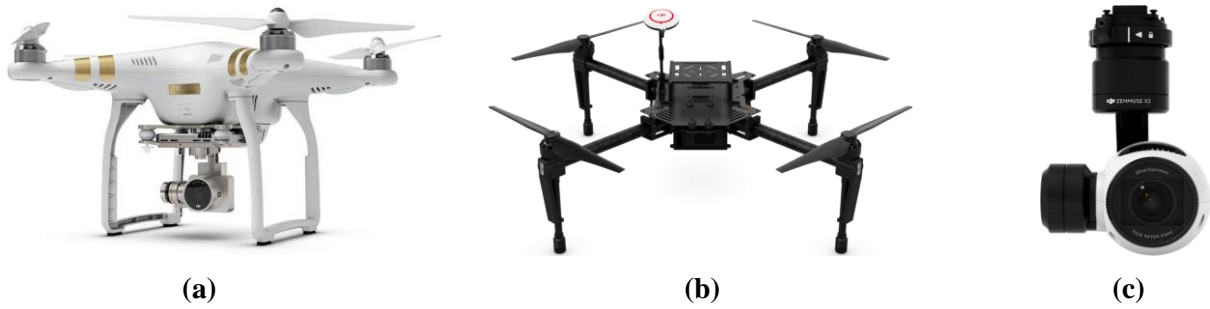
Figure 3-3. Equipment used to monitor the coastal zones: **(a)** DJI Phantom 3 Pro; **(b)** DJI Matrice 100; and **(c)** Zenmuse X3 Camera

3.2.2 Data Processing

Images were processed to generate DSMs, Digital Terrain Models (DTMs), and ortho-mosaic photos using Pix4Dmapper. DSMs are models that contain the elevation of the top of reflective surfaces such as buildings and vegetation; DTM are models with bare-earth elevations. Pix4Dmapper automatically processes the images collected from the UAVs and recognizes the pixels in order to create a 3D model of the area covered by the survey. The software processes the data automatically and calibrates each image to obtain a good precision and at the same time allows verifying the quality of recording directly on the field (Car et al. 2016). Also, allows generating 3D point cloud, measuring lines, polylines, areas and volumes, and making cross sections and contour drawings.

During the initial process, the software calibrates the camera using an algorithm that takes the whole information of each pixel of the images to estimate the optimal camera and lens calibration for each flight. After that, it performs the point cloud densification to filter and smooth the point cloud data. Since generating point cloud can lead to noisy and erroneous points, the noise filtering algorithm is used to correct the altitude of these points. Once the noise filter

12

has been applied, a surface is generated from the point cloud. Since this surface can contain areas with erroneous small bumps, the surface smoothing algorithm is used to correct these areas by flattening them. The DSM, DTM, and ortho-mosaic images are then generated. The ortho-mosaic removes the perspective distortions from the images using the 3D model and then blends the ortho-rectified images together. Since distances are preserved, ortho-rectified images can be used for measurement purposes (Visockiene et al. 2014).

A network of horizontal and vertical controls was established for each site to validate the measurements. The horizontal and vertical network of permanent controls was established using Static and Real time Kinematics (RTK) Global Positioning System (GPS), and instantly corrected with Virtual Reference Stations (VRS). Control points were marked using white paint over asphalt and observations were made for 3 minutes using VRS and 4 hours using Static/RTK at each point. Horizontal positions were referenced to the North American Datum of 1983 (NAD83) High Accuracy Reference Networks (HARN) State Plane Coordinate System (SPCS) for Puerto Rico and Virgin Islands FIPS 5200. Vertical positions for the Static RTK solutions were referenced to the Puerto Rico Vertical Datum of 2002 (PRVD02) by the use of the Online Positioning User Service (OPUS) provided by the National Geodetic Survey (NGS) which used the GEOID12B model to transform the positions from ellipsoid to ortho-metric heights.

After developing the DSM, DTM, and obtaining the ortho-rectified images, ArcGIS software was used to delineate the shorelines for each site, in addition to a unique dataset of historical aerial photography that covers from 1930 to 2010. All images were projected to the NAD83 HARN SPCS for Puerto Rico and Virgin Islands FIPS 5200 and same unit measure (meters). The wet/dry line was used as the shoreline indicator to represent the "true" shoreline position of each

image. This indicator was manually detected, identifying the maximum wet line (Boak and Turner 2005). The final output consisted of six digitized shoreline positions for each site: 1930, 2004, 2010, 2016, 2017, and 2018.

3.2.3 Data Analysis

The Digital Shoreline Analysis System (DSAS) was implemented to compute the rate-of-change statistics from the delineated shorelines. The statistical measures allowed in DSAS include: Shoreline Change Envelope (SCE), Net Shoreline Movement (NSM), End Point Rate (EPR), Linear Regression Rate (LRR), and other standard methods. The SCE method measures the total change in shoreline movement considering all the shorelines. The NSM method reports the distance between the oldest and most recent shoreline in the data. The EPR determines the distance between the oldest and most recent shoreline in the dataset and divides it by the number of years between them. The LRR method determines the rate of change statistic by fitting a least square regression to all shorelines at a specific transect (Thieler et al. 2009). These statistics were calculated at each transects along the shore to evaluate the historical shoreline changes and trends.

For each site, a baseline was constructed adjacent to the shoreline positions to serve as the starting point for all transect cast by the application. These transects were cast perpendicular to the baseline with 15 meters spacing and intersect each shoreline at the measurement points used to calculate shoreline-change rate. They were also used to study the beach changes occurred along the coast.

3.3 Case Study: Effects of Hurricane Matthew at Cofresí Beach, Rincón, PR

In October 2016, UAVs were deployed to perform a rapid assessment and evaluate the effects of the Hurricane Matthew (Category 4) at Rincón, PR. This hurricane was 500 nautical miles away and the southwestern direction of the generated swell severely impacted the western region of Puerto Rico (Figure 3-4).
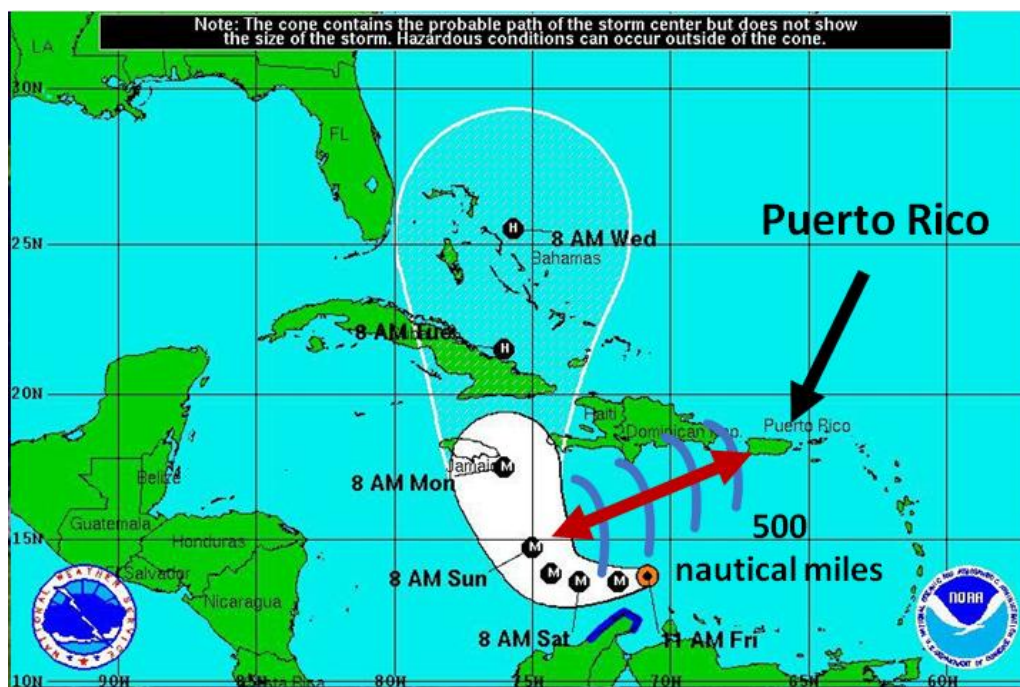
Figure 3-4. Hurricane Matthew trajectory (NOAA)

Additionally, XBeach was used to evaluate the morphological changes at the foreshore induced by this storm event at Rincón and results were validated using UAV data. This analysis was performed with the purpose of evaluating whether XBeach showed potential to determine the

morphological changes in the coastal zone and quantify the erosion or accretion events caused by the hurricane.

3.3.1 Numerical Model

XBeach was modeled in the hydrostatic surfbeat mode (in stationary), where the short wave variations on the wave group scale and the long waves associated with them are resolved. This mode is necessary when the focus is on swash zone processes rather than time-averaged currents and setup (Roelvink et al. 2015).

3.3.1.1 Short Wave Action

The wave action balance was necessary to determine the wave forcing of short waves in shallow waters for the hydrostatic mode. The short wave action balance equation is given below:

$$\frac{dA}{dt} + \frac{dc_{gx}A}{dx} + \frac{dc_{gy}A}{dy} + \frac{dc_{\theta}A}{d\theta} = -\frac{D_w + D_f + D_v}{\sigma} \qquad (3\text{-}1)$$

Where A represents the wave action, c_g represent the wave action propagation speed in the x- and y- direction, θ represents the angle of incidence with respect to the x-axis, σ represents the intrinsic wave frequency, and D_w, D_f and D_v represents the dissipation terms for respectively waves, bottom friction and vegetation. The equations to calculate the separate terms in the wave action balance can be found in the manual of XBeach (Roelvink et al. 2015).

3.3.1.2 Shallow Water Equations

Shallow water equations were used to model the infragravity waves and flow caused by currents. In order to solve the long waves caused by wave groups and the return flow, the horizontal viscosity was required, and it was computed using the Smagorinsky method shown below:

$$\nu_h = c_s^2 2^{\frac{1}{2}} \sqrt{\left(\frac{\delta u}{\delta x}\right)^2 + \left(\frac{\delta v}{\delta y}\right)^2 + \frac{1}{2}\left(\frac{\delta u}{\delta x} + \frac{\delta v}{\delta y}\right)^2} \Delta x \Delta y \qquad (3\text{-}2)$$

Where ν_h represents the horizontal viscosity and c_s represents the Smagorinsky constant set at 0.1 in all model simulations.

3.3.1.3 Sediment Transport

XBeach models the sediment concentration in the water column using the following advection-diffusion equation:

$$\frac{\partial hC}{\partial t} + \frac{\partial hCu^E}{\partial x} + \frac{\partial hCv^E}{\partial y} + \frac{\partial}{\partial x}\left[D_h h \frac{\partial C}{\partial x}\right] + \frac{\partial}{\partial y}\left[D_h h \frac{\partial C}{\partial y}\right] = \frac{hC_{eq} - hC}{T_s} \qquad (3\text{-}3)$$

Where C represents the depth-averaged sediment concentration, D_h represents the sediment diffusion coefficient which is 1 by default, h represents the water depth, T_s represents the adaption time for the sediment to respond to wave forcing, and C_{eq} represents the equilibrium sediment concentration.

3.3.2 Model setup

3.3.2.1   Model Input Parameters

Figure 3-5 shows the workflow implemented in the numerical simulation.

XBeach Simulation

↓

Input Data

Initial Beach Profile

- Bathymetry
- Grid coordinates

Sediment Properties

- D_{50} and D_{90}
- Density
- Porosity

Wave Conditions

- Flow boundary
- Initial water level
- Significant wave height
- Representative Period

Duration of Impact

- Model time
- Start/stop time
- Morphological factor

↓

Process Data

- Run XBeach executable

↓

Output Data

- Run MATLAB to visualize results
- Output variables:
  - Total bed change due to avalanching
  - Bed erosion rate per fraction
  - Suspended sediment transport in x, y direction
  - Rate of change bed level
  - Cumulative sedimentation/erosion
  - Fraction breaking waves

Figure 3-5. XBeach workflow

The following table indicates the parameters used as the model input for the simulation:

Table 3-1. Input parameters used for the XBeach simulation

Grid parameters	gridform	Delft3D
	depfile	bed.dep
	alfa (°)	0
	posdwn	-1
	xyfile	xy.grd
Spectral grid parameters	thetamin (°)	-90
	thetamax (°)	90
	dtheta (°)	10
	thetanaut	0
Model time	tstart (s)	0
	tstop (s)	18000
	tintg (s)	60
	tintp (s)	60
Physical constants and sediments	rho (kg/m^3)	1025
	g (m/s^2)	9.81
	D_{50} (m)	0.00097
	rhos (kg/m^3)	2650
	por	0.3
	D_{90} (m)	0.00157
Flow boundary conditions	front	abs_1d
	back	abs_1d
	left	neumann
	right	neumann
Tide boundary conditions	tideloc	0
	zs0 (m)	0.225
Wave boundary conditions	instat	0
	dir0 (°)	279
	Hrms (m)	1.67
	Trep (s)	11.11
	lwave	0
Morphology conditions	morfac	1
	morstart	0
Output variables	outputformat	netcdf
	nglobalvar	4: zb, zb0, sedero, ero

The simulation was made for 5 hours under uniform water level conditions. In order to implement the model, a directional grid for short waves was needed. This spectral grid was determined by a minimum and maximum angle and width per bin (*thetamin* – lower directional limit; *thetamax* – upper directional limit; *dtheta* – directional resolution). Additionally, boundary conditions were needed and established at the front, back, and lateral locations. The absorbing-generating boundary in 1D (Abs1d) option was selected for the front and back locations. This option allows for a time-varying water level to be specified at the boundary while allowing any waves propagating perpendicularly towards the boundary to be absorbed (i.e. passed through the boundary with a minimum of reflection. The "no-gradient" or Neumann boundaries option was selected for the lateral boundaries. This option state that there is locally no change in surface elevation and velocity (Roelvink et al. 2015)

In addition to the previous parameters, XBeach also required data regarding bathymetry, wind, waves, tide, and sediment properties.

3.3.2.2 Bathymetry Data

The pre-storm topo-bathymetry data was obtained from the 2016 United States Army Corps of Engineers (USACE) Topobathy LiDAR dataset for Puerto Rico (NOAA - Digital Coast 2016). The LiDAR dataset was collected from January 28, 2016 to February 7, 2016 by the Joint Airborne LiDAR Bathymetry Technical Center of Expertise (JALBTCX) using the Coastal Zone Mapping and Imaging Lidar (CZMIL) system which integrates a LiDAR sensor with simultaneous topographic and bathymetric capabilities, a digital camera and a hyperspectral

imager on a single remote sensing platform. The horizontal positions were referenced to the NAD83 HARN SPCS for Puerto Rico and Virgin Islands FIPS 5200 with 1-meter resolution. The vertical positions were referenced to the PRVD02 with a vertical accuracy of 0.01 meters. This data was used to establish the model computational domain that defines the area of interest for the modeling (Figure 3-6). The grid was generated with a 2-meter resolution using ArcGIS and Delft3D software and was aligned parallel to the coastline with 22.5 degrees of inclination. The elevation values for the study area were from 3.45 to -6.05 meters; negative values correspond to the bathymetry data portion.
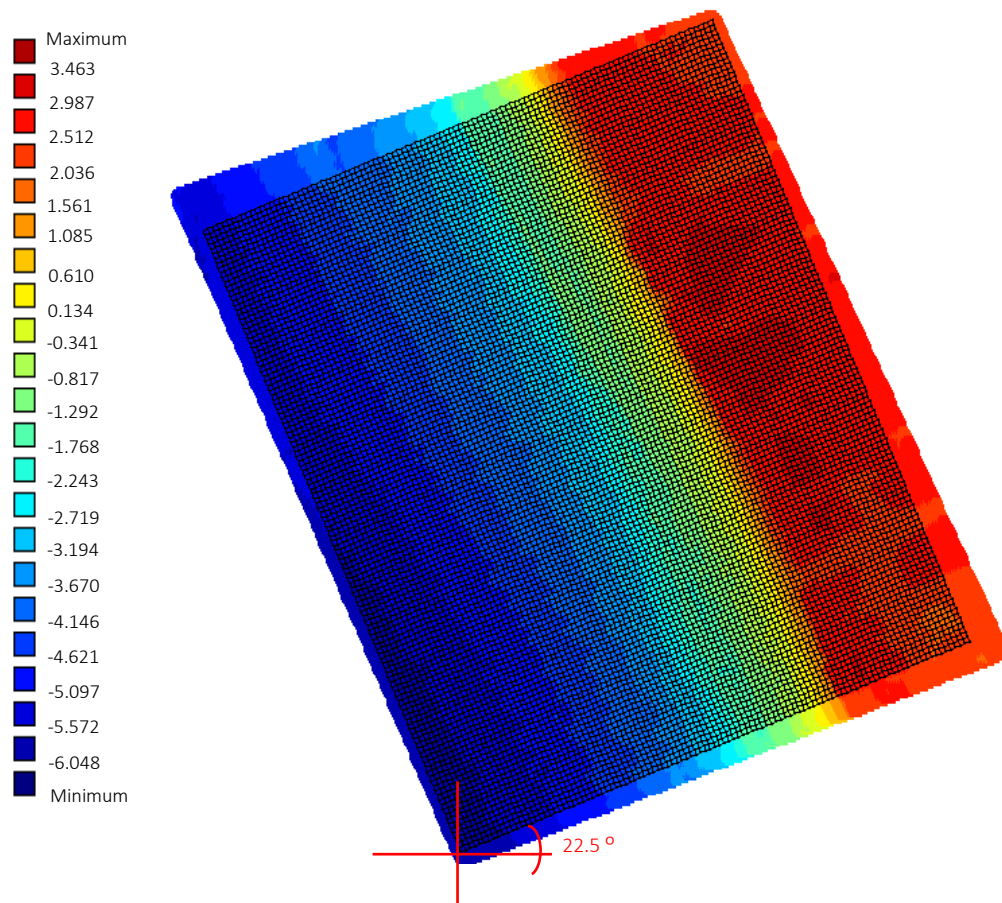
Figure 3-6. USACE topo-bathy LiDAR data and Delft3D grid (2-meter resolution in *x-* and *y-* direction) used for the XBeach simulation

21

3.3.2.3   Hydrodynamic Data

In addition to the topo-bathymetry data, wind, wave, and tide data generated during the Hurricane Matthew event were also needed. Wind and wave data were obtained from the Caribbean Coastal Ocean Observing System (CARICOOS) Rincón wave buoy and anemometer, respectively (Figures 3-7 and 3-8). Tide data was obtained from the NOAA tidal station at Mayaguez, P.R (Figures 3-7 and 3-9) (NOAA 2018); values are shown in Table 3-2 and 3-3.
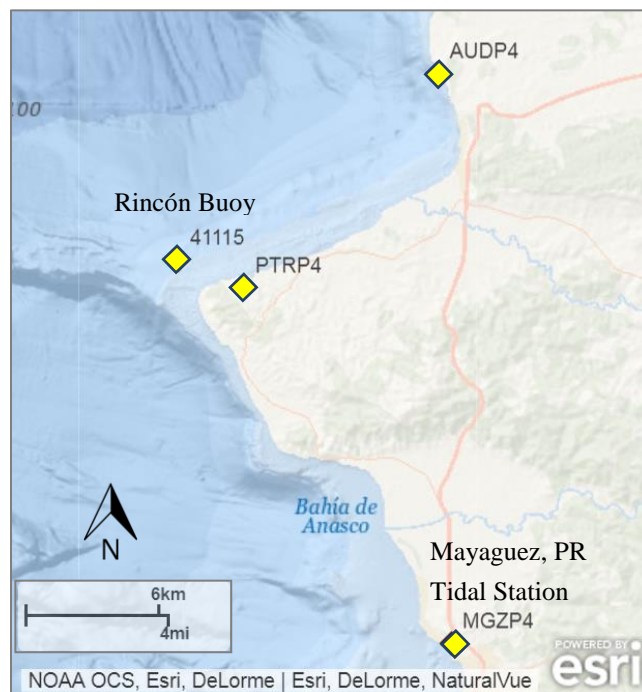
Figure 3-7. Location of NOAA buoy and tidal station for the hindcast
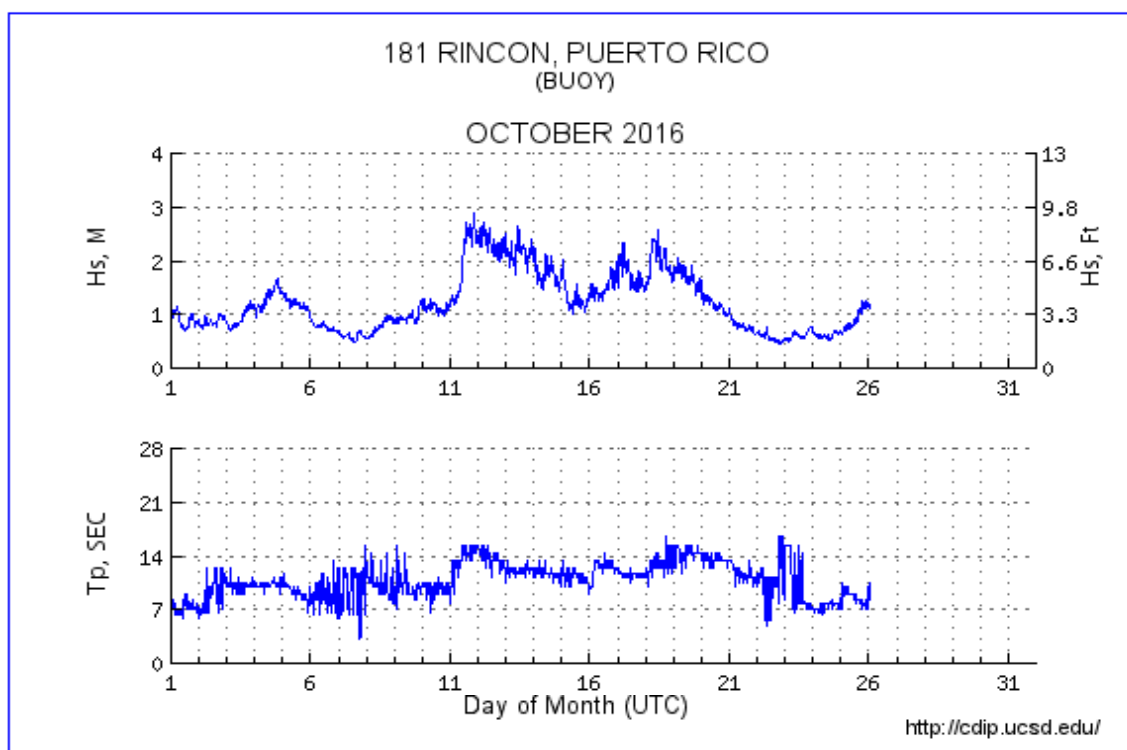
Figure 3-8. CARICOOS buoy data at Rincón, P.R (The Coastal Data Information Program)
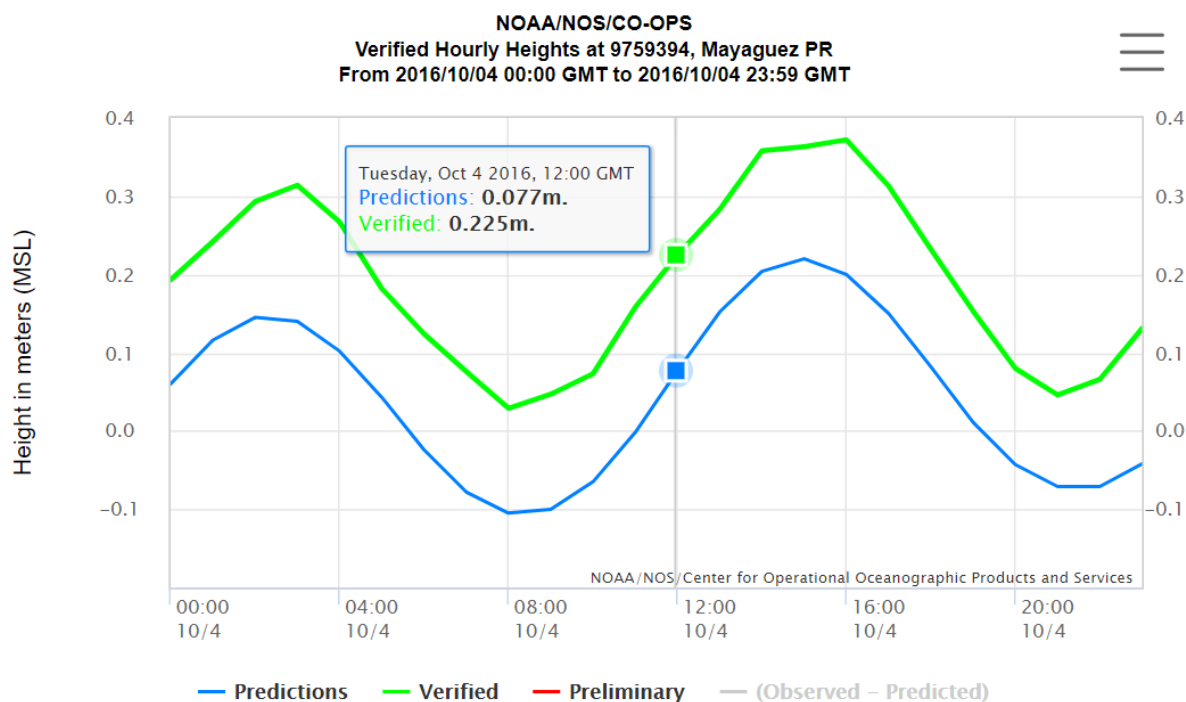
Figure 3-9. NOAA tide/water levels data for October 4, 2016

23

Table 3-2. Tide boundary conditions

Parameter	Value
Time varying water level, tideloc	0 - Uniform water level
Initial water level, zs0	0.225 meters

Table 3-3. Wave boundary conditions

Parameter	Value
Wave direction, dir0	279 $^\circ$
Significant wave height, Hrms	1.67 meters
Dominant wave period, Trep	11.11 seconds

3.3.2.4   Sediment Properties

The uniform D_{50} sediment diameter and D_{90} diameter were needed for the XBeach simulation. Both diameters were obtained through the characterization of the soil conducting the sieve analysis test using the Standard of the American Society for Testing and Materials ASTM-C136. Samples were collected on September 4th, 2016 as part of a thesis project lead by Professor Miguel Canals. The samples were collected from four different areas: (a) berm, (b) beach face/front, (c) swash zone, and (d) nearshore (Figures 3-10 and 3-11). These four areas were selected to obtain a clearly idea of the sediments found on the beach.

(a)   **(b)**

(c)   **(d)**
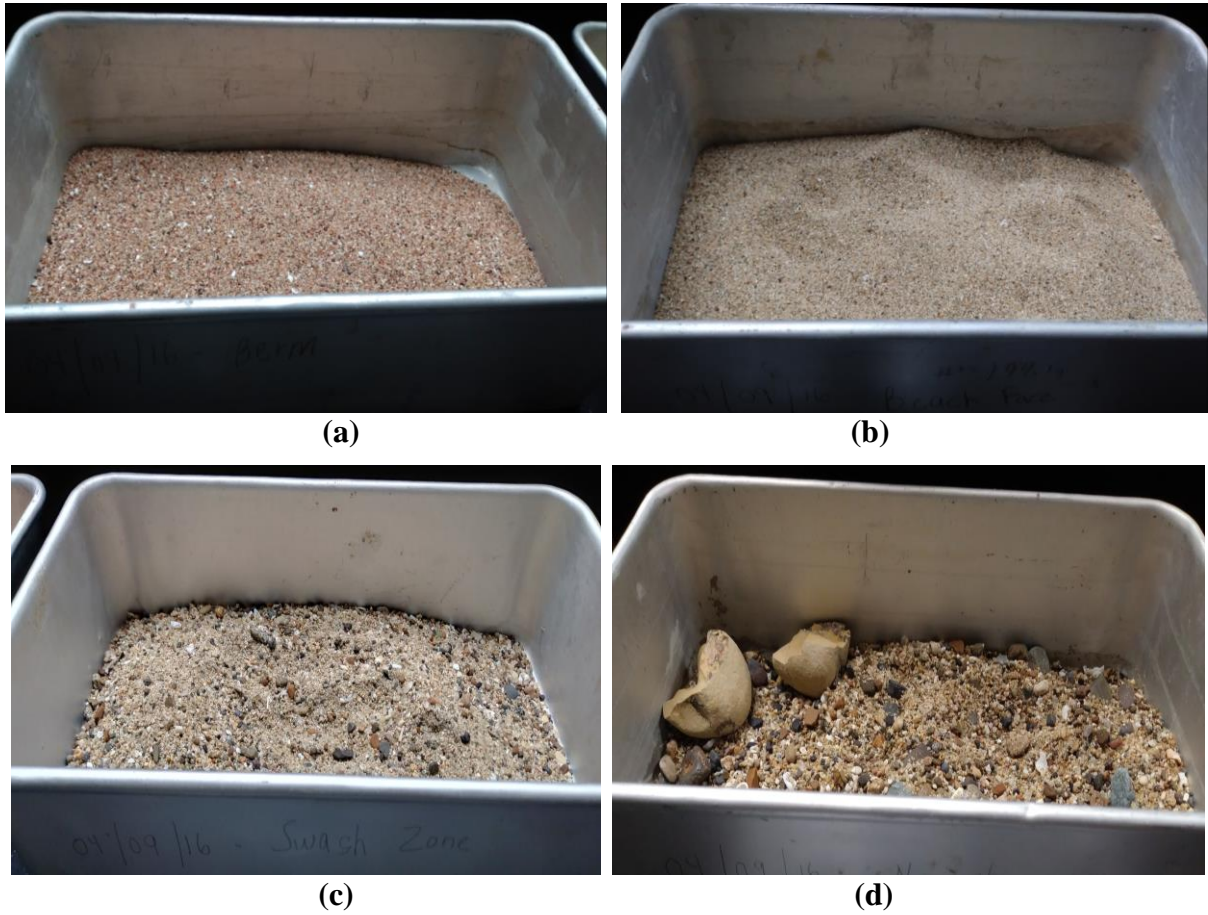
Figure 3-10. Samples collected from **(a)** berm; **(b)** beach face; **(c)** swash zone; and **(d)** nearshore
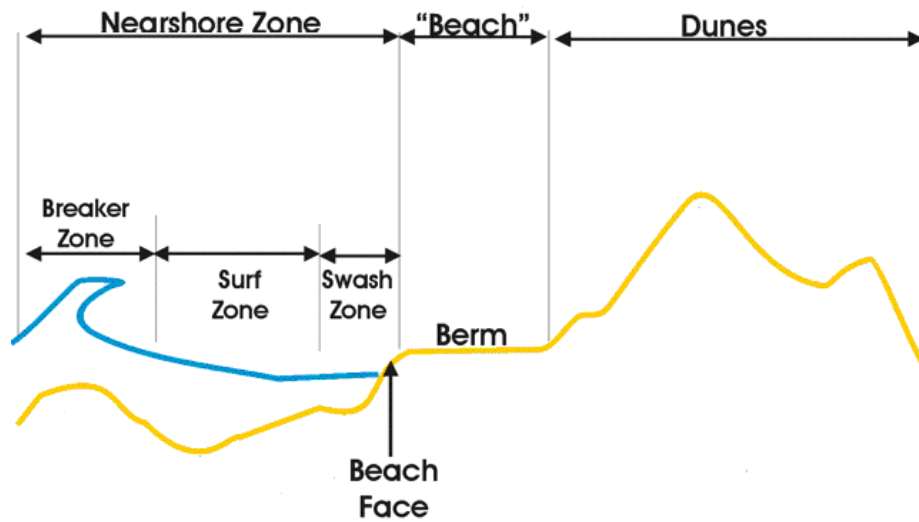
Figure 3-11. Typical beach system (Maine Geological Survey)

25

In order to perform the sieve analysis, the sequence of sieves shown in Figure 3-12 was used.
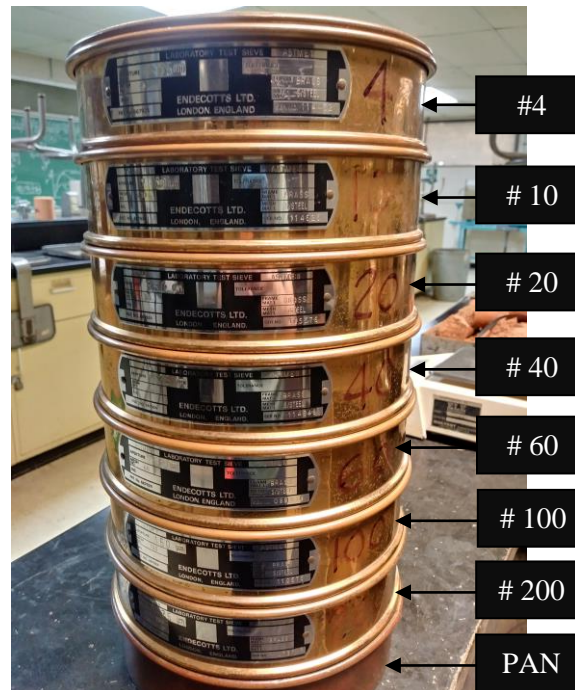
Figure 3-12. Sieve size sequence

The following tables show the sieve analysis of samples collected at the berm (Table 3-4), beach face (Table 3-5), swash zone (Table 3-6), and nearshore (Table 3-7). These tables allow the quantification of the percent of gravel, sand, and silt. This percent is needed to classify each sample. According to the standard practice for classification of soils provided in the ASTM D 2487 (Figure 3-13), which uses the Unified Soil Classification System (USCS), the samples collected from the berm, beach face, and swash zone were classified as SP or poorly graded sand; the sample collected from the nearshore was classified as SP with gravel.

26

Table 3-4. Sieve analysis of samples collected at the berm

							Berm
Sieve #	Sieve Size (mm)	Sieve Weight (g)	Sieve + Soil Weight (g)	Weight Retained (g)	% Retained	Cumulative % Retained	% Passing
4	4.75	461.5	461.5	0	0	0	100
10	2.0	426.0	426.3	0.3	0.1	0.1	99.9
20	0.85	384.2	391.2	7.0	3.0	3.1	96.9
40	0.425	348.7	427.9	79.2	33.4	36.5	63.5
60	0.250	329.8	420.7	90.9	38.4	74.9	25.1
100	0.150	314.2	369.3	55.1	23.3	98.1	1.9
200	0.074	305.0	309.4	4.4	1.9	100	0
Pan	0	362.4	362.4	0	0	100	0

Σ 236.9

Table 3-5. Sieve analysis of samples collected at the beach face

							Beach Face / Front
Sieve #	Sieve Size (mm)	Sieve Weight (g)	Sieve + Soil Weight (g)	Weight Retained (g)	% Retained	Cumulative % Retained	% Passing
4	4.75	461.5	461.5	0	0	0	100
10	2.0	426.2	426.3	0.1	0	0	100
20	0.85	384.3	387.5	3.2	1.4	1.5	98.5
40	0.425	348.3	396.5	48.2	21.3	22.7	77.3
60	0.250	329.8	415.9	86.1	38.0	60.7	39.3
100	0.150	314.2	398.7	84.5	37.3	98	2
200	0.074	305.1	309.6	4.5	2	100	0
Pan	0	362.4	362.4	0	0	100	0

Σ 226.6

Table 3-6. Sieve analysis of samples collected at the swash zone

							Swash Zone
Sieve #	Sieve Size (mm)	Sieve Weight (g)	Sieve + Soil Weight (g)	Weight Retained (g)	% Retained	Cumulative % Retained	% Passing
4	4.75	461.4	469.9	8.5	3.2	3.2	96.8
10	2.0	425.9	473.6	47.7	17.9	21.1	78.9
20	0.85	384.3	471.3	87.0	32.7	53.9	46.1
40	0.425	348.8	411.7	62.9	23.7	77.5	22.5

				Swash Zone			
Sieve #	Sieve Size (mm)	Sieve Weight (g)	Sieve + Soil Weight (g)	Weight Retained (g)	% Retained	Cumulative % Retained	% Passing
60	0.250	329.9	359.5	29.6	11.1	88.7	11.3
100	0.150	314.1	342.5	28.4	10.7	99.4	0.6
200	0.074	305.1	306.7	1.6	0.6	100	0
Pan	0	362.3	362.4	0.1	0	100	0

$$\Sigma \quad 265.8$$

Table 3-7. Sieve analysis of samples collected at the nearshore

				Nearshore			
Sieve #	Sieve Size (mm)	Sieve Weight (g)	Sieve + Soil Weight (g)	Weight Retained (g)	% Retained	Cumulative % Retained	% Passing
4	4.75	461.4	530.9	69.5	28.7	28.7	71.3
10	2.0	426.0	485.8	59.8	24.7	53.4	46.6
20	0.85	384.5	455.5	71.0	29.4	82.8	17.2
40	0.425	348.9	378.1	29.2	12.1	94.9	5.1
60	0.250	329.8	336.9	7.1	2.9	97.8	2.2
100	0.150	314.1	319.1	5.0	2.1	99.9	0.1
200	0.074	305.0	305.3	0.3	0.1	100	0
Pan	0	362.3	362.4	0.1	0	100	0

$$\Sigma \quad 242$$

Figure 3-13. ASTM D 2487 standard section for the classification of soils

Figure 3-14 shows the sieve analysis results for the four collected samples. This graph was generated using the sieve size and passing percent data from each collected sample. These results were used to determine the diameters D_{50} and D_{90} of each sample. Results are summarized in Table 3-8, in addition to the average diameter results of the four samples needed for the XBeach simulation.
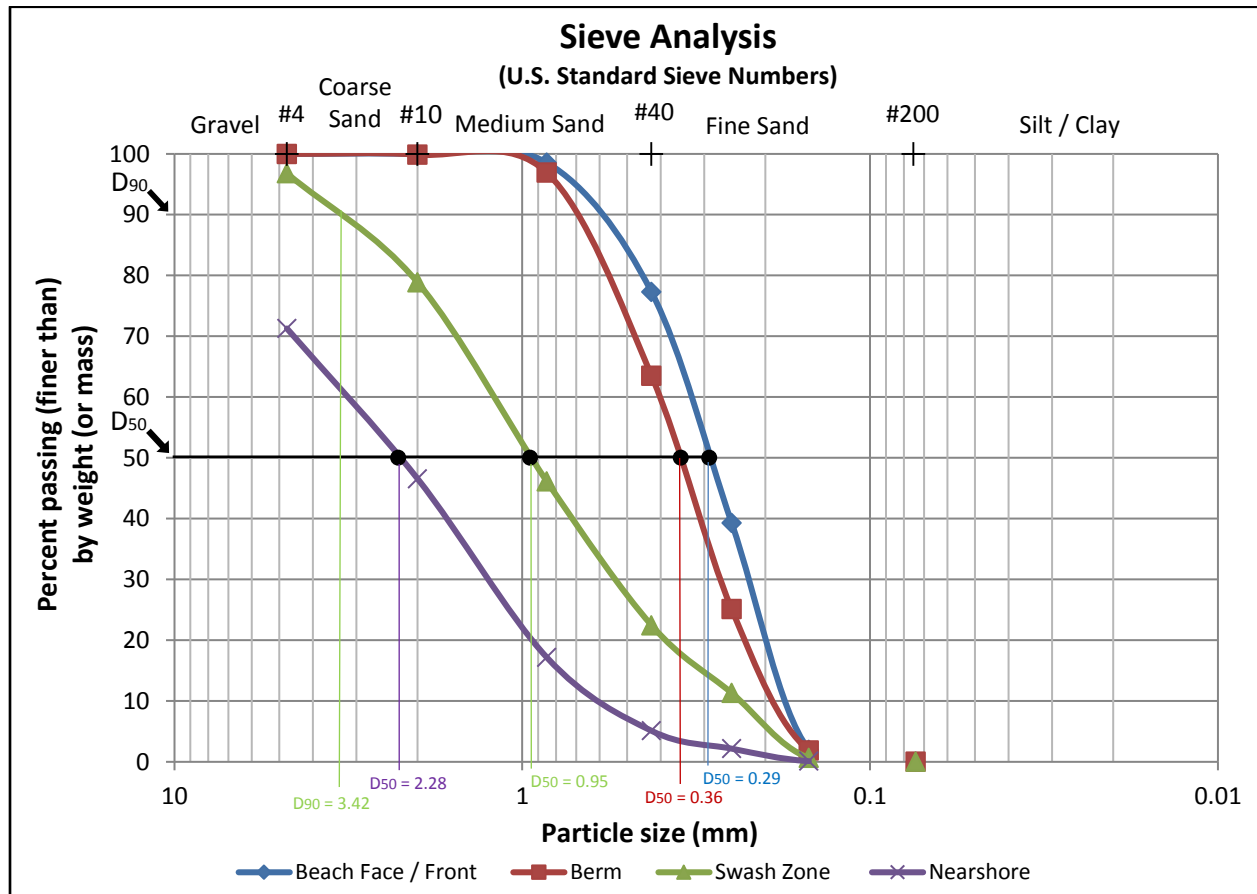
Figure 3-14. Sieve analysis graph for the four samples collected

Table 3-8. Sieve analysis diameter results

Soil Sample	Gravel (%)	Sand (%)	Silt (%)	D50 (mm)	D90 (mm)
Beach Face / Front	0	100	0	0.29	0.59
Berm	0	100	0	0.36	0.69
Swash Zone	3.2	96.8	0	0.95	3.42
Nearshore	28.7	71.3	0	2.28	-
			Average:	0.97	1.567

3.3.2.5 Model Output Data Processing

XBeach simulation results were managed using MATLAB and Microsoft Office Excel. Eleven transects were cast perpendicular to the coastline with 10 meters spacing (Figure 3-15). Erosion and accretion results were added to the initial bed level results to develop the simulated bed level.
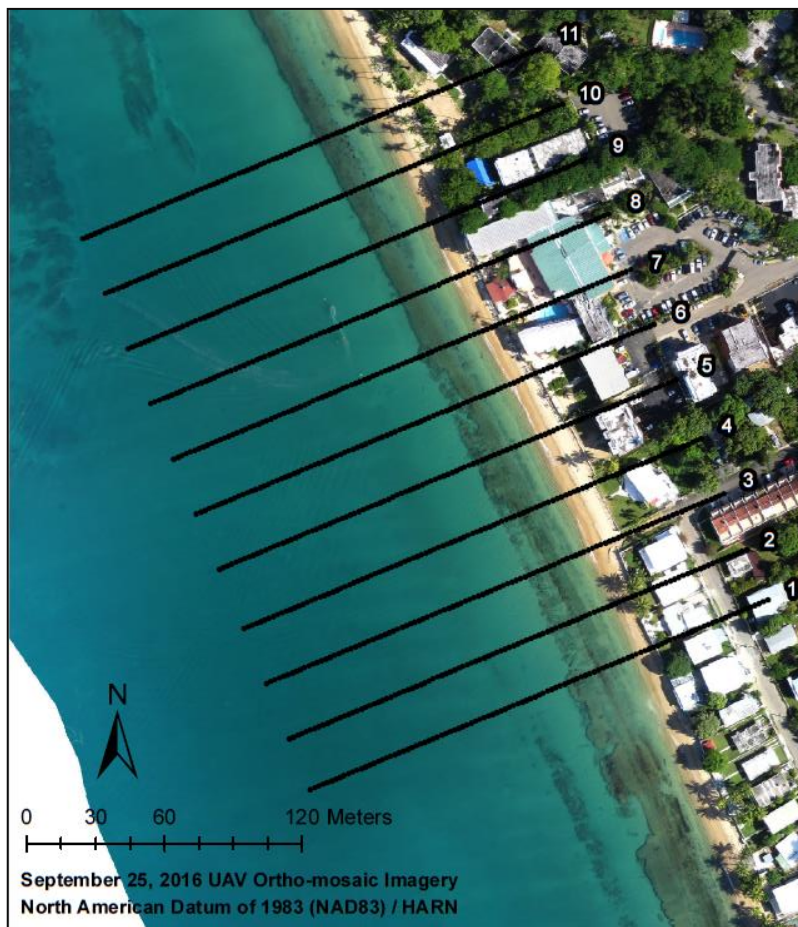
Figure 3-15. Transect used for the profiles creation

3.3.2.6   Model Validation

XBeach simulation results were validated in two coordinates: longitudinal (x) and vertical (z); the longitudinal refers to planimetric data, and vertical refers to topographic data. For the longitudinal validation, UAV's high-resolution images were used to generate the ortho-mosaic images before and after Hurricane Matthew. After generating the ortho-mosaics, ArcGIS software was used to delineate the shorelines. DSAS was then implemented to cast 18 perpendiculars transects with 15 meters spacing which provided the change-of rate statistics with the EPR results (see section 3.2.2 and 3.2.3 for details). For the vertical validation, XBeach simulated profiles and UAV measured profiles were generated at each of the 11 transects with 10-meters spacing between them. Pre- and post-storm XBeach simulated profiles were generated using the DTM elevations. Pre- and post-storm UAV profiles were generated using two DSMs and a DTM after the hurricane event. The DSM before Hurricane Matthew was obtained through the Sea Grant project R/75-1-14, where UAV images were collected at Rincón, P.R. This DSM was a hybrid model that contained the topography and bathymetry data from another source. The other DSM and DTM generated after the storm event were obtained using the DJI Phantom 3 UAV for the image collection and Pix4Dmapper for the data processing. Both models only contain the topographical information because our UAV visible camera was not capable to determine the elevation of water surfaces. In addition to the profiles, the elevation results from the XBeach simulation and UAVs DSMs pre- and post-storm were subtracted to quantify the erosion or accretion events at each transect.

31

For both validations, a statistical analysis was conducted to measure the efficiency of the model results. This analysis included the standard deviation (s), Mean Absolute Error (MAE), Mean Bias Error (MBE), Root Mean Square Error (RMSE), correlation coefficient (R), and the coefficient of determination (R^2); their respective equations are shown below:

$$s = \sqrt{\frac{\sum_{i=1}^{n}(x_i - \bar{x})}{n-1}} \tag{3-4}$$

$$MAE = \frac{1}{n}\sum_{i=1}^{n}|y_i - \hat{y}_i| \tag{3-5}$$

$$MBE = \frac{1}{n}\sum_{i=1}^{n}y_i - \hat{y}_i \tag{3-6}$$

$$RMSE = \sqrt{\frac{\sum_{i=1}^{n}(y_i - \hat{y}_i)^2}{n}} \tag{3-7}$$

$$R = \frac{\left\{\sum_{i=1}^{n}\left[(x_{i,obs} - \bar{x}_{obs})\cdot(x_{i,sim} - \bar{x}_{sim})\right]\right\}}{\sqrt{\sum_{i=1}^{n}(x_{i,obs} - \bar{x}_{obs})^2 \cdot \sum_{i=1}^{n}(x_{i,sim} - \bar{x}_{sim})^2}} \tag{3-8}$$

$$R^2 = \frac{\left(\sum_{i=1}^{n}\left[(x_{i,obs} - \bar{x}_{obs})\cdot(x_{i,sim} - \bar{x}_{sim})\right]\right)^2}{\sum_{i=1}^{n}(x_{i,obs} - \bar{x}_{obs})^2 \cdot \sum_{i=1}^{n}(x_{i,sim} - \bar{x}_{sim})^2} \tag{3-9}$$

Where n represent the number of observed/simulated points, x_i represent the observed/simulated point at n position, $\bar{x}$ represent the sample average, y_i represent the observed variable at n position, and $\hat{y}_i$ represent the simulated variable at n position.

These statistics are widely used throughout the scientific community and will define how close the simulations are to the observed data. The standard deviation is a measure of how spreads out numbers are; low values indicates that the data tend to be close to the mean of the set, while high values indicates that the data are spread out over a wider range of values. The MAE is the average over the test sample of the absolute differences between the predicted and observed values. It measures the average magnitude of the errors in a set of prediction, without considering their direction. The MBE is the average over the test sample of the differences between the predicted and observed values. It measures the average model bias and should be interpreted cautiously because positive and negative errors will cancel out. A negative MBE occurs when predictions are smaller in value than observations (Willmott and Matsuura 2006). The RMSE is a measure of the differences between values predicted by a model and observed values. In general, the larger the RMSE values, the more significant the errors associated with the simulation. The coefficient of correlation is a measure of how strong a relationship is between two variables, in addition to the direction of the linear relationship. It is expressed as a value between +1 and -1; +1 indicates a perfect positive correlation where one variable increases as the other increases, -1 indicates a perfect negative correlation where one variable decreases as the other increases, and 0 indicate no linear relationship. The R^2 is a measure of how close the data are to the fitted regression line; low R^2 values will indicate low ability of the model to represent the variability of the phenomena (Infante-Corona et al. 2015).

3.3.2.7 Sensitivity Analysis

A sensitivity analysis was performed to evaluate the changes in the simulation results by varying the uniform D_{50} sediment diameter. For this analysis, values corresponding to the minimum (0.29 mm) and maximum (2.28 mm) diameter were used as data input for the model. Similar to the previous section (section 3.3.2.6), both XBeach simulation results were validated in two coordinates: longitudinal (*x*) and vertical (*z*). For the longitudinal validation, UAV's high-resolution images were used to generate the ortho-mosaic images before and after Hurricane Matthew, and DSAS was then implemented to provide the change-of rate statistics with the EPR results. For the vertical validation, the UAVs DSMs pre- and post-storm were subtracted to quantify the erosion or accretion events at each transect.

For both validations, a statistical analysis was conducted to measure the efficiency of the model results. This analysis included the standard deviation (s), Mean Absolute Error (MAE), Mean Bias Error (MBE), Root Mean Square Error (RMSE), and the correlation coefficient (R). Additionally, both results were compared with the average (0.97 mm) D_{50} diameter used in this study.

CHAPTER 4 - DATA PRODUCTS

This chapter presents the data products processed from the UAV data collection, using Pix4Dmapper. These products include the generation of ortho-mosaics images for the three sites, in addition to a DSM and DTM for Cofresí Beach at Rincón. All the data will be available to the scientific community through Geospatial Research Laboratory at the University of Puerto Rico at Mayaguez (UPRM) website (https://wordpress.uprm.edu/elige/mdocuments-library/).

4.1   Ortho-mosaics

Ortho-mosaics were developed for Jobos Beach at Isabela, Crash Boat Beach at Aguadilla, and Cofresí Beach at Rincón as shown in Figures 4-16 to 4-18. These images were projected using the NAD83 HARN SPCS for Puerto Rico and Virgin Islands FIPS 5200 in meters and generated for years 2016 and 2018 with a 2.05 centimeter/pixel resolution. The ortho-mosaic images had an approximately extension of 0.6 kilometers for Jobos Beach at Isabela, 0.5 kilometers for Crash Boat Beach at Aguadilla, and 0.3 kilometers for Cofresí Beach at Rincón.

4.1.1 Jobos Beach, Isabela

Figure 4-16. Ortho-mosaic images from 2016 and 2018 for Jobos Beach, Isabela

4.1.2 Crash Boat Beach, Aguadilla
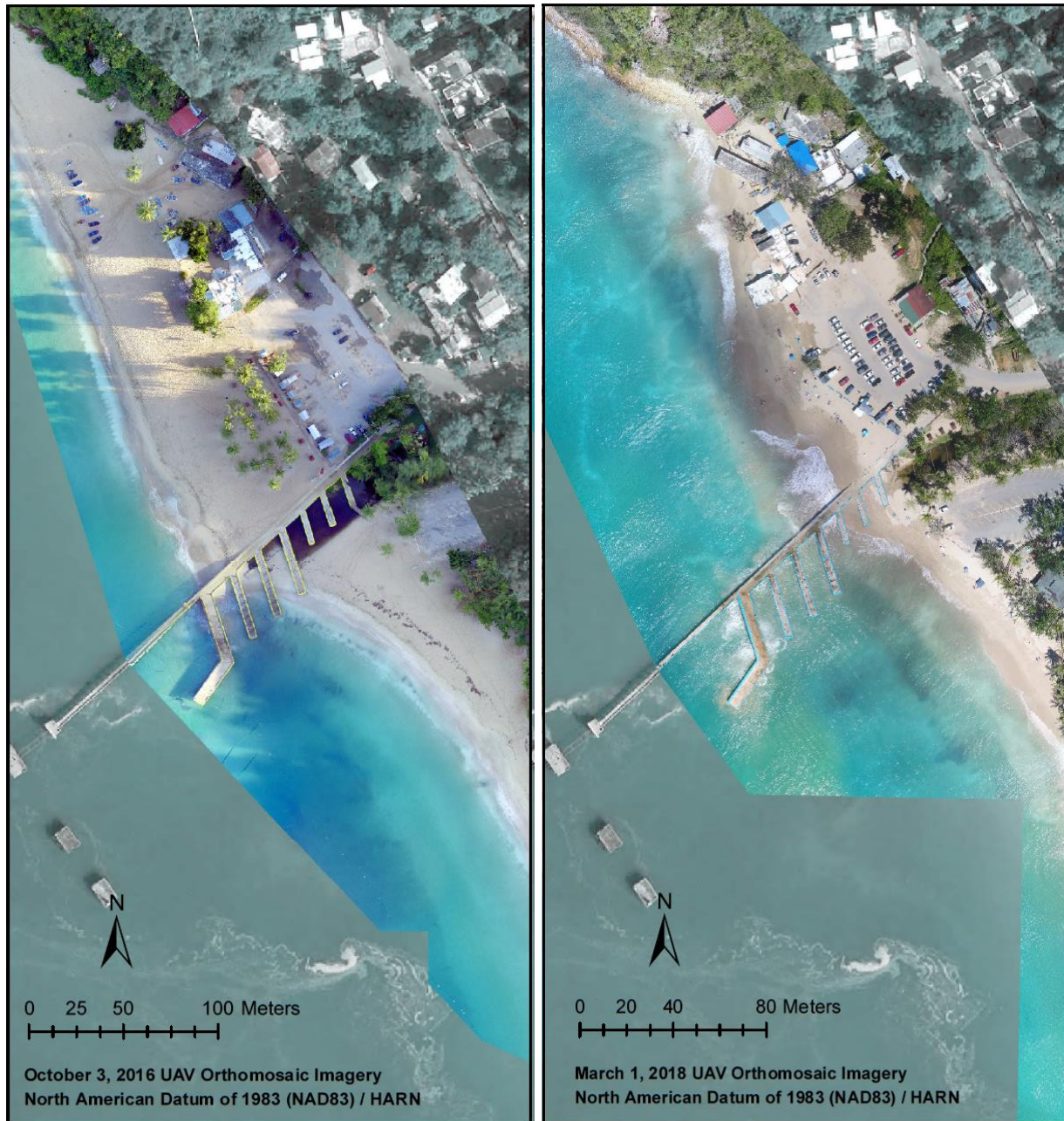
Figure 4-17. Ortho-mosaic images from 2016 and 2018 for Crash Boat Beach, Aguadilla

4.1.3 Cofresí Beach, Rincón

Figure 4-18. Ortho-mosaic images from 2016 and 2018 for Cofresí Beach, Rincón

4.2 Digital Surface and Terrain Models (DSMs and DTMs)

A DSM and DTM were developed for the validation of the XBeach simulation at Cofresí Beach, Rincón (Figure 4-19). Both models were generated in 2016, after the Hurricane Matthew with a 2.05 centimeter/pixel resolution. These models were projected using the NAD83 HARN SPCS for Puerto Rico and Virgin Islands FIPS 5200 in meters. The DSM from the Sea Grant project R/75-1-14 was also used.
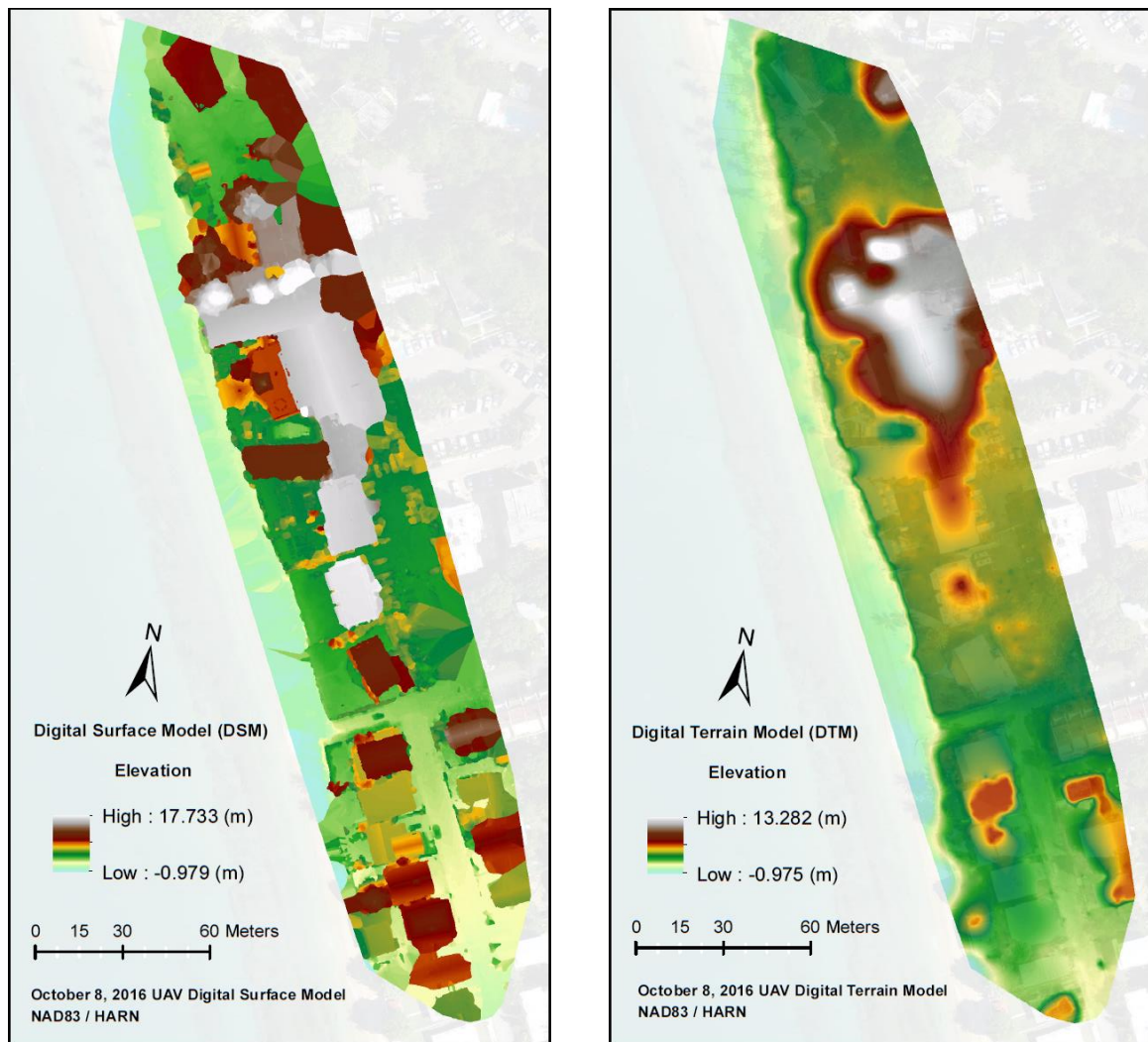
Figure 4-19. DSM and DTM of Cofresí Beach, Rincón

CHAPTER 5 - RESULTS AND DISCUSSION

This chapter contains the results and discussion of the shoreline changes maps and DSAS analysis for the three selected areas, as well as the case study results of the erosion effects of Hurricane Matthew at Cofresí Beach, Rincón.

5.1   Shoreline Changes Maps

A qualitative analysis of shoreline changes was perform using maps of historical shoreline positions. These maps were developed for each site using the ortho-mosaic images (Figures 5-20 to 5-28). The maps represent the shoreline changes for periods 1930-2004, 2004-10, 2010-16, 2016-17, and 2017-18 in addition of the net shoreline changes from 1930 to 2018. Aerial images for 2017 were used from the Vexcel Imaging Puerto Rico post Maria imagery available at ArcGIS Online. These images were collected in September 2017 with approximately 3" to 6" resolution, using a Vexcel Imaging UltraCam Eagle.

5.1.1 Jobos Beach, Isabela

The analysis of the historical shoreline positioning maps for Jobos Beach at Isabela, for the periods from 1930 to 2004 (Figure 5-20a), showed retreat events. This could be due to the conditions generated during several meteorological events that have occurred in that period. During the period from 2004 to 2010 (Figure 5-20b), the shoreline remained almost in the same position, except for a few small segments. It is important to recognize that the delineation of the coast varies over time and is influenced by the waves and tides. Similarly, for the period from 2010 to 2016 (Figure 5-21a), the shoreline remained almost in the same position, with the exception of some areas that showed retreat. For the period from 2016 to 2017 (Figure 5-21b), the coastline had a significant setback. Taking into account the past periods, this beach did not present problems of retreat in the coastline, until Hurricane Maria (Category 4) event on September 20, 2017 which directly impacted the complete island of Puerto Rico. On September 21, 2017 CARICOOS buoy measured waves with a maximum significant wave height of 6.40 meters, 12 seconds peak period and peak wave direction of 290°. This event completely altered the trend of the coastline at Jobos Beach at Isabela. For the period from 2017 to 2018 (Figure 5-22a), the coastline recovered in large part compared to its initial position before Hurricane Maria. The comparison of the period from 1930 to 2018 (Figure 5-22b), showed mild erosion in some transects.
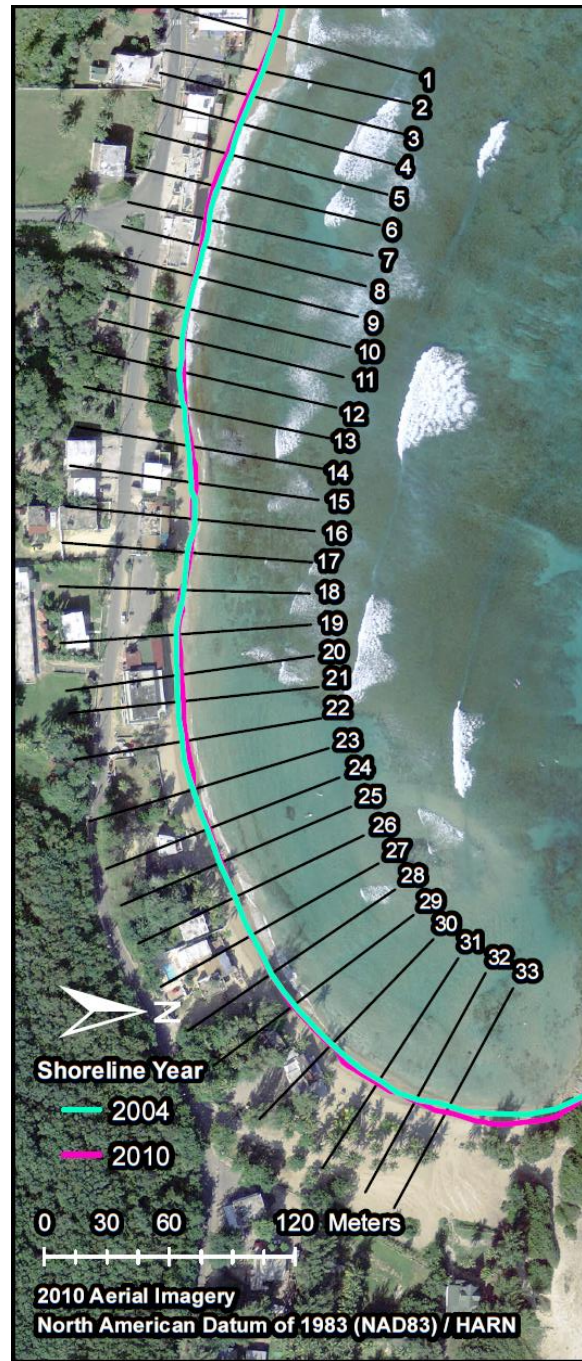
Figure 5-20. Shoreline changes at Jobos Beach, Isabela for periods **(a)** 1930-2004 and **(b)** 2004-10

42
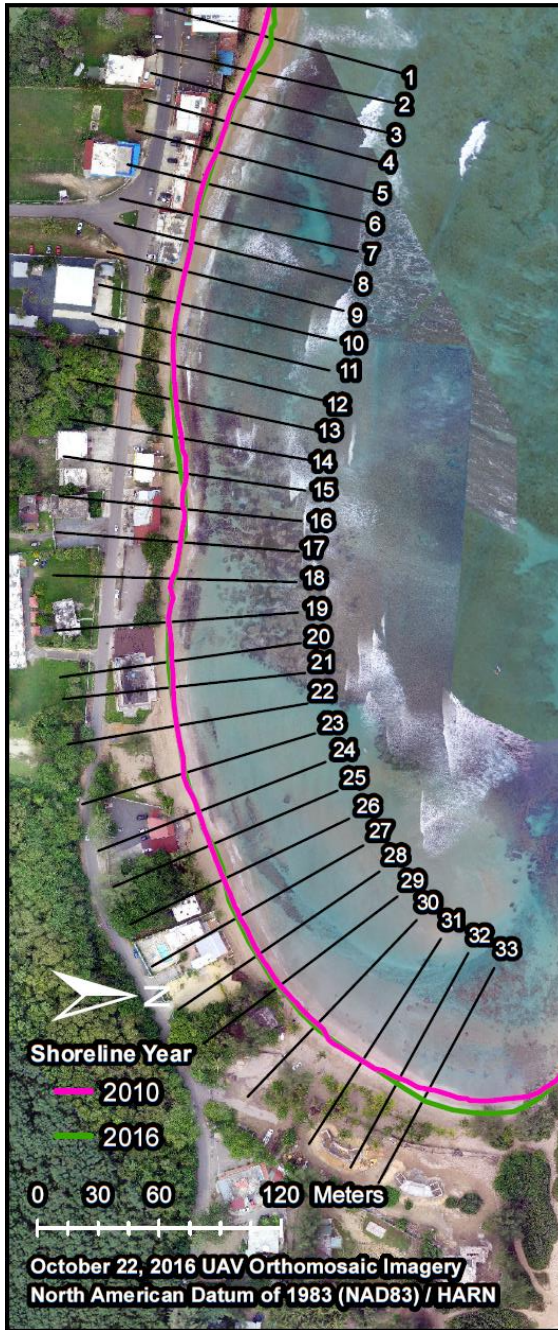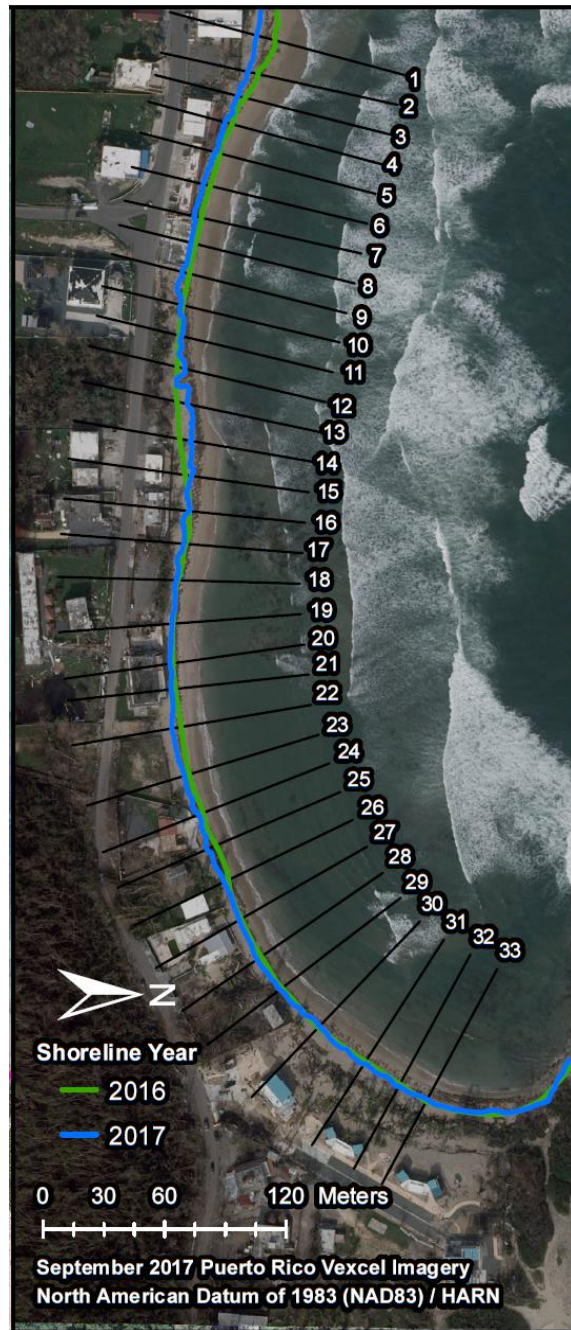
Figure 5-21. Shoreline changes at Jobos Beach, Isabela for periods **(a)** 2010-16 and **(b)** 2016-17
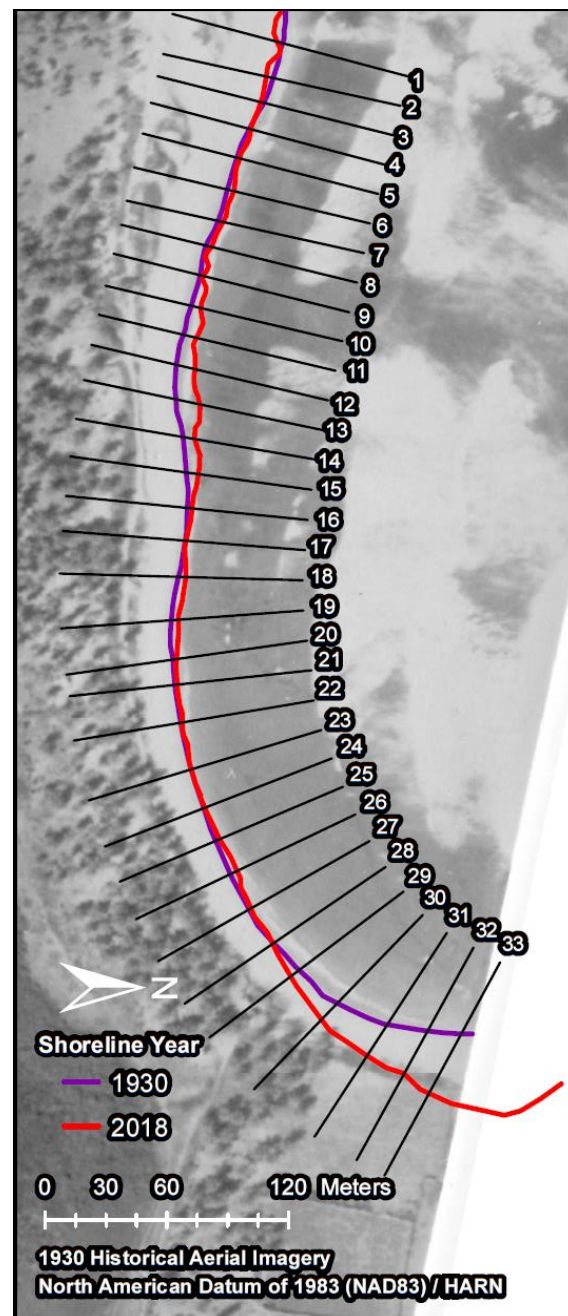
Figure 5-22. Shoreline changes at Jobos Beach, Isabela for period **(a)** 2017-18 and **(b)** net shoreline change from 1930 to 2018

44

5.1.2 Crash Boat Beach, Aguadilla

The analysis of the historical shoreline positioning maps for Crash Boat Beach at Aguadilla, for the period from 1930 to 2004 (Figure 5-23a), presented a recovery in the coastline. This behavior was due to the construction of a pier / dock for the Ramey Air Force Base. For the period from 2004 to 2010 (Figure 5-23b), the coastline also presented a recovery similarly for the period from 2010 to 2016 (Figure 5-24a). A possible caused for the accretion could be to the sediment transport by means of the swell. For the period from 2016 to 2017 (Figure 5-24b), the coastline had a significant retrieve. Based on the digitized coastline, the beach was completely lost as a result of Hurricane Maria. Similar to Jobos Beach, this beach did not showed retrieve events along the coastline until the impact of Hurricane Maria. For the period from 2017 to 2018 (Figure 5-25a), the coastline presented a recovery due to the onshore sediment transport induced by the waves. Considering the period of 1930 and 2018 (Figure 5-25b), the beach has had a change in its entirety.
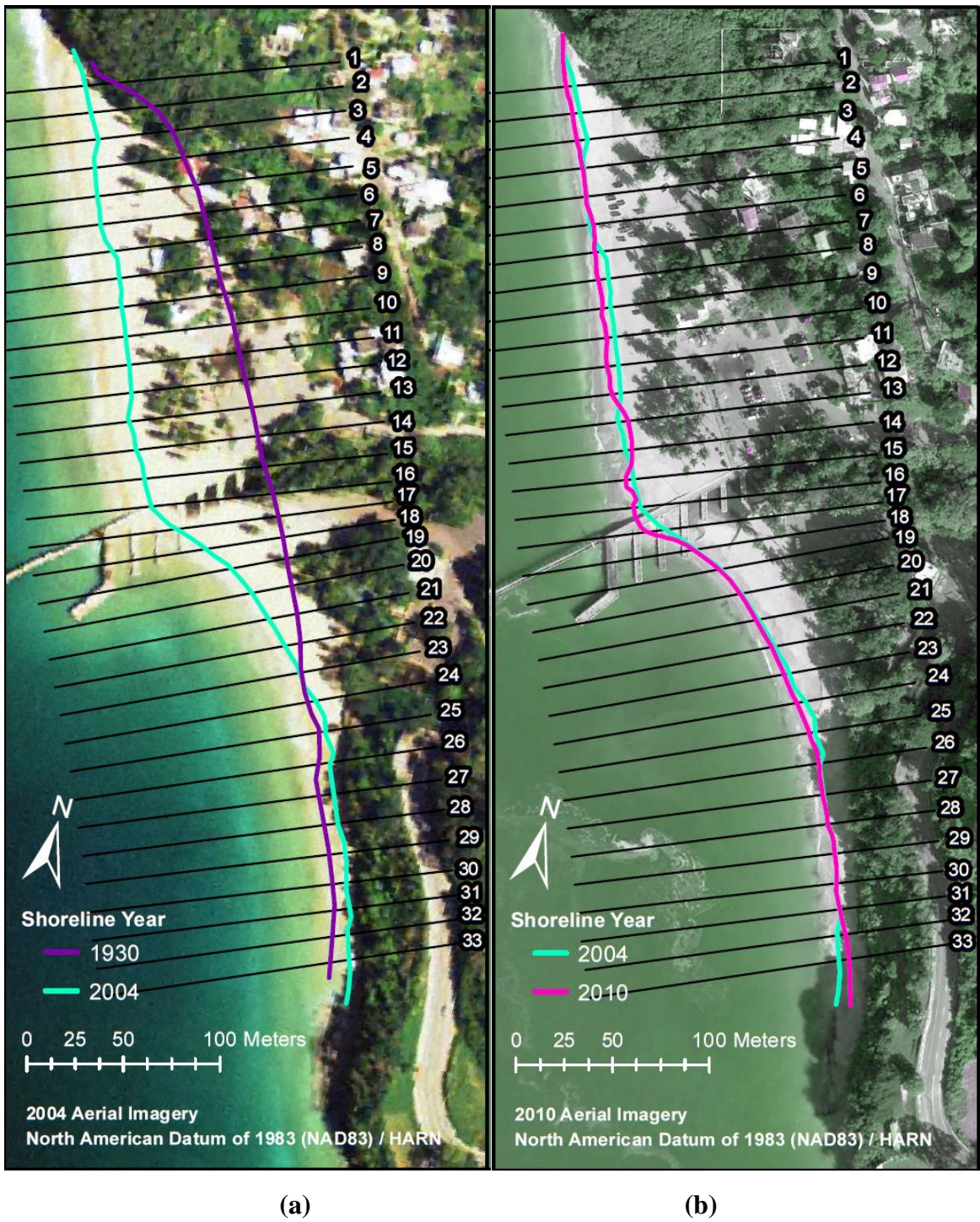
Figure 5-23. Shoreline changes at Crash Boat Beach, Aguadilla for periods **(a)** 1930-2004 and **(b)** 2004-10
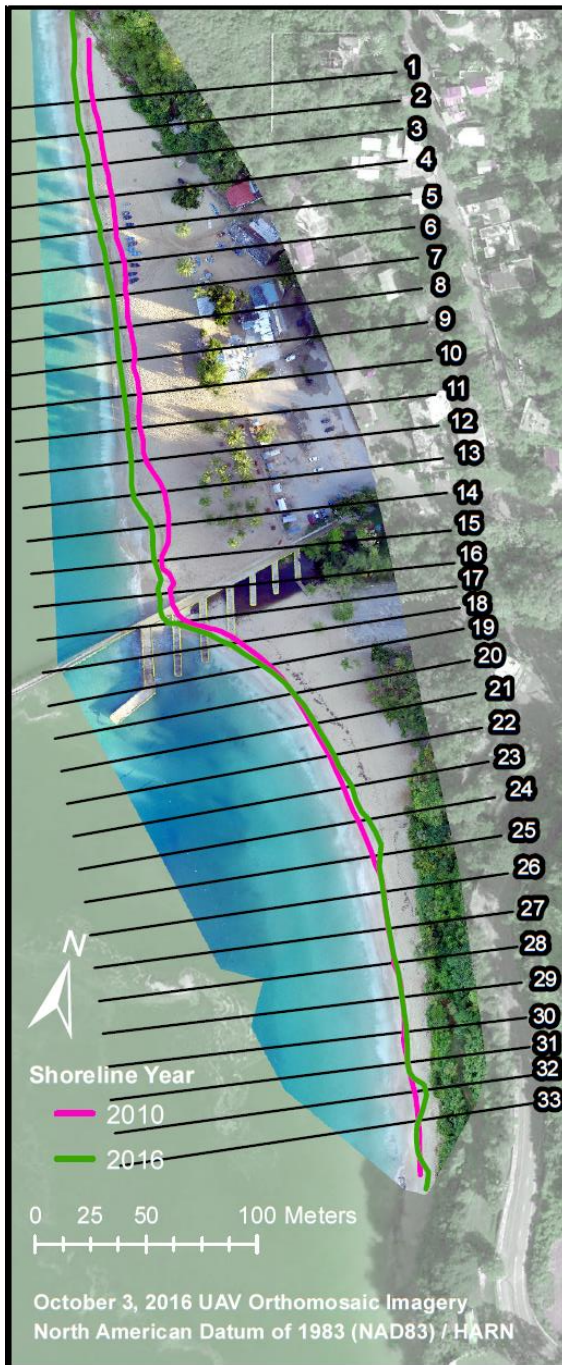
Figure 5-24. Shoreline changes at Crash Boat Beach, Aguadilla for periods **(a)** 2010-16 and **(b)** 2016-17
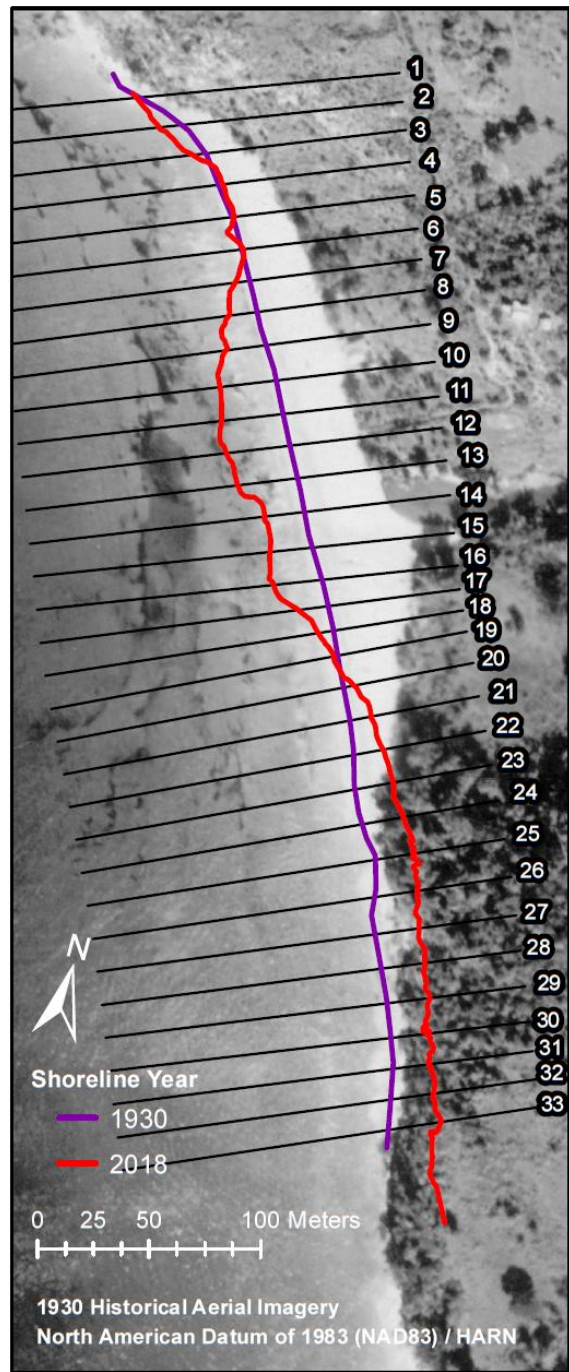
Figure 5-25. Shoreline changes at Crash Boat Beach, Aguadilla for period **(a)** 2017-18 and **(b)** net shoreline change from 1930 to 2018

5.1.3 Cofresí Beach, Rincón

The analysis of the historical shoreline positioning maps for Cofresí Beach at Rincón, for the period from 1930 to 2004 (Figure 5-26a), presented a significant retrieve. A possible cause may have been the development of homes and tourist places along the coast. Meanwhile, from 2004 to 2010 the coastline presented a recovery (Figure 5-26b). Possible causes could have been the sand nourishment for beach restoration or other methods that compensate for the regression. During the period 2010 to 2016 (Figure 5-27a), the coastline had a significant setback; this was caused by Hurricane Matthew (Category 4) event on October 4, 2016 during its near passage to the west coast of Puerto Rico. Although Hurricane Matthew was not a direct threat to Puerto Rico since he was 500 nautical miles away, the direction of the swell was extremely rare to rhis stretch of coast which severely impacted western coast of Puerto Rico. On October 4, 2016 CARICOOS Rincón buoy measured waves with a maximum significant wave height of 1.67 meters, 11 seconds peak period and peak wave direction of 279°, which highly affected the shoreline position. Likewise, during the period 2016 to 2017 (Figure 5-27b), the coastline presented a retrieve, causing the total loss of the beach. This behavior was caused by the passage of the Hurricane Maria through Puerto Rico. From 2017 to 2018 (Figure 5-28a), the coastline remained almost in the same place, continuing with the loss of the beach. Comparing the period of 1936 with 2018 (Figure 5-28b), the beach has gone backwards, showing severe erosion events.

(a)

(b)

50
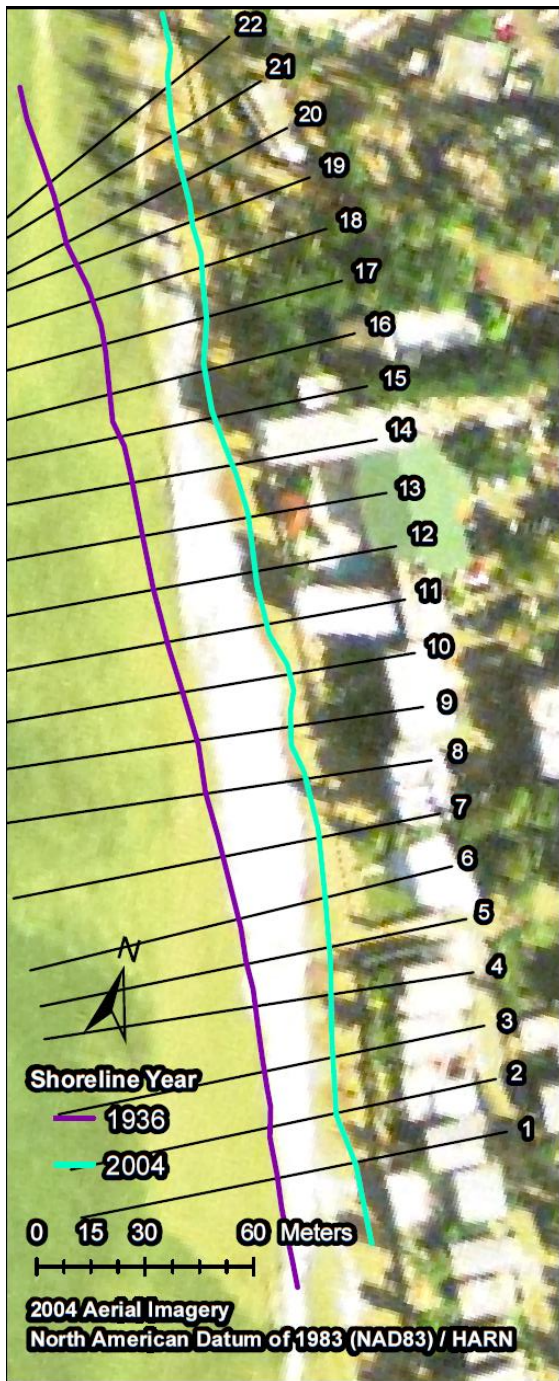
Figure 5-26. Shoreline changes at Cofresí Beach, Rincón for periods **(a)** 1936-2004 and **(b)** 2004-10

(a)   (b)
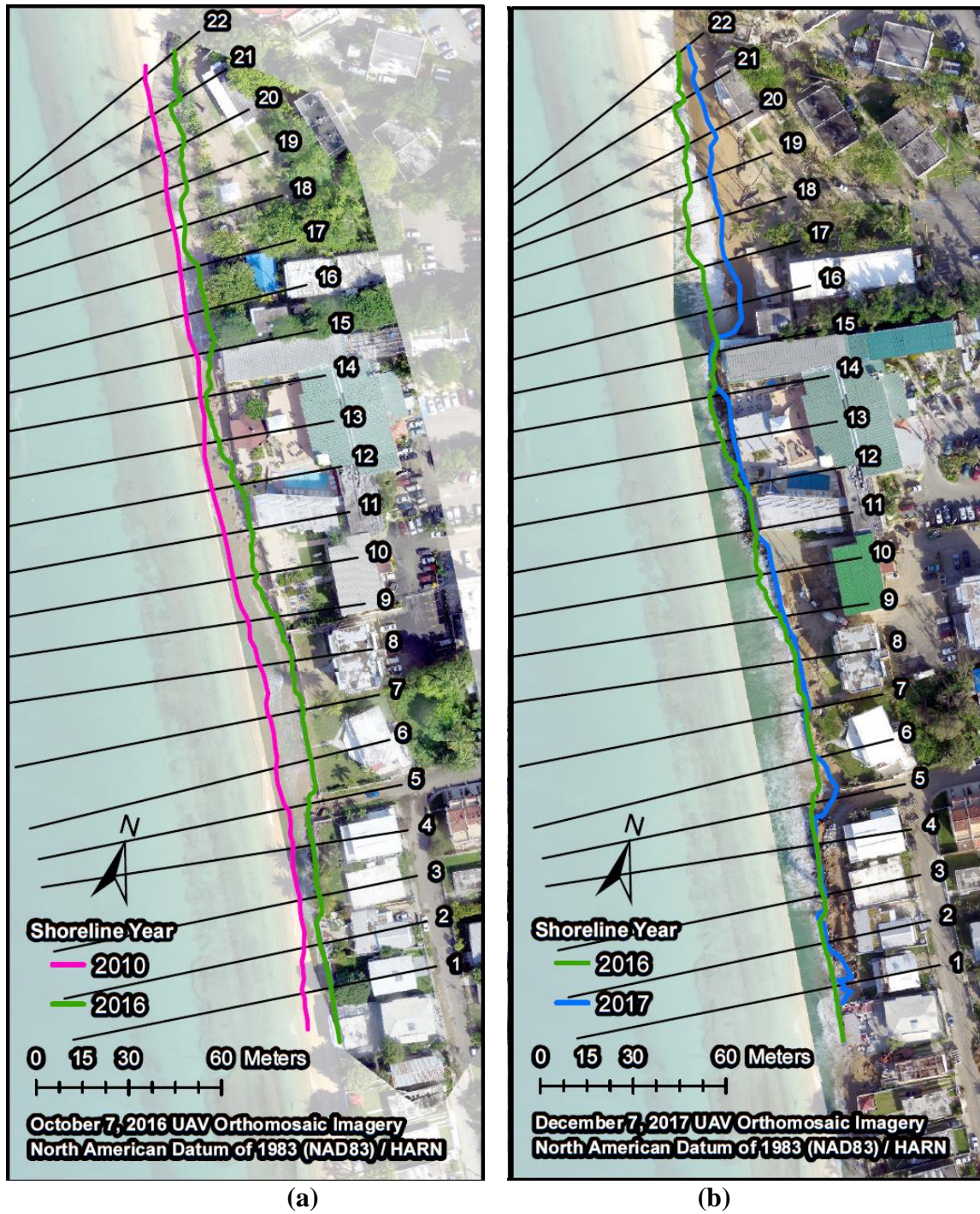
Figure 5-27. Shoreline changes at Cofresí Beach, Rincón for periods **(a)** 2010-16 and **(b)** 2016-17
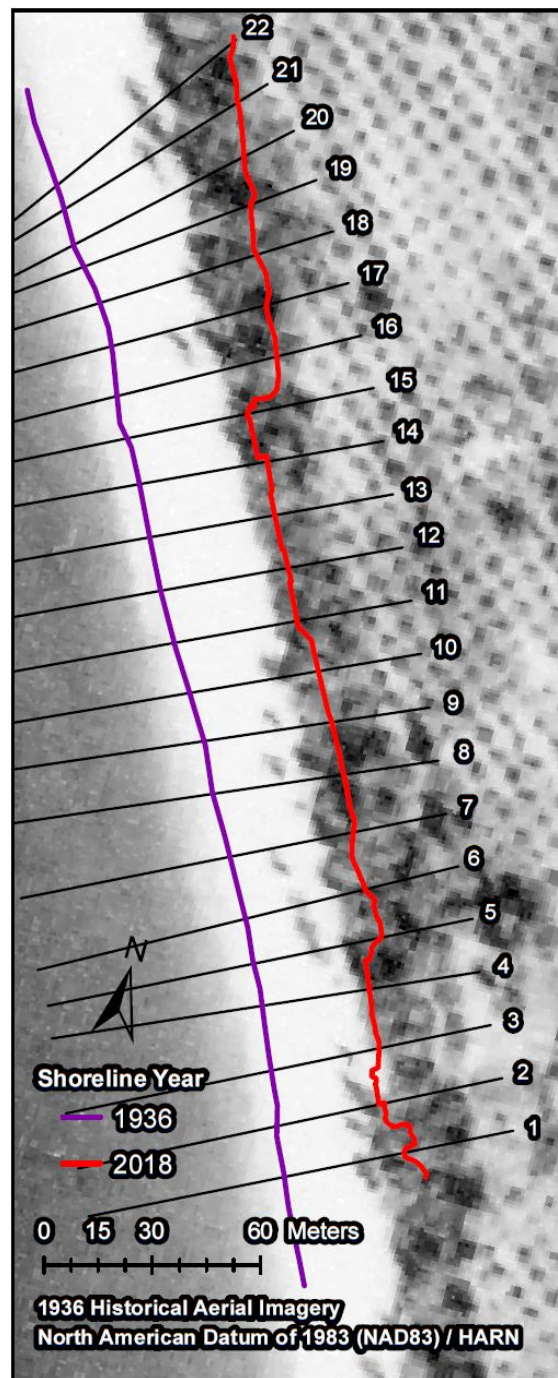
Figure 5-28. Shoreline changes at Cofresí Beach, Rincón for period **(a)** 2017-18 and **(b)** net shoreline change from 1936 to 2018

52

5.2 Digital Shoreline Analysis System (DSAS)

As previously mentioned, DSAS was used to determine the rate of change statistics at each site for periods 1930-2004, 2004-10, 2010-16, 2016-17, 2017-18, and 1930-2018. For the following analysis, the EPR method was applied. The next sections provide a quantitative analysis of the DSAS results, in addition to the scheme of the transects created by DSAS, the values of the distance from baseline needed to compute the EPR, the EPR results, and the average EPR values for the three areas selected.

5.2.1 Jobos Beach, Isabela

The rate of change for Jobos Beach at Isabela was obtained from the statistical calculations provided by DSAS, using the 33 transects (Figure 5-29). The distance from the baseline values needed for the EPR calculations are indicated in Table 5-9. The EPR results determined by DSAS for each transect and for the periods 1930-2018, 1930-2004, 2004-10, 2010-16, 2016-17, and 2017-18, are indicated in Table 5-10. Additionally, the EPR results and the average EPR for each period are shown in Figures 5-30 and 5-31. Based on the average EPR results, Jobos Beach showed a net erosion rate of -0.01 m/yr for the period 1930 to 2018 (Figure 5-30a). Analyzing the other periods, Jobos beach eroded -0.06 m/yr from 1930 to 2004 (Figure 5-30b), -0.02 m/yr from 2004 to 2010 (Figure 5-30c), -0.04 m/yr from 2010 to 2016 (Figure 5-31a), -1.42 m/yr from 2016 to 2017 (Figure 5-31b), and accreted 5.30 m/yr from 2017 to 2018 (Figure 5-31c). According to previous studies, Jobos beach accreted from 1964 to 1971, eroded from 1971 to 1977, accreted from 1977 to 1987, and eroded from 1987 to 1993 (Barreto-Orta 1997).

Comparing these results, there is a pattern of shoreline behavior that may be an indicator of future trends assuming continuity in the environment. Additionally, as previously mentioned, the higher erosion event from 2016 to 2017 was due the Hurricane María event in 2017.
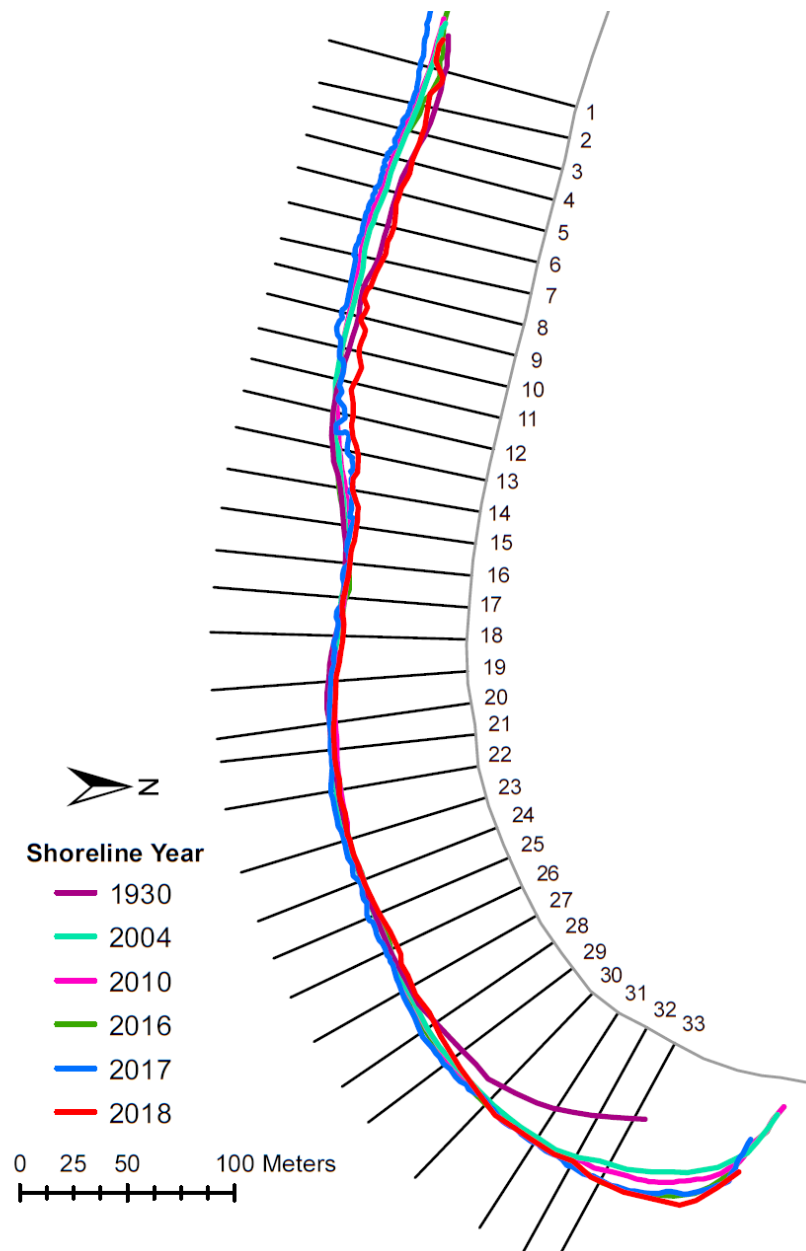
Figure 5-29. Transect numbers for the shoreline changes analysis at Jobos Beach, Isabela

Table 5-9. Distance from baseline for each shoreline year at Jobos Beach, Isabela

Transect #	1930	2004	2010	2016	2017	2018
1	-63.72	-70.53	-70.90	-66.38	-75.60	-66.34
2	-64.18	-72.34	-73.76	-70.67	-75.72	-67.78
3	-66.17	-74.45	-76.15	-74.27	-78.13	-67.62
4	-69.47	-76.37	-77.86	-77.14	-80.78	-68.79
5	-71.93	-77.30	-79.08	-79.36	-81.89	-70.56
6	-72.37	-79.27	-81.44	-79.95	-83.52	-69.32
7	-73.49	-79.95	-81.66	-80.94	-84.73	-71.24
8	-76.80	-79.59	-80.83	-80.92	-83.32	-74.12
9	-75.76	-79.69	-80.29	-80.18	-83.89	-74.38
10	-76.63	-79.98	-79.83	-79.89	-80.87	-71.76
11	-77.12	-79.41	-78.66	-78.19	-76.88	-70.65
12	-76.94	-76.95	-75.08	-75.41	-71.57	-67.39
13	-73.60	-70.99	-70.26	-71.92	-66.54	-61.53
14	-66.53	-65.71	-64.05	-67.04	-61.78	-60.79
15	-62.23	-61.65	-59.13	-61.80	-58.46	-56.29
16	-59.58	-57.80	-58.42	-57.68	-57.56	-57.28
17	-59.28	-59.78	-58.55	-58.01	-58.93	-58.98
18	-61.32	-60.45	-61.22	-60.51	-61.17	-57.78
19	-65.27	-64.37	-63.65	-63.54	-64.00	-61.81
20	-66.98	-66.27	-64.21	-65.80	-67.04	-64.95
21	-67.72	-67.57	-65.24	-66.41	-68.41	-66.47
22	-66.44	-67.42	-65.42	-65.31	-69.84	-65.77
23	-67.10	-68.15	-67.75	-67.05	-69.44	-66.99
24	-67.73	-67.97	-67.06	-67.04	-69.11	-67.08
25	-68.33	-68.49	-67.79	-66.90	-71.72	-66.21
26	-68.45	-68.53	-68.53	-68.17	-70.57	-64.80
27	-68.37	-69.96	-70.26	-71.52	-72.70	-67.16
28	-66.87	-71.86	-71.87	-72.84	-75.31	-67.43
29	-64.51	-71.51	-72.53	-73.63	-74.87	-69.67
30	-60.78	-70.12	-70.59	-72.28	-71.41	-71.99
31	-53.82	-69.79	-71.28	-71.26	-72.65	-72.22
32	-47.11	-69.02	-70.01	-72.82	-74.01	-71.42
33	-40.21	-64.28	-67.72	-73.61	-72.85	-73.65

Table 5-10. End Point Rate results for each period at Jobos Beach, Isabela

Transect #	1930-2018	1930-2004	2004-10	2010-16	2016-17	2017-18
1	-0.03	-0.09	-0.06	0.75	-9.22	9.27
2	-0.04	-0.11	-0.24	0.52	-5.05	7.95
3	-0.02	-0.11	-0.28	0.31	-3.86	10.50
4	0.01	-0.09	-0.25	0.12	-3.64	11.98
5	0.02	-0.07	-0.30	-0.05	-2.53	11.33
6	0.03	-0.09	-0.36	0.25	-3.57	14.20
7	0.03	-0.09	-0.29	0.12	-3.79	13.49
8	0.03	-0.04	-0.21	-0.02	-2.41	9.20
9	0.02	-0.05	-0.10	0.02	-3.71	9.51
10	0.06	-0.05	0.03	-0.01	-0.98	9.10
11	0.07	-0.03	0.12	0.08	1.32	6.23
12	0.11	0.00	0.31	-0.06	3.85	4.18
13	0.14	0.04	0.12	-0.28	5.39	5.01
14	0.07	0.01	0.28	-0.50	5.26	0.99
15	0.07	0.01	0.42	-0.44	3.34	2.18
16	0.03	0.02	-0.10	0.12	0.12	0.28
17	0.00	-0.01	0.21	0.09	-0.92	-0.05
18	0.04	0.01	-0.13	0.12	-0.66	3.39
19	0.04	0.01	0.12	0.02	-0.46	2.19
20	0.02	0.01	0.34	-0.27	-1.24	2.09
21	0.01	0.00	0.39	-0.20	-1.99	1.94
22	0.01	-0.01	0.33	0.02	-4.52	4.07
23	0.00	-0.01	0.07	0.12	-2.39	2.45
24	0.01	0.00	0.15	0.00	-2.07	2.03
25	0.02	0.00	0.12	0.15	-4.82	5.51
26	0.04	0.00	0.00	0.06	-2.40	5.77
27	0.01	-0.02	-0.05	-0.21	-1.18	5.55
28	-0.01	-0.07	0.00	-0.16	-2.47	7.89
29	-0.06	-0.09	-0.17	-0.18	-1.24	5.19
30	-0.13	-0.13	-0.08	-0.28	0.87	-0.58
31	-0.21	-0.22	-0.25	0.00	-1.39	0.42
32	-0.28	-0.30	-0.16	-0.47	-1.19	2.59
33	-0.38	-0.33	-0.57	-0.98	0.76	-0.79
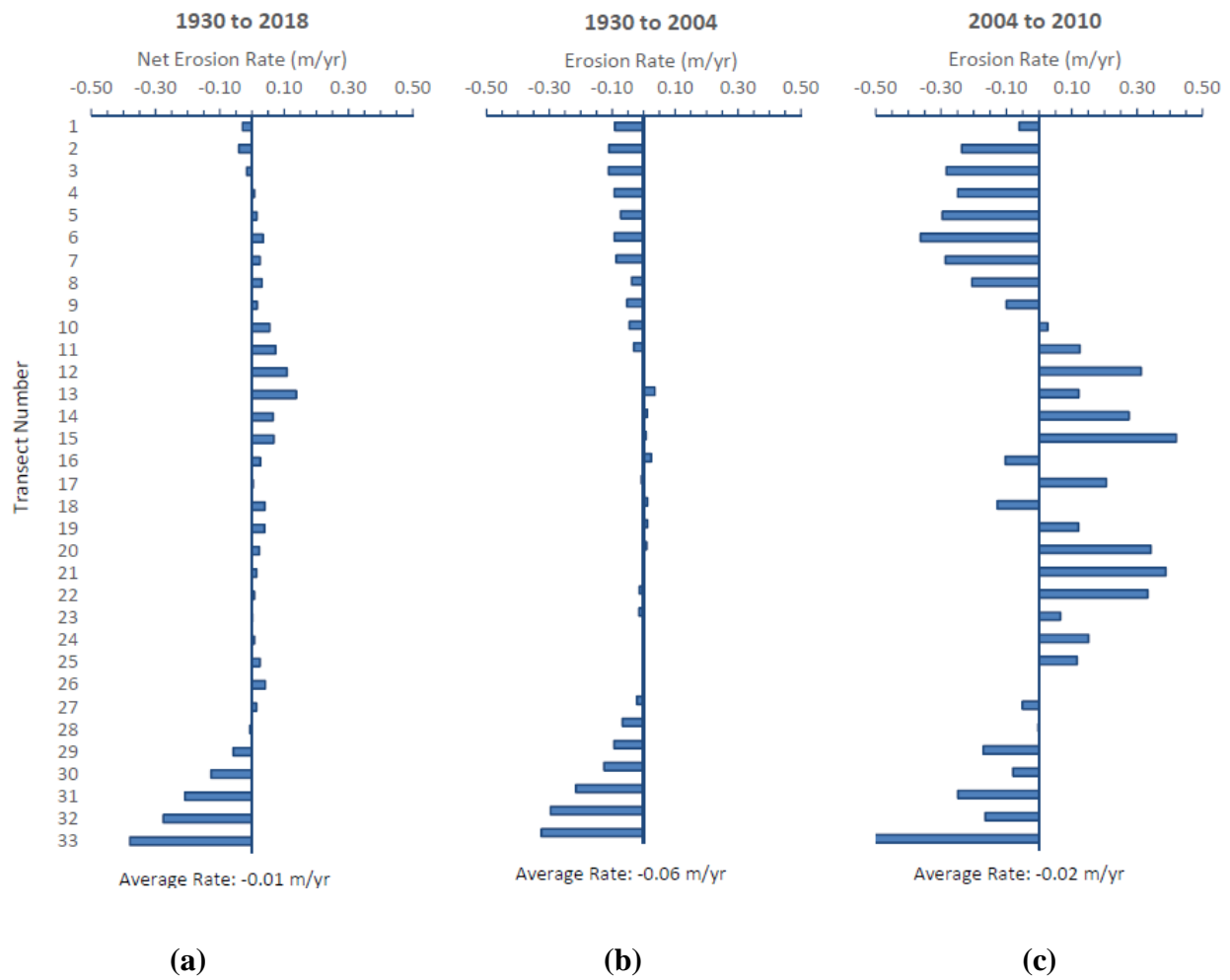
Figure 5-30. Average EPR results for periods **(a)** 1930-2018, **(b)** 1930-2004, and **(c)** 2004-10 at Jobos Beach, Isabela

57
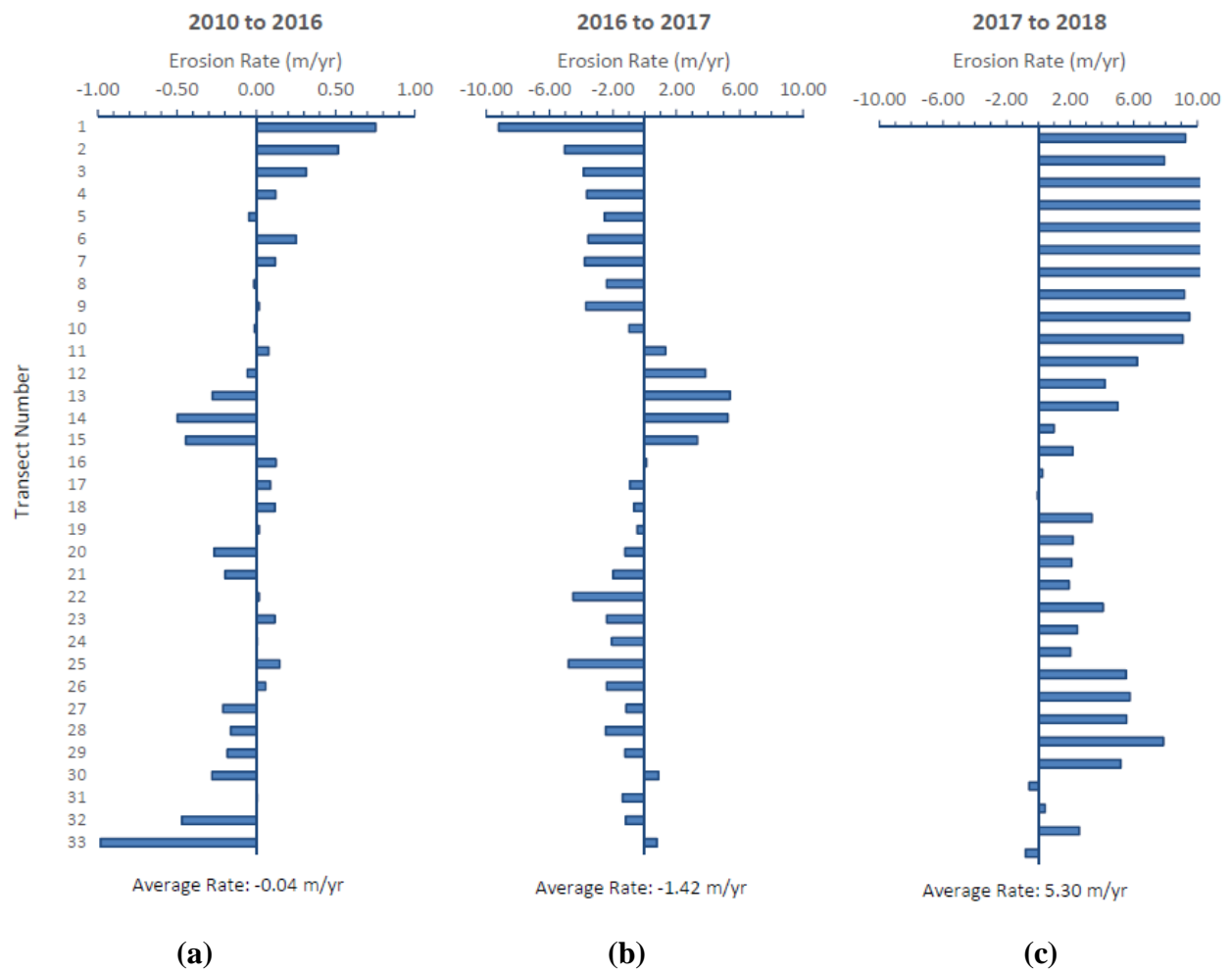
Figure 5-31. Average EPR results for periods **(a)** 2010-16, **(b)** 2016-17, and **(c)** 2017-18 at Jobos Beach, Isabela

5.2.2 Crash Boat Beach, Aguadilla

Figure 5-32 shows the rate of change for Crash Boat Beach at Aguadilla obtained from the statistical calculations provided by DSAS, using the 33 transects. The distance from baseline values needed for the EPR calculations are indicated in Table 5-11. The EPR results determined by DSAS for each transect and for the periods 1930-2018, 1930-2004, 2004-10, 2010-16, 2016-17, and 2017-18, are indicated in Table 5-12. Additionally, the EPR results and the average EPR for each period are shown in Figures 5-33 and 5-34. Based on the average EPR results, Crash Boat Beach showed a net erosion rate of 0.00 m/yr for the period 1930 to 2018 (Figure 5-33a). Analyzing the other periods, Crash Boat accreted 0.38 m/yr from 1930 to 2004 (Figure 5-33b), 0.28 m/yr from 2004 to 2010 (Figure 5-33c), 0.54 m/yr from 2010 to 2016 (Figure 5-34a), eroded -38.11 m/yr from 2016 to 2017 (Figure 5-34b), and accreted 5.51 m/yr from 2017 to 2018 (Figure 5-34c). As previously mentioned, the accretion for the period 1930 to 2004 was induced by the construction of a pier/dock for the Ramey Air Force Base. Although the erosion rate for the period 2016 to 2017 is significant, it does not affect the net result due to the small year period, compared to the 1930 to 2004 period (1 vs. 74 yrs). This erosion event was due the impact of Hurricane María. The accretion for the period 2017 to 2018 was due to the onshore sediment transport.
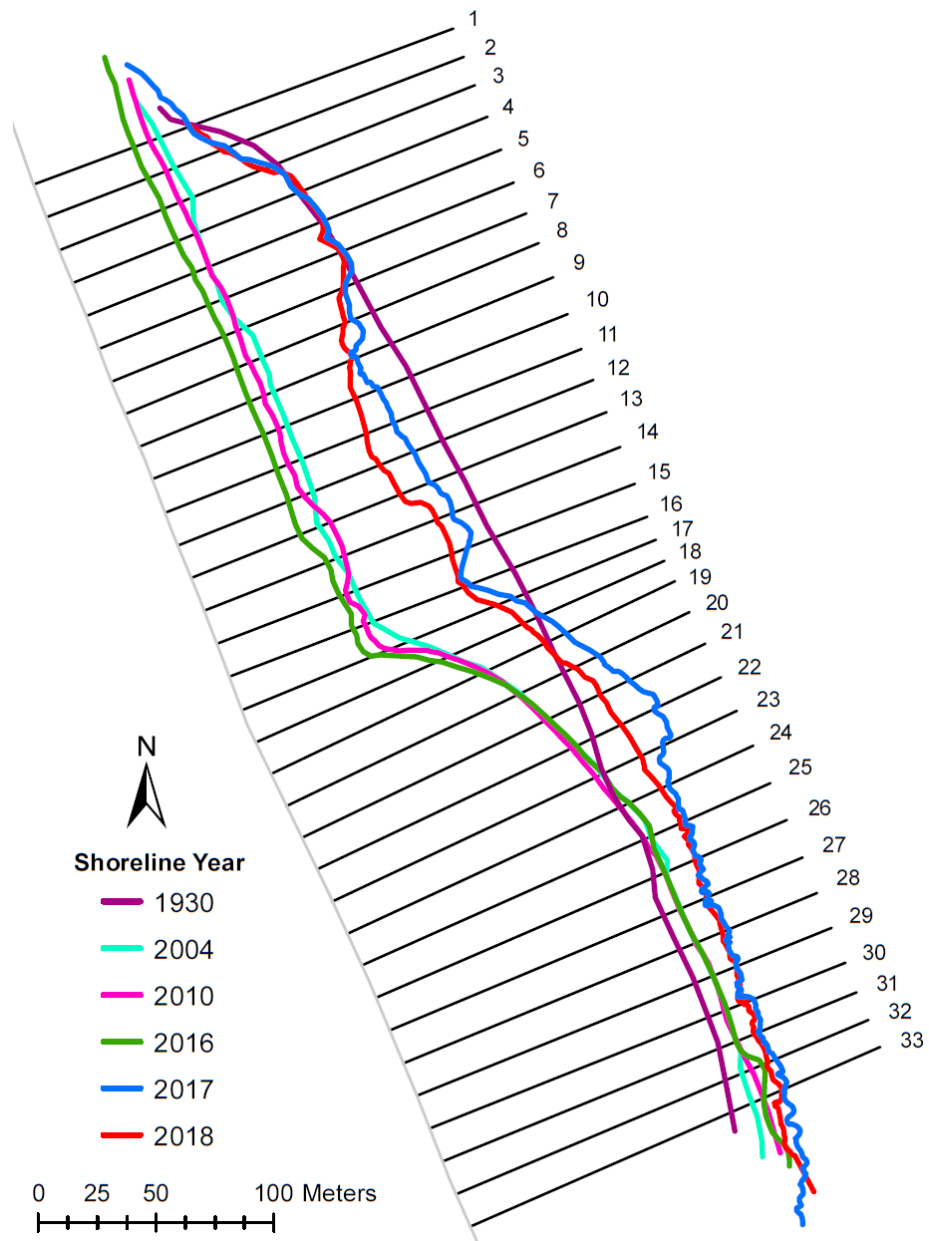
Figure 5-32. Transect numbers for the shoreline changes analysis at Crash Boat Beach, Aguadilla

Table 5-11. Distance from baseline for each shoreline year at Crash Boat Beach, Aguadilla

Transect #	1930	2004	2010	2016	2017	2018
1	-72.57	-56.94	-52.63	-45.43	-70.56	-71.24
2	-89.96	-58.41	-54.58	-46.18	-82.37	-79.91
3	-99.47	-60.76	-55.28	-47.63	-97.47	-93.46
4	-103.47	-57.08	-56.42	-47.70	-103.13	-105.28
5	-107.60	-56.27	-56.28	-49.13	-109.11	-108.44
6	-110.37	-56.32	-58.24	-50.32	-111.92	-110.86
7	-112.38	-61.02	-57.58	-51.47	-107.27	-105.90
8	-113.70	-62.64	-57.30	-51.24	-104.70	-100.76
9	-115.66	-61.68	-57.23	-50.46	-99.76	-97.43
10	-118.25	-61.87	-57.65	-50.93	-103.41	-92.87
11	-119.74	-62.10	-56.33	-50.92	-104.25	-91.80
12	-121.03	-61.64	-57.37	-50.60	-107.66	-92.33
13	-122.68	-58.65	-63.62	-49.80	-109.19	-95.69
14	-124.08	-60.47	-64.04	-56.07	-113.24	-105.96
15	-125.95	-63.06	-59.06	-55.96	-113.98	-106.70
16	-128.68	-65.20	-61.58	-56.34	-109.19	-106.75
17	-130.35	-77.13	-67.50	-60.13	-124.60	-116.80
18	-131.08	-90.67	-89.66	-84.72	-132.75	-124.33
19	-130.75	-101.60	-100.84	-98.23	-138.82	-128.93
20	-130.71	-109.93	-109.04	-109.38	-147.09	-135.59
21	-130.88	-115.94	-114.75	-116.40	-154.26	-140.37
22	-129.62	-121.62	-119.86	-121.95	-158.65	-142.94
23	-127.38	-126.49	-123.72	-127.41	-155.43	-144.90
24	-127.99	-131.84	-127.66	-131.85	-150.39	-146.67
25	-130.97	-134.38	-131.23	-134.70	-150.39	-148.38
26	-128.19	-134.39	-133.58	-133.56	-149.82	-147.46
27	-126.08	-133.86	-133.49	-133.74	-146.22	-145.98
28	-126.75	-134.02	-134.03	-134.62	-149.38	-146.50
29	-127.38	-135.76	-135.63	-135.59	-146.46	-146.63
30	-127.21	-134.56	-134.64	-135.80	-148.00	-143.83
31	-126.62	-134.78	-134.92	-134.62	-144.87	-142.73
32	-123.97	-131.74	-136.08	-140.98	-147.13	-143.49
33	-120.83	-130.52	-135.74	-136.01	-145.91	-144.57

Table 5-12. End Point Rate results for each period at Crash Boat Beach, Aguadilla

Transect #	1930-2018	1930-2004	2004-10	2010-16	2016-17	2017-18
1	0.02	0.21	0.72	1.20	-25.14	-0.68
2	0.11	0.43	0.64	1.40	-36.19	2.46
3	0.07	0.52	0.91	1.27	-49.84	4.01
4	-0.02	0.63	0.11	1.45	-55.43	-2.15
5	-0.01	0.69	0.00	1.19	-59.98	0.68
6	-0.01	0.73	-0.32	1.32	-61.60	1.06
7	0.07	0.69	0.57	1.02	-55.80	1.37
8	0.15	0.69	0.89	1.01	-53.46	3.93
9	0.21	0.73	0.74	1.13	-49.30	2.33
10	0.29	0.76	0.70	1.12	-52.48	10.54
11	0.32	0.78	0.96	0.90	-53.33	12.45
12	0.33	0.80	0.71	1.13	-57.06	15.34
13	0.31	0.87	-0.83	2.30	-59.39	13.50
14	0.21	0.86	-0.60	1.33	-57.17	7.28
15	0.22	0.85	0.67	0.52	-58.02	7.28
16	0.25	0.86	0.60	0.87	-52.85	2.44
17	0.15	0.72	1.60	1.23	-64.48	7.81
18	0.08	0.55	0.17	0.82	-48.03	8.42
19	0.02	0.39	0.13	0.43	-40.58	9.89
20	-0.06	0.28	0.15	-0.06	-37.71	11.50
21	-0.11	0.20	0.20	-0.27	-37.87	13.89
22	-0.15	0.11	0.29	-0.35	-36.71	15.72
23	-0.20	0.01	0.46	-0.62	-28.02	10.53
24	-0.21	-0.05	0.70	-0.70	-18.54	3.72
25	-0.20	-0.05	0.52	-0.58	-15.69	2.01
26	-0.22	-0.08	0.14	0.00	-16.26	2.35
27	-0.23	-0.11	0.06	-0.04	-12.48	0.24
28	-0.22	-0.10	0.00	-0.10	-14.75	2.88
29	-0.22	-0.11	0.02	0.01	-10.87	-0.17
30	-0.19	-0.10	-0.01	-0.19	-12.20	4.17
31	-0.18	-0.11	-0.02	0.05	-10.25	2.14
32	-0.22	-0.10	-0.72	-0.82	-6.15	3.64
33	-0.27	-0.13	-0.87	-0.04	-9.90	1.34
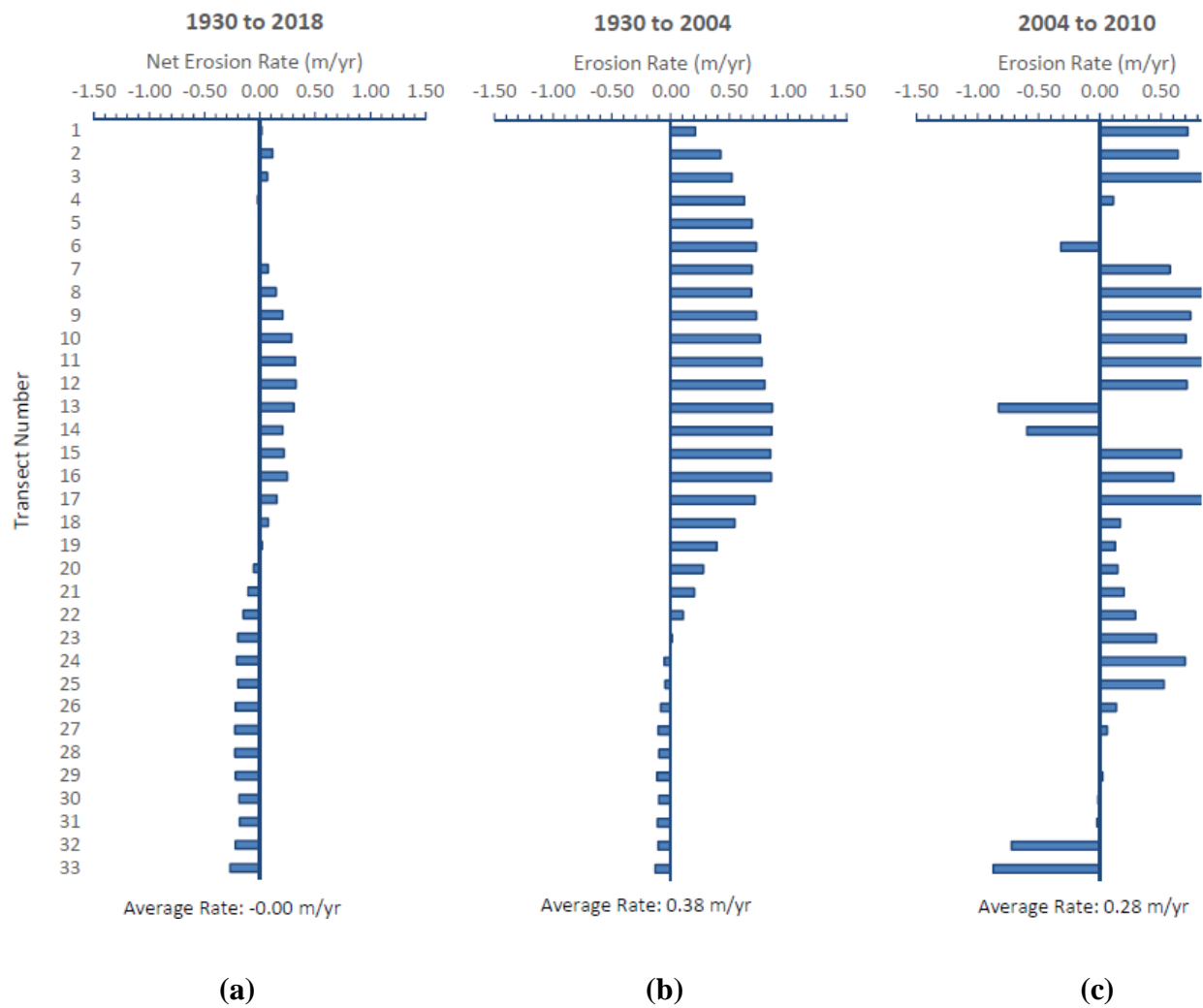
Figure 5-33. Average EPR results for periods **(a)** 1930-2018, **(b)** 1930-2004, and **(c)** 2004-10 at Crash Boat Beach, Aguadilla
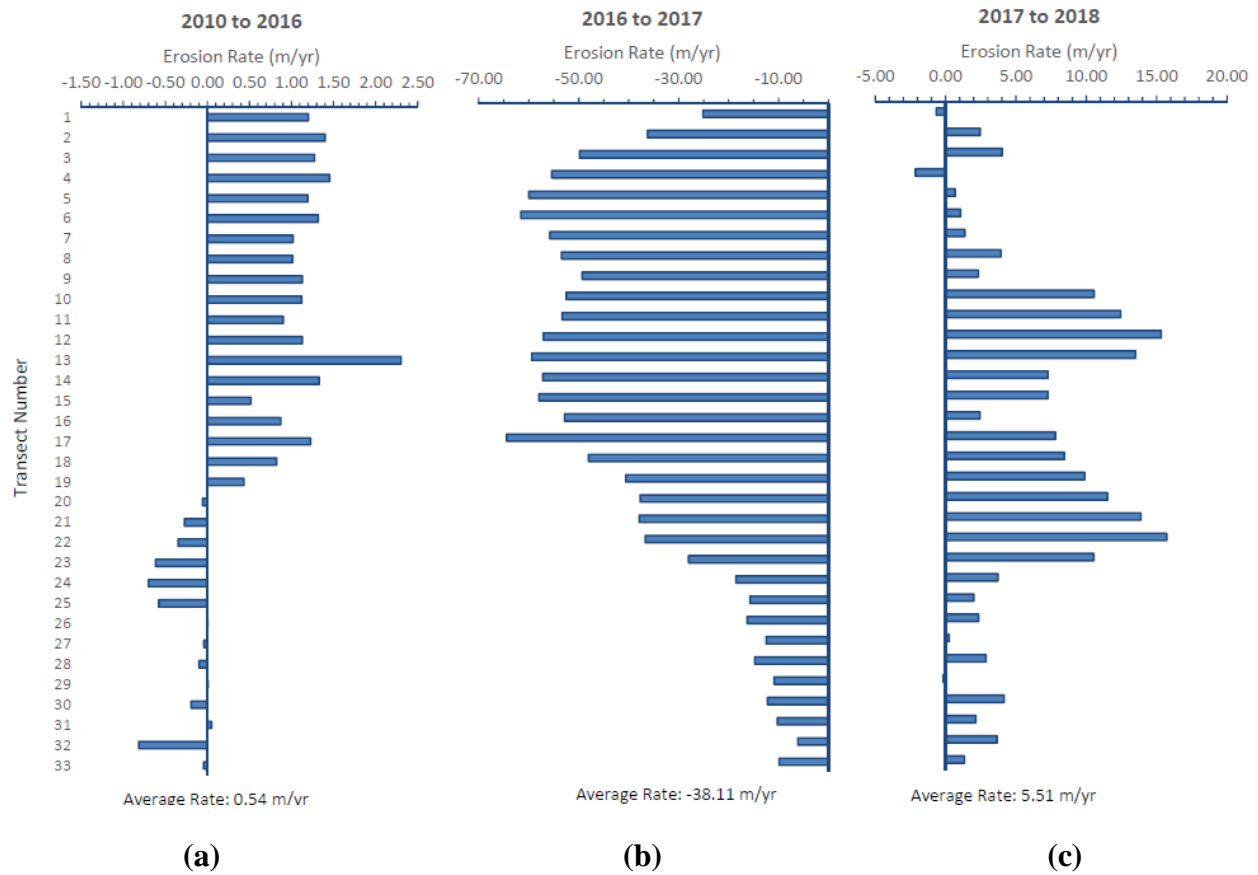
Figure 5-34. Average EPR results for periods **(a)** 2010-16, **(b)** 2016-17, and **(c)** 2017-18 at Crash Boat Beach, Aguadilla

5.2.3 Cofresí Beach, Rincón

Figure 5-35 shows the rate of change for Cofresí Beach at Rincón obtained from the statistical calculations provided by DSAS, using the 22 transects. The distance from baseline values are indicated in Table 5-13. The EPR results determined by DSAS for each transect and for the periods 1936-2018, 1936-2004, 2004-10, 2010-16, 2016-17, and 2017-18, are indicated in Table 5-14. Additionally, the EPR results and the average EPR for each period are shown in Figures 5-36 and 5-37. Based on the average EPR results, Cofresí Beach showed a net erosion rate of -0.48 m/yr for the period 1936 to 2018 (Figure 5-36a). Analyzing the other periods, Cofresí Beach eroded -0.41 m/yr from 1936 to 2004 (Figure 5-36b), accreted 0.08 m/yr from 2004 to 2010 (Figure 5-36c), and eroded -1.27 m/yr from 2010 to 2016 (Figure 5-37a), -3.82 m/yr from 2016 to 2017 (Figure 5-37b), and -0.34 m/yr from 2017 to 2018 (Figure 5-37c). The short-term period of 2016 to 2017 is nearly eight times the long-term average. This could be due storm influences, sea-level change, and other factors. According to previous studies, this area had an average long-term erosion rate of -0.4 m/yr for the period 1936 to 2006, and -0.7 m/yr for the period 1994 to 2006 (Thieler et al. 2007). Comparing these results, there is a very consistent trend over time that continues to happen, showing severe erosion events. If no action is taken and the trend continues, infrastructures along the coastline will be permanently damaged.
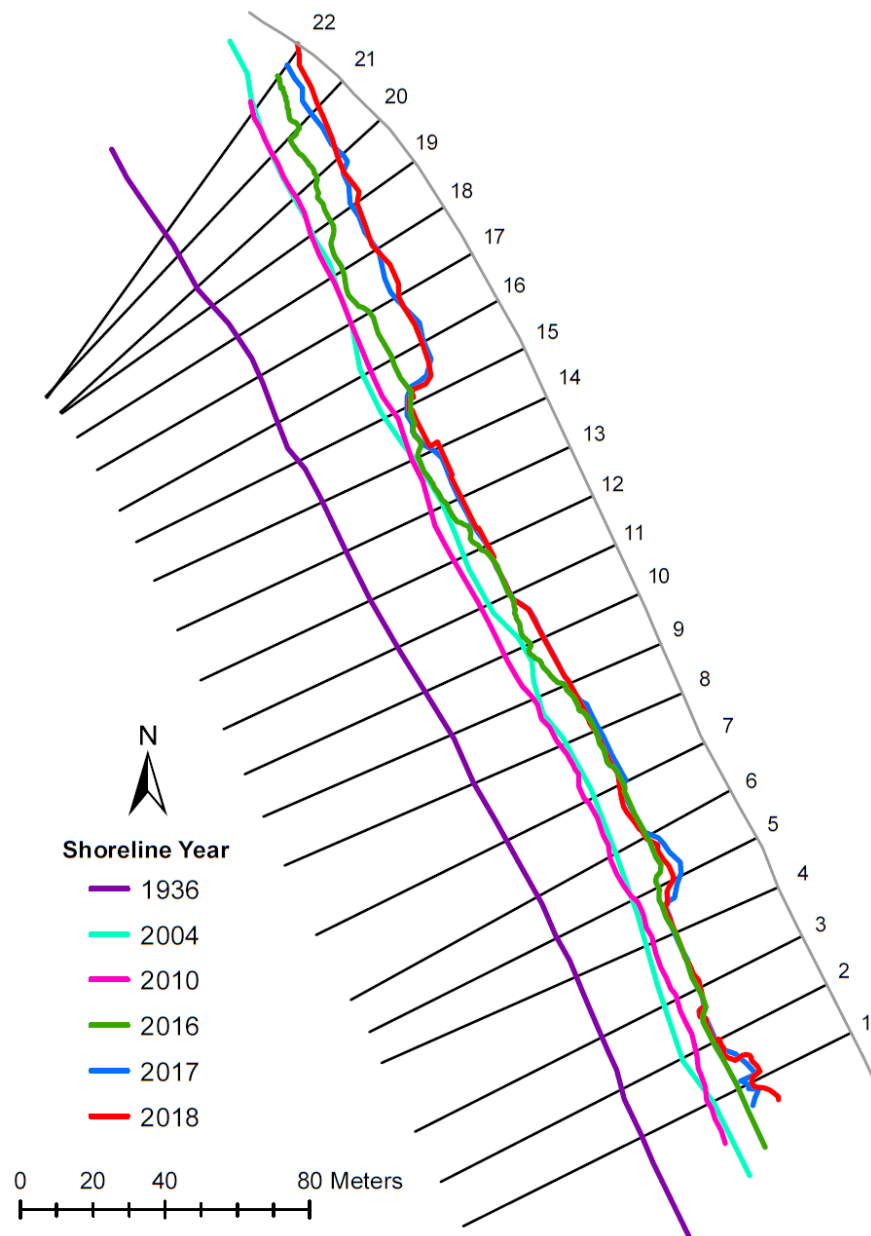
Figure 5-35. Transect numbers for the shoreline changes analysis at Cofresí Beach, Rincón

Table 5-13. Distance from baseline for each shoreline year at Cofresí Beach, Rincón

Transect #	1936	2004	2010	2016	2017	2018
1	64.59	42.87	44.08	34.86	31.98	30.71
2	63.70	44.99	40.72	35.25	34.53	34.08
3	62.04	42.64	38.79	32.18	31.64	31.55
4	60.98	39.88	37.73	31.09	31.29	31.04
5	61.90	38.58	37.91	30.52	23.83	25.83
6	60.75	36.18	37.96	26.30	25.20	26.63
7	61.01	34.03	36.33	25.21	24.60	26.32
8	62.90	35.12	36.71	26.20	25.03	26.31
9	63.15	37.03	38.41	28.97	27.64	27.52
10	65.02	35.10	40.78	33.11	28.87	29.00
11	66.73	38.86	41.18	32.54	32.13	32.32
12	67.94	39.45	42.49	34.33	32.28	32.13
13	68.34	38.61	42.36	37.59	33.92	33.21
14	68.53	40.44	41.19	39.23	34.58	32.65
15	69.75	43.08	40.04	35.12	36.16	35.53
16	69.72	42.75	40.31	33.46	23.50	24.19
17	67.86	38.70	38.69	32.78	24.56	23.42
18	67.54	36.07	36.77	33.03	21.93	22.18
19	68.64	34.69	35.14	28.49	21.27	19.39
20	68.76	32.22	31.60	23.76	14.32	15.75
21	66.08	28.15	28.10	17.47	12.42	9.64
22	64.03	21.73	22.72	10.57	6.38	1.13

Table 5-14. End Point Rate results for each period at Cofresí Beach, Rincón

| Transect #	1936-2018	1930-2004	2004-10	2010-16	2016-17	2017-18
1	-0.41	-0.32	0.20	-1.54	-2.88	-1.27
2	-0.36	-0.28	-0.71	-0.91	-0.72	-0.45
3	-0.37	-0.29	-0.64	-1.10	-0.54	-0.09
4	-0.37	-0.31	-0.36	-1.11	0.20	-0.25
5	-0.44	-0.34	-0.11	-1.23	-6.70	2.00
6	-0.42	-0.36	0.30	-1.94	-1.10	1.42
7	-0.42	-0.40	0.38	-1.85	-0.60	1.72
8	-0.45	-0.41	0.26	-1.75	-1.17	1.27
9	-0.43	-0.38	0.23	-1.57	-1.33	-0.12
10	-0.44	-0.44	0.95	-1.28	-4.24	0.14
11	-0.42	-0.41	0.39	-1.44	-0.41	0.19
12	-0.44	-0.42	0.51	-1.36	-2.05	-0.15
13	-0.43	-0.44	0.63	-0.79	-3.67	-0.71
14	-0.44	-0.41	0.12	-0.33	-4.64	-1.93
15	-0.42	-0.39	-0.51	-0.82	1.04	-0.64
16	-0.56	-0.40	-0.41	-1.14	-9.96	0.69
17	-0.54	-0.43	0.00	-0.99	-8.22	-1.14
18	-0.55	-0.46	0.12	-0.62	-11.10	0.25
19	-0.60	-0.50	0.07	-1.11	-7.21	-1.88
20	-0.65	-0.54	-0.10	-1.31	-9.44	1.43
21	-0.69	-0.56	-0.01	-1.77	-5.05	-2.78
22	-0.77	-0.62	0.16	-2.02	-4.19	-5.25
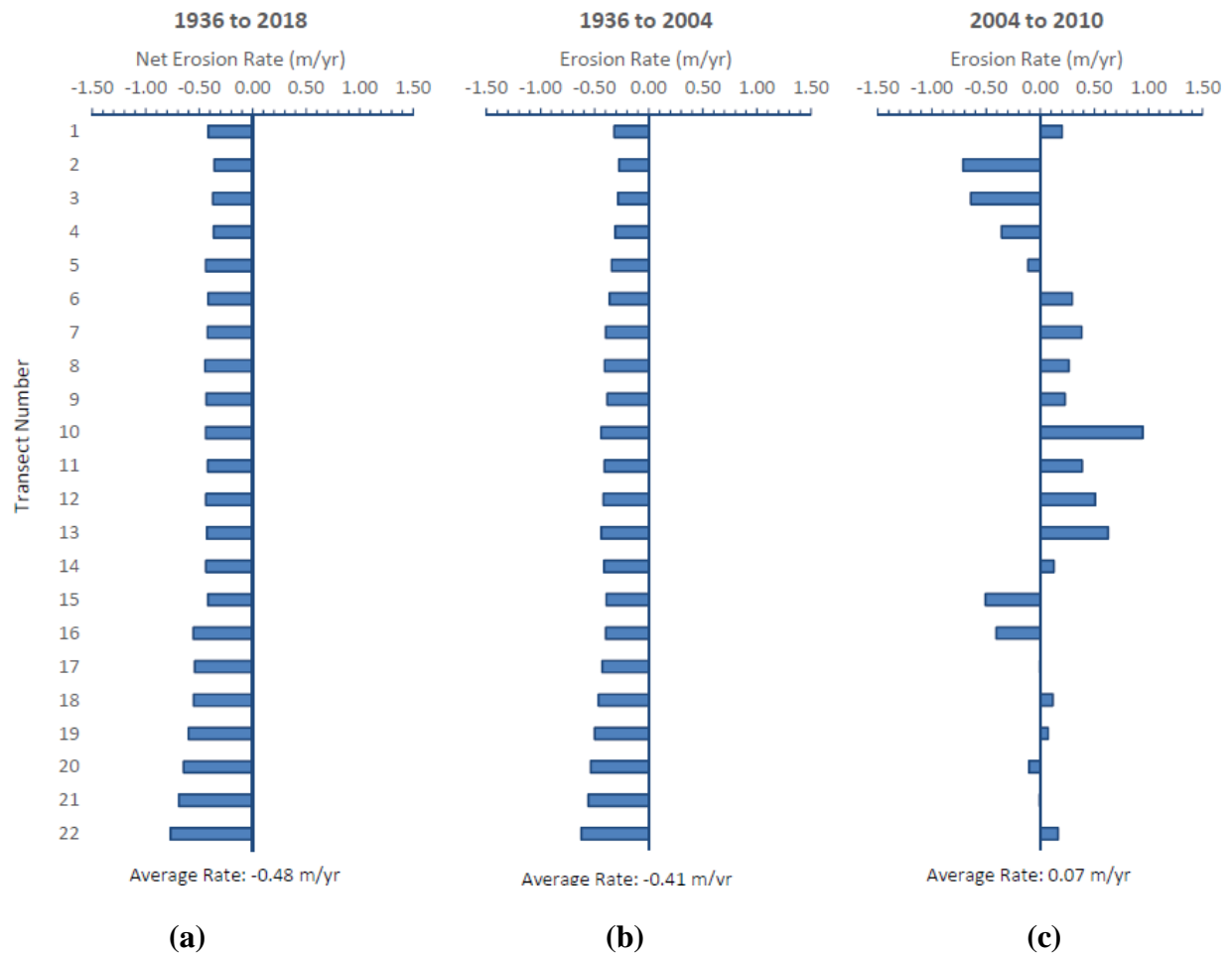
Figure 5-36. Average EPR results for periods **(a)** 1936-2018, **(b)** 1936-2004, and **(c)** 2004-10 at Cofresí Beach, Rincón
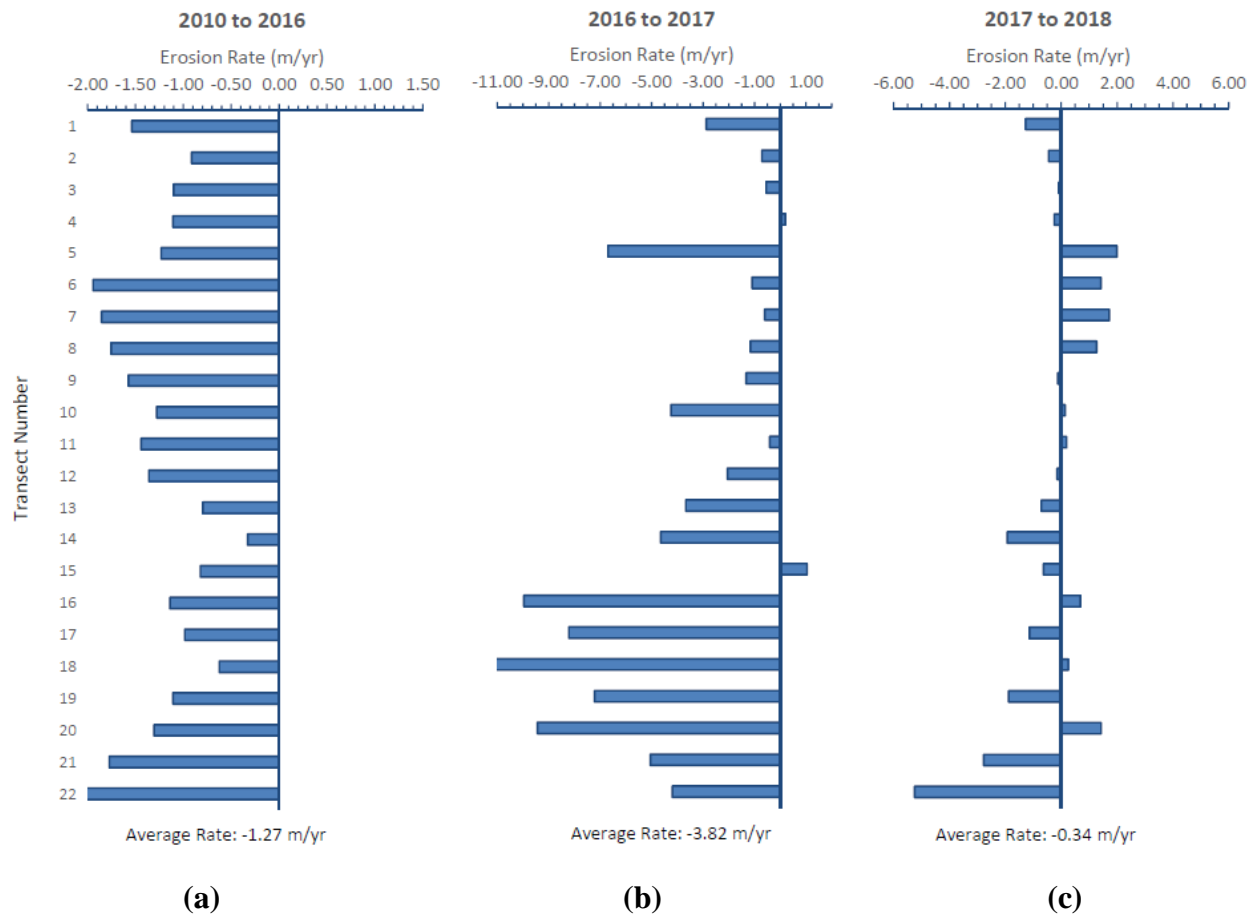
Figure 5-37. Average EPR results for periods **(a)** 2010-16, **(b)** 2016-17, and **(c)** 2017-18 at Cofresí Beach, Rincón

5.3   Case Study: Effect of Hurricane Matthew at Cofresí Beach, Rincón

As previously mentioned, in October 2016, Hurricane Matthew severely affected the western region of Puerto Rico. A few days after the hurricane event, UAVs were deployed to evaluate these effects. Also, a five-hours numerical simulation of the hurricane, using a spatial uniform wave variation, was carried out for Cofresí Beach. This simulation was performed with the intention of testing the application of the XBeach model to quantify the morphological changes along the coast. The following sections provide the modeled simulation, the comparison between numerical simulation and field observations, and a correlation analysis of beach profiles.

5.3.1 Modeled Simulation

The profiles (Figures 5-38 to 5-41) represent the initial bed level and simulated bed level results obtained from the numerical simulations, as well to the pre- and post-storm DSMs and DTM elevations obtained with UAVs. Each profile has a subplot that contains the beach portion of each transect to easily compare the variation. For transects 1, 2, and 3 (Figure 5-38), the initial and simulated results were quite similar with the UAV's DSM and DTM pre- and post-storm, except for a longitudinal displacement in the first two transects. Comparing the DSM and DTM generated after the hurricane, both were quite similar on the beach portion giving similar behaviors. For transects 4, 5 and 6 (Figure 5-39), profiles showed agreement between the model simulations and observations. For transects 7, 8, and 9 (Figure 5-40), profiles were also quite similar, except for the transect 8 which showed accretion in the UAV comparison. These particular elevations may be influenced by vegetation (i.e. palm trees) located along the transect,

leading to overestimate the actual elevation. Similarly, for transects 10 and 11 (Figure 5-41), both profiles were quite similar in behavior; except for transect 10 in were the elevation from the DSM pre-storm was also overestimate. This could also be due to vegetation located along the transect that could cause wrong assignment to the pixel value.
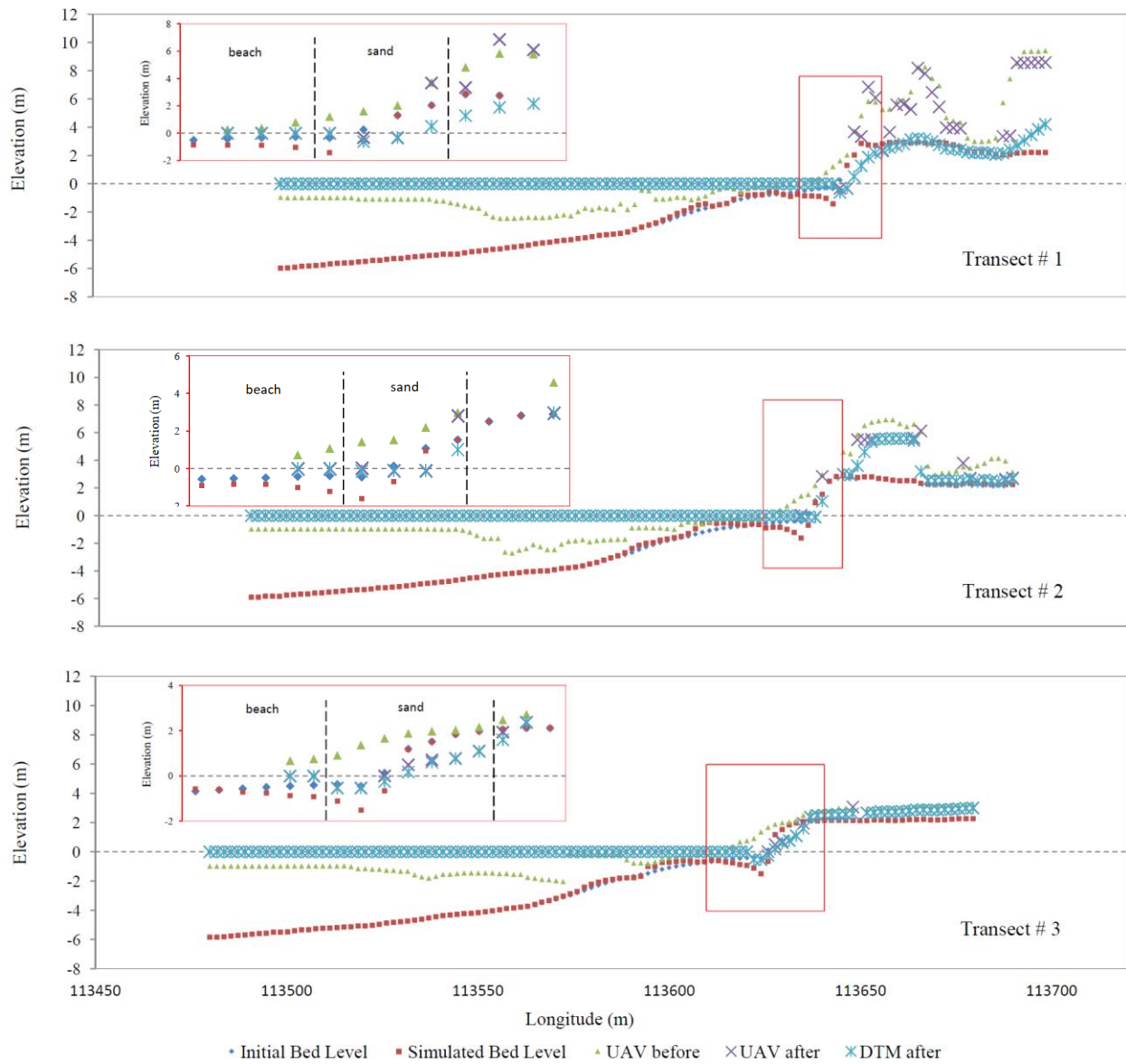
Figure 5-38. Profiles of the bed level change for transects 1 to 3 before and after Hurricane Matthew
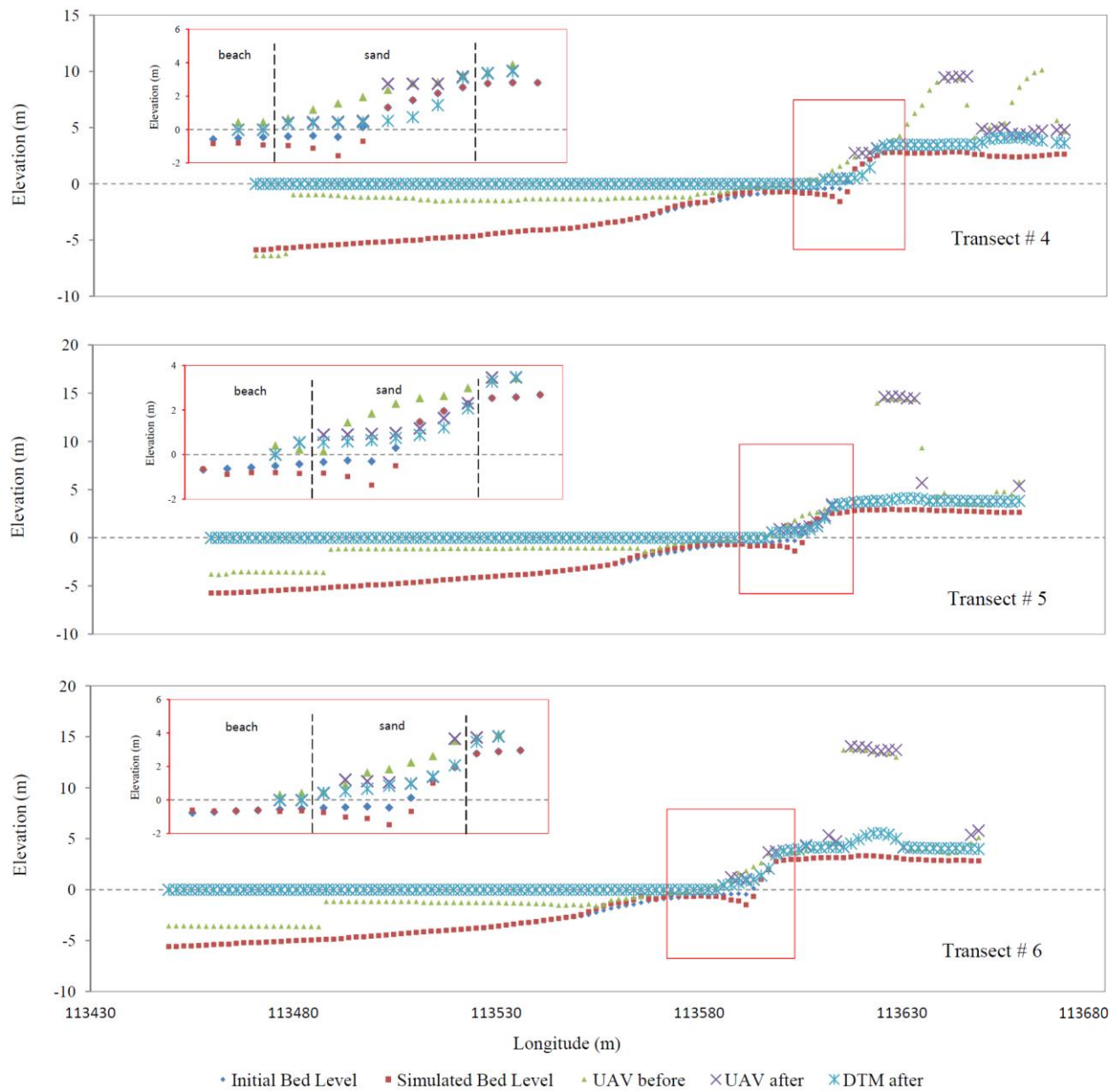
Figure 5-39. Profiles of the bed level change for transects 4 to 6 before and after Hurricane Matthew
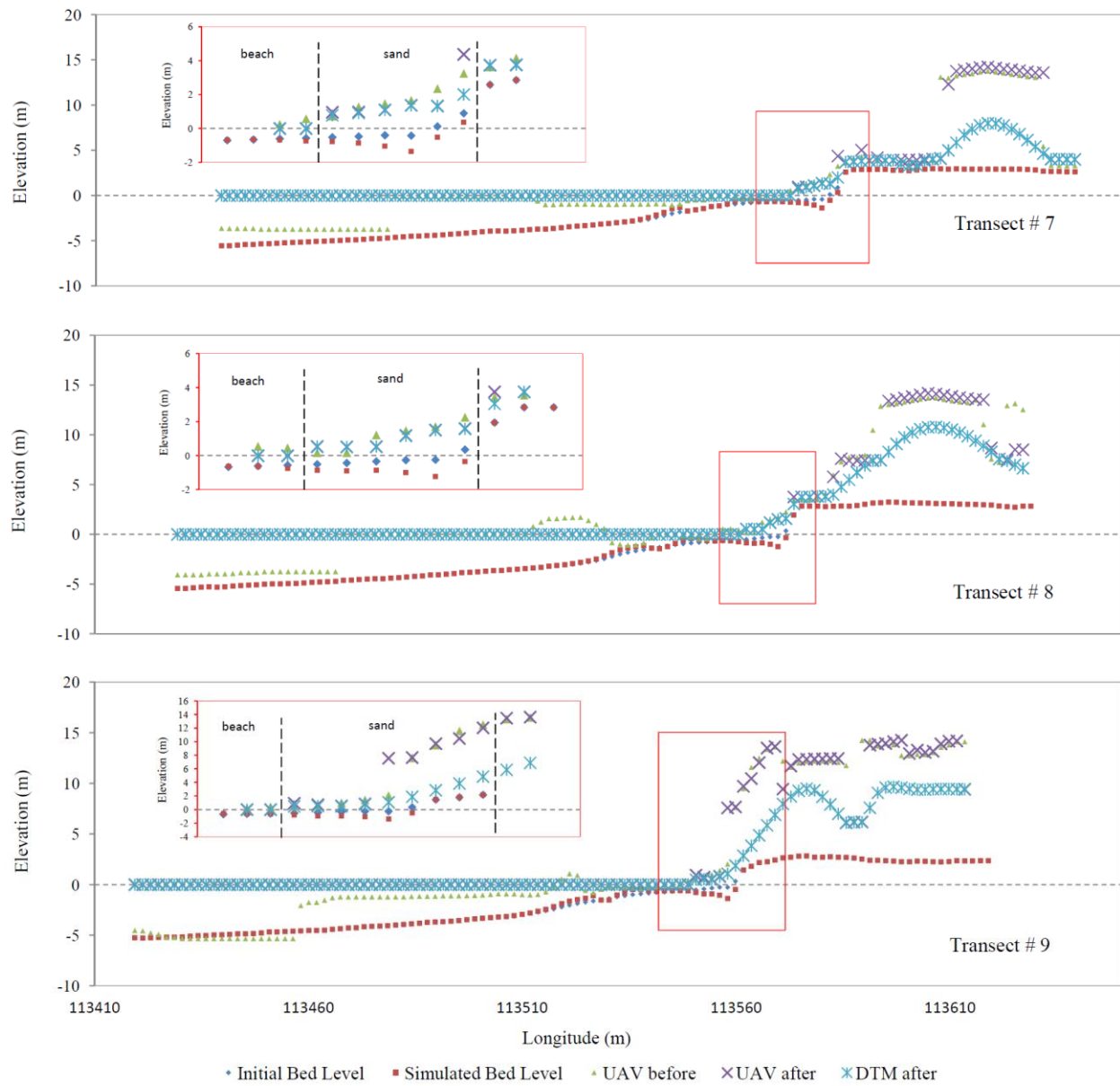
Figure 5-40. Profiles of the bed level change for transects 7 to 9 before and after Hurricane Matthew
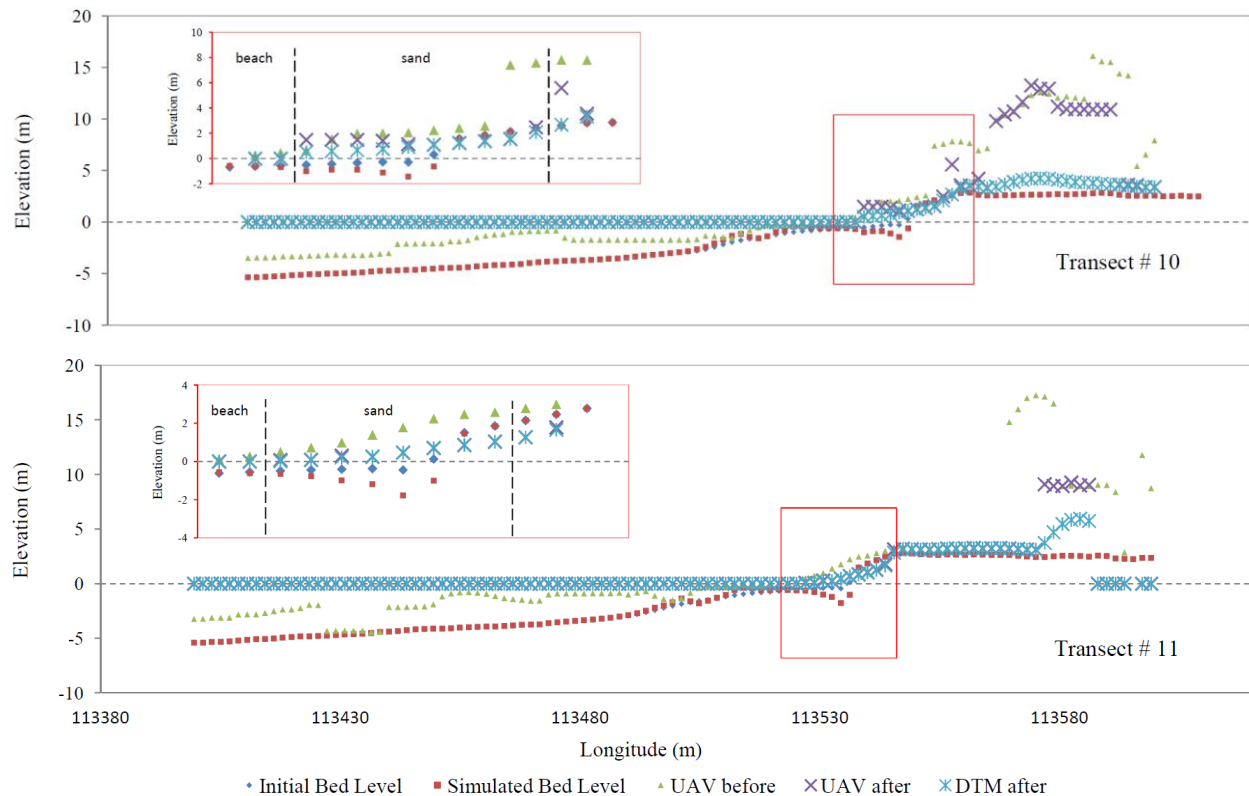
Figure 5-41. Profiles of the bed level change for transects 10 to 11 before and after Hurricane Matthew

The averaged erosion results in the vertical direction of the numerical simulation were determined and summarized in Table 5-15. These values were obtained for each transects from the subtraction of the simulated erosion results and the initial bed level values obtained from the USACE DTM. All the transect values were then averaged obtaining the overall erosion value of -0.693 meters in the vertical direction. These results were used to generate the maps shown in Figure 5-42.

Longitudinal erosion displacement was also determined and summarized in Table 5-16. These values were obtained for each transect, from the numerical model 2-meters grid resolution, by calculating the distance between two points. The results were then averaged obtaining the overall erosion value of -6.22 meters.

Table 5-15. Average erosion results of the XBeach simulation in the vertical direction

Transect #	Average Erosion (m)
1	-0.936
2	-0.719
3	-0.653
4	-0.819
5	-0.772
6	-0.593
7	-0.560
8	-0.625
9	-0.586
10	-0.731
11	-0.630
Average	-0.693

(a)   (b)
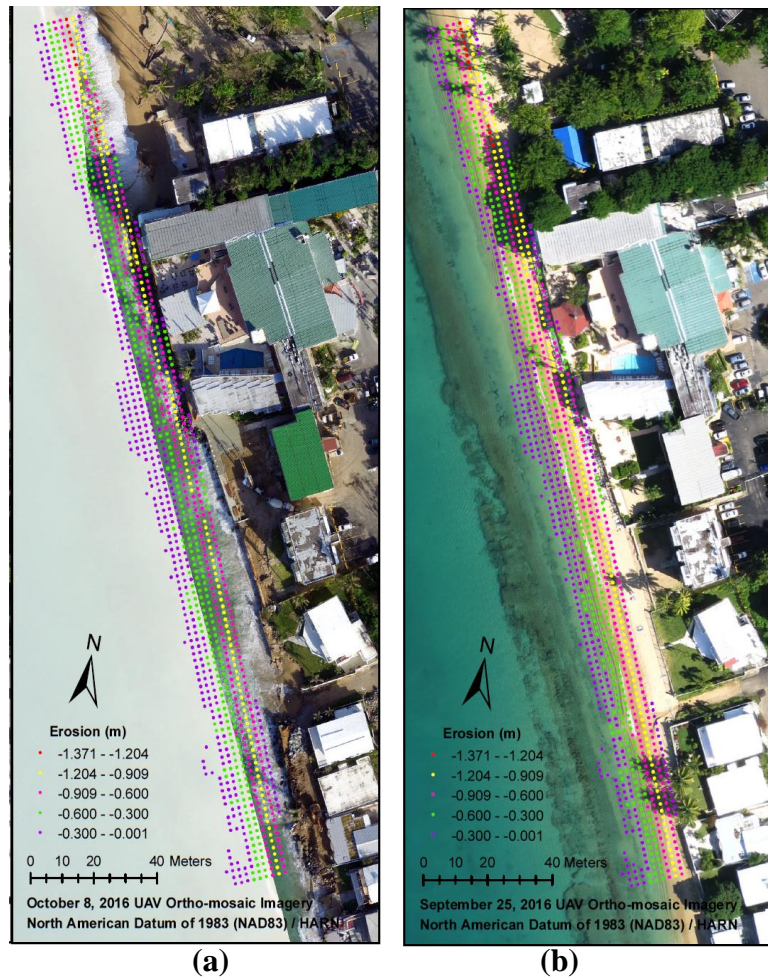
Figure 5-42. Erosion values from the simulation results along the coastline using UAV ortho-mosaic images **(a)** before and **(b)** after Hurricane Matthew

Table 5-16. XBeach results of longitudinal erosion values at each transect

Transect #	Pt.	X (m)	Y (m)	EPR (m/yr)
1	1	113642.68	254827.01	-2.00
	2	113640.83	254826.24	
2	1	113639.17	254840.71	-4.00
	2	113635.47	254839.18	
3	1	113633.04	254855.49	-6.00
	2	113627.50	254853.19	
4	1	113626.92	254870.27	-6.00
	2	113621.38	254867.97	
5	1	113618.95	254884.29	-4.00
	2	113615.25	254882.76	
6	1	113613.59	254897.22	-4.00
	2	113609.90	254895.69	
7	1	113606.70	254913.85	-6.00
	2	113601.16	254911.56	
8	1	113601.35	254926.79	-8.00
	2	113593.96	254923.72	
9	1	113595.99	254939.72	-8.00
	2	113588.60	254936.66	
10	1	113588.78	254951.89	-8.00
	2	113581.39	254948.83	
11	1	113583.43	254964.82	-8.00
	2	113576.04	254961.76	
12	1	113574.69	254980.69	-8.00
	2	113567.30	254977.63	
13	1	113567.49	254992.86	-6.00
	2	113561.94	254990.56	
14	1	113562.13	255005.79	-6.00
	2	113556.58	255003.50	
15	1	113556.00	255020.57	-8.00
	2	113548.61	255017.51	
16	1	113548.80	255032.74	-6.00
	2	113543.26	255030.45	
17	1	113542.68	255047.52	-6.00
	2	113537.13	255045.23	
18	1	113537.32	255060.46	-8.00
	2	113529.93	255057.40	
			Average:	-6.22

5.3.2 Numerical Simulations vs. Field Observations

The following section will provide the vertical and longitudinal validation results of the XBeach simulation, in addition to the correlation analysis of the beach profiles.

5.3.2.1 Vertical Validation

The vertical validation was made using the DSMs pre- and post-storm. Table 5-17 summarizes the averaged erosion results in the vertical direction of the UAV DSMs. These values were obtained for each transects from the subtraction of the elevations pre- and post-storm. All transects were then averaged obtaining the overall erosion value of -0.802 meters in the vertical direction.

Table 5-17. Average erosion results of the UAV profiles in the vertical direction

Transect #	Average Erosion (m)
1	-1.581
2	-1.767
3	-1.601
4	-0.889
5	-0.513
6	-0.609
7	-0.107
8	-0.190
9	-0.104
10	-0.402
11	-1.053
Average	-0.802

For the vertical validation, the average and the standard deviation was calculated from the UAV and XBeach average erosion. A statistical analysis including the MBE, MAE, RMSE, and R was performed considering both data sets (Table 5-18).

Table 5-18. Statistical analysis for the erosion results in the vertical direction

	UAV	XBeach	UAV and XBeach
Average Erosion (m)	-0.802	-0.693	-0.747
Std. Dev (m)	0.622	0.115	

MBE (m)	MAE (m)	RMSE (m)	R
-0.108	0.464	0.556	0.513

Based on the average results, XBeach underestimated the erosion in the vertical direction. The average erosion obtained between UAVs and XBeach was -0.747 meters. For the standard deviation, UAV values seemed to be more spread out compared to the XBeach values. When determining the MAE among all the analyzed profiles, a discrepancy of 0.464 meters was observed between both samples. This discrepancy was equivalent to a 62% of the total erosion. However, when determining the MBE, an error of -10 centimeter was obtained; indicating that positive and negative errors cancelled out. The XBeach model and UAV results showed great variability, however, the overall results were consistent between both. The negative error indicated that XBeach prediction results were smaller in value than UAV observations. The RMSE value was 0.556 meters, indicating a moderate error associated with the simulation results; and the coefficient of correlation was 0.513, indication a moderate lineal relationship.

5.3.2.2 Longitudinal Validation

The rate of change for Cofresí Beach at Rincón pre- and post-storm obtained from the statistical calculations provided by DSAS, using the UAV images and the 18 transects shown in Figure 5-43. The distance from baseline values needed for the EPR calculations, and the EPR results are shown in Table 5-19. The EPR values for each transect were then averaged obtaining the overall erosion value of -7.21 meters in the longitudinal direction.
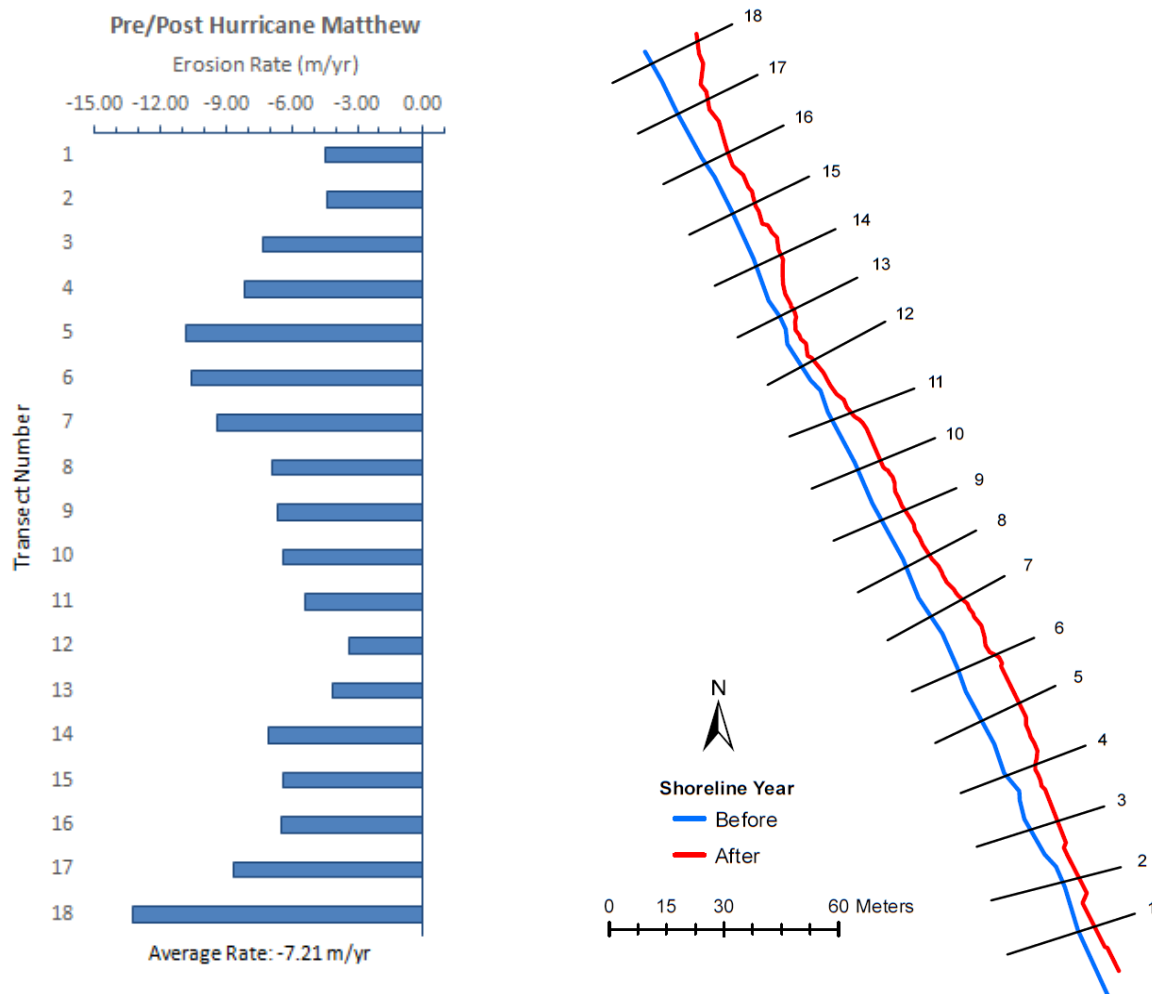

Figure 5-43. Shoreline changes results before and after Hurricane Matthew

81

Table 5-19. Values of distance from baseline before and after hurricane Matthew and EPR results

Transect #	Before Hurricane Matthew	After Hurricane Matthew	EPR (m/yr)
1	-19.47	-23.96	-4.48
2	-19.36	-23.71	-4.35
3	-14.79	-22.12	-7.33
4	-12.78	-20.95	-8.17
5	-13.54	-24.37	-10.82
6	-13.31	-23.87	-10.56
7	-12.94	-22.34	-9.39
8	-14.30	-21.17	-6.87
9	-13.69	-20.33	-6.64
10	-13.04	-19.43	-6.39
11	-11.83	-17.22	-5.39
12	-10.23	-13.64	-3.42
13	-12.26	-16.39	-4.13
14	-12.05	-19.09	-7.04
15	-12.80	-19.22	-6.41
16	-12.34	-18.79	-6.45
17	-11.66	-20.33	-8.67
18	-11.56	-24.80	-13.24
		Average	-7.21

However, for the statistical analysis in the longitudinal direction, transects 5, 6, 7, 12, and 18 were not selected since at the moment of capturing the UAV image, the swell was at its peak and it was difficult to accurately determine the wet/dry line. It should be noted that a temporary erosion event was detected. Days after the hurricane the beach returned to its initial state (Figure 5-44).

<center>(a)</center> <center>(b)</center>

Figure 5-44. Temporary erosion event **(a)** during Hurricane Matthew on October 8, 2016 and **(b)** after Hurricane Matthew on October 14, 2016

A statistical analysis including the MBE, MAE, RMSE, and R was performed considering both data sets; results are shown in Table 5-20.

Table 5-20. Statistical analysis for the erosion results in the longitudinal direction

	UAV	XBeach	UAV and XBeach
Average Erosion (m)	-6.332	-6.308	-6.320
Std. Dev (m)	1.410	1.797	

MBE (m)	MAE (m)	RMSE (m)	R
-0.023	1.589	1.748	0.377

Based on the average results, XBeach also underestimated the erosion in the longitudinal direction. The average erosion obtained between UAVs and XBeach was -6.320 meters. For the standard deviation, XBeach values seemed to be more spread out compared to the UAV values. When determining the MAE among all the analyzed profiles, a discrepancy of 1.589 meters was

observed between both samples. This discrepancy was equivalent to a 25% of the total erosion. However, similar to the vertical validation, when determining the MBE, an error of -2 centimeter was obtained; indicating that positive and negative errors cancelled out. This negative error indicates that XBeach prediction were smaller than UAV observations. The RMSE value was 1.748 meters and the coefficient of correlation was 0.377. Higher errors and lower correlations were due to the fact that a 2-meter resolution grid in the x- and y- direction was used. Using a 2-meter resolution grid caused the details to be lost and high variability in the data that may result in bias.

5.3.2.3 Correlation Analysis of Beach Profiles

The following charts (Figures 5-45 to 5-48) were generated to evaluate how the profiles behaved in their shape. Charts were created using the beach portion of the XBeach and UAV DSMs data pre- and post-storm. The pre-storm values corresponded to the comparison of the XBeach and UAV DSM data before Hurricane Matthew; the after values corresponded to the comparison of the XBeach and UAV DSM data after Hurricane Matthew. The DTM post-storm values corresponded to the comparison of the XBeach and UAV DTM data after Hurricane Matthew. It includes the DTM elevations after the hurricane in order to evaluate if there is any difference using a DSM or DTM to detect morphological changes.
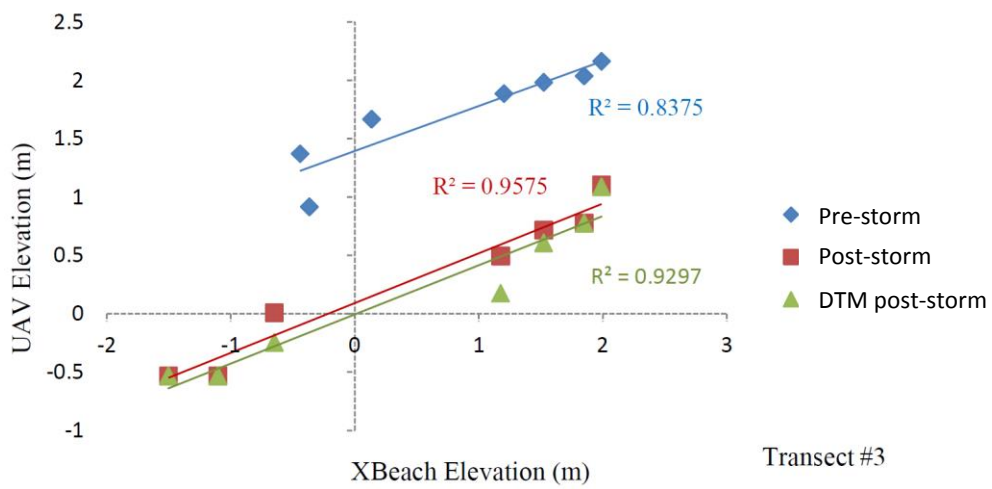
Figure 5-45. Correlation analysis for transects 1, 2, and 3

85

Figure 5-46. Correlation analysis for transects 4, 5, and 6

Figure 5-47. Correlation analysis for transects 7, 8, and 9

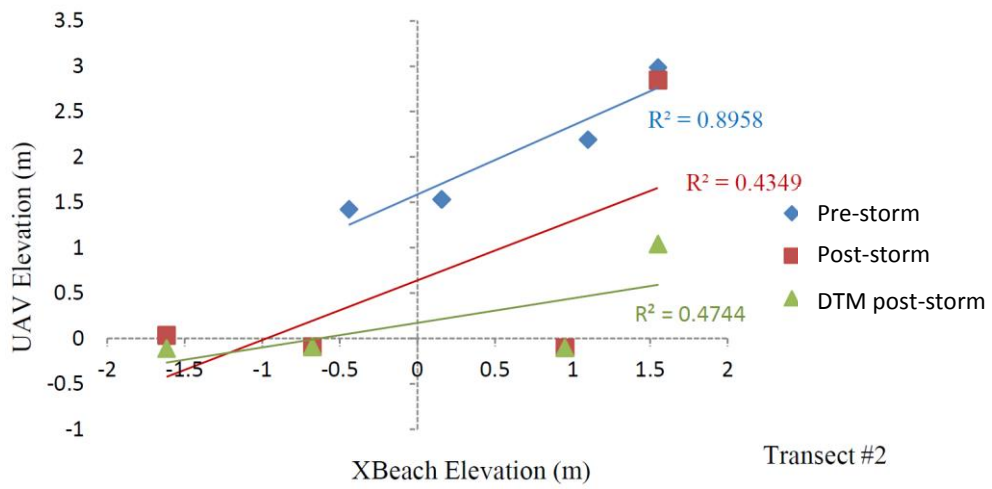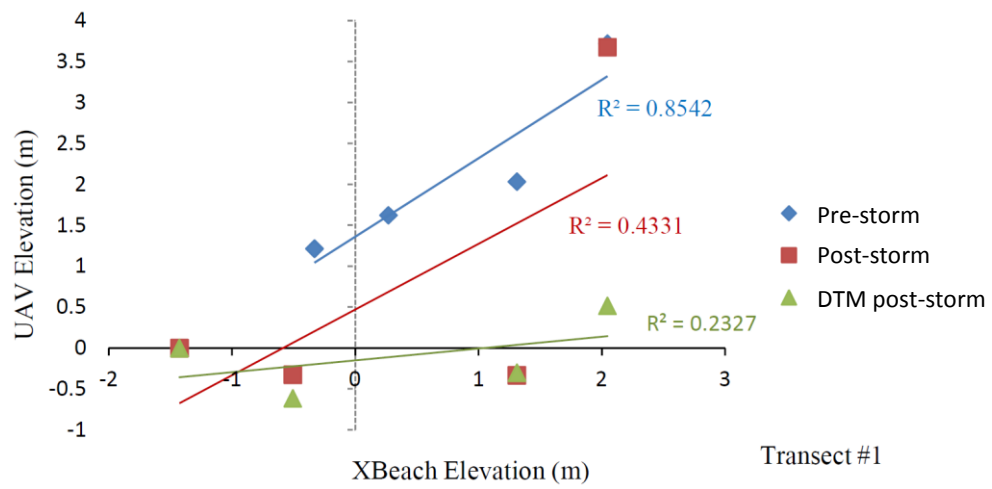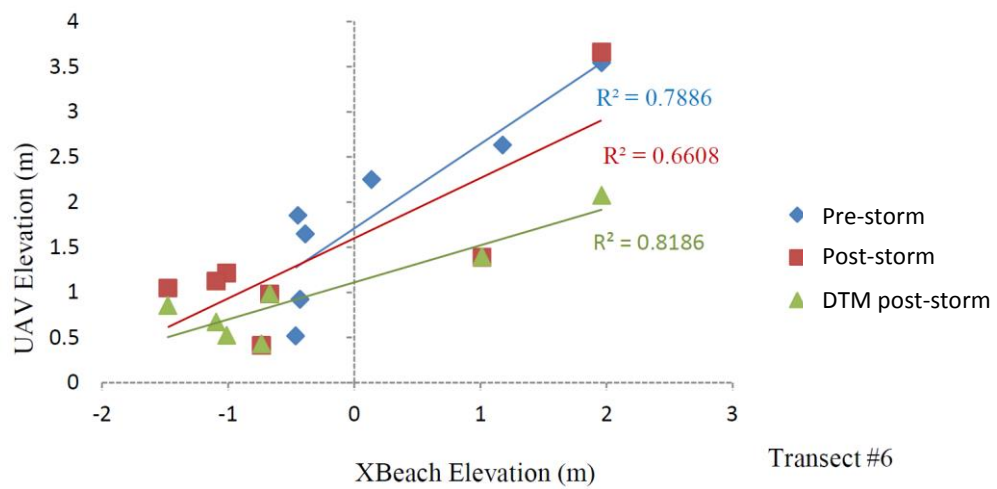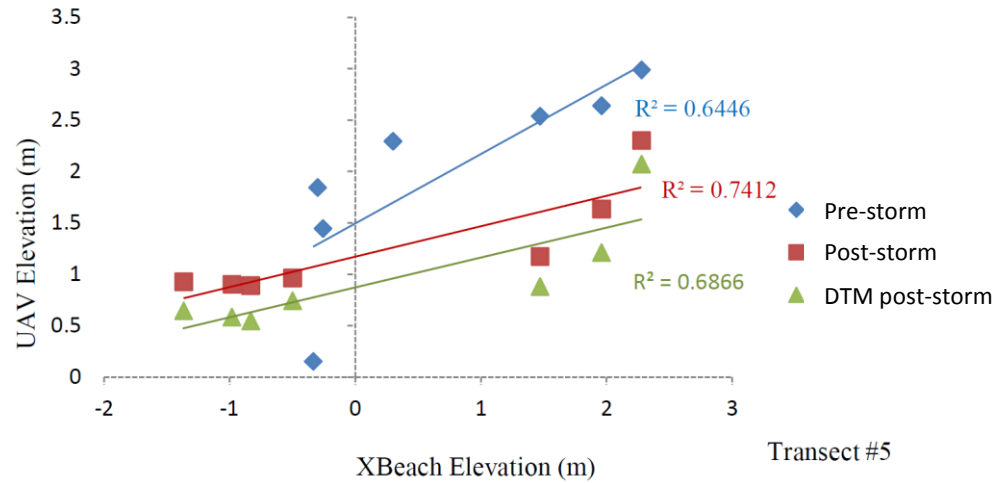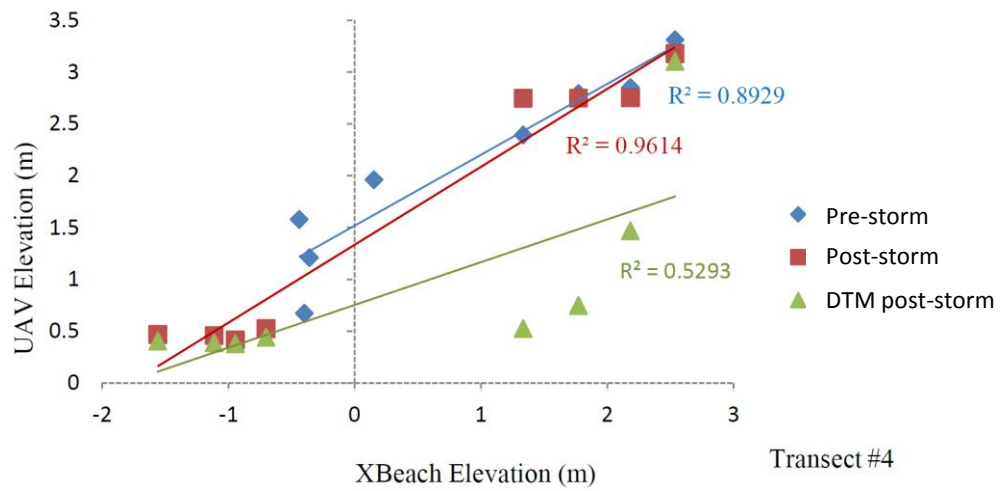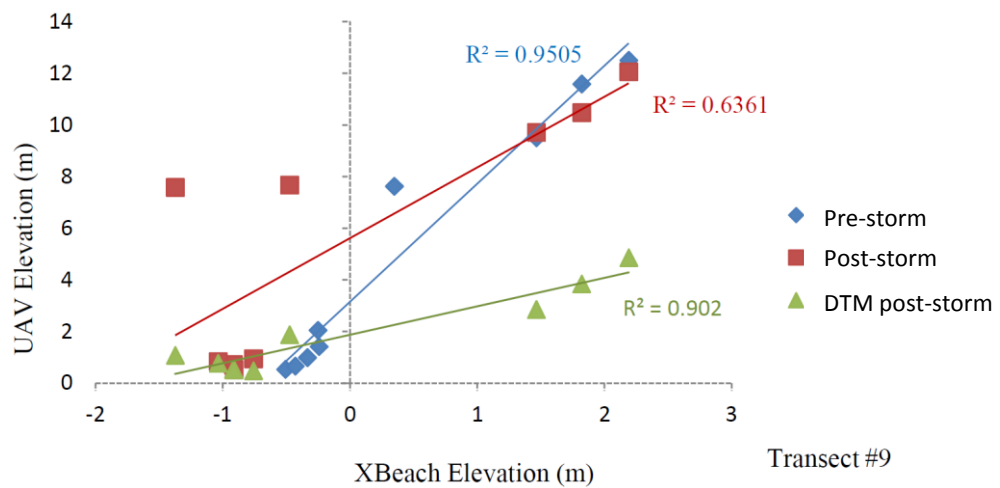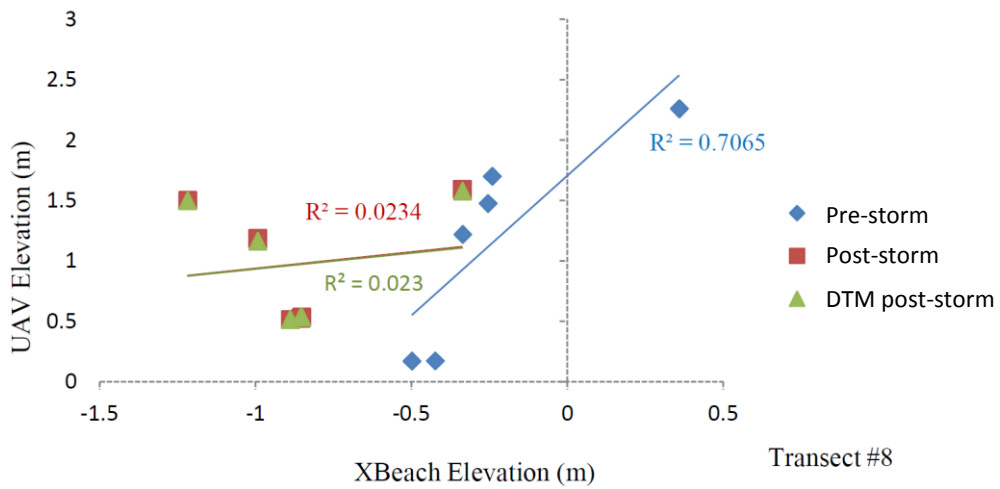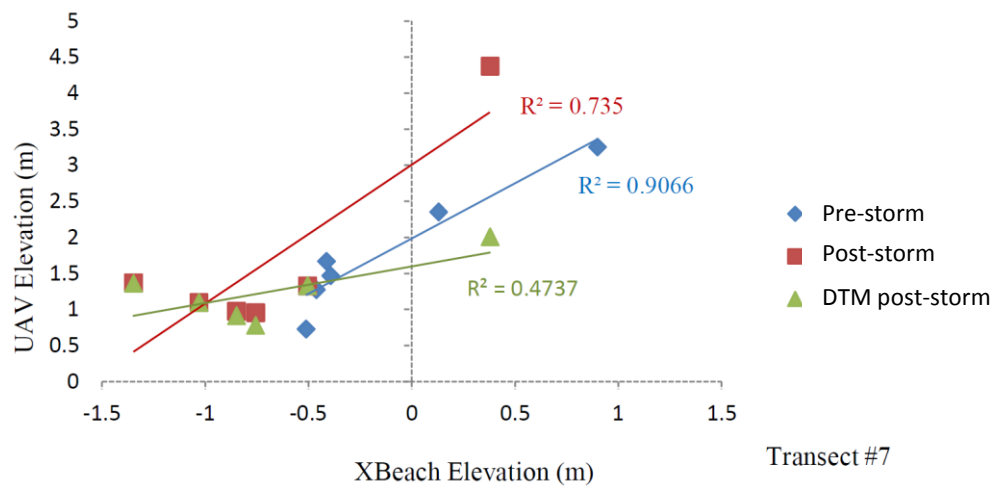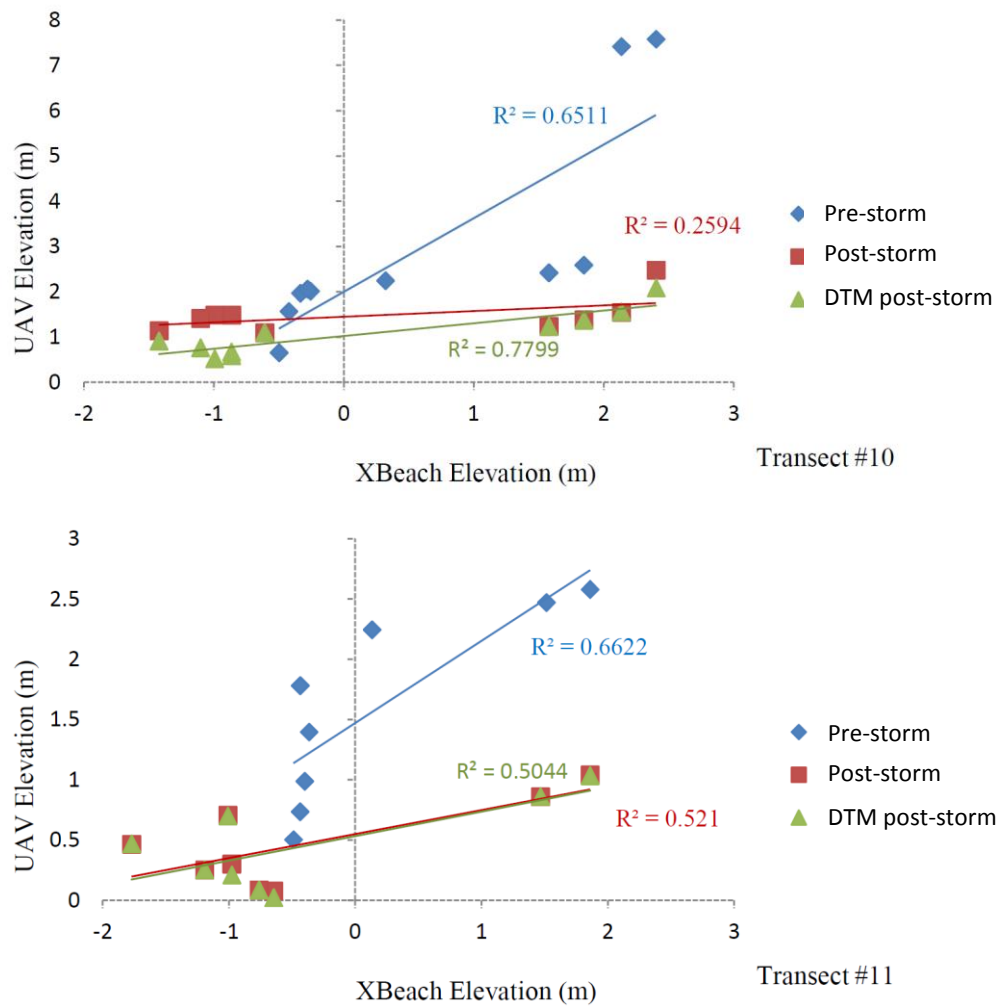**Figure 5-48.** Correlation analysis for transects 10 and 11

For the correlation analysis, transect 8 was removed since a point generated in the UAV point cloud was out of position. The R^2 analysis was used as the statistical measure of how close the XBeach results respect to the UAV data. R^2 results are summarized in Table 5-21.

Table 5-21. UAV and XBeach pre- and post-storm profile correlation results

Transect #	R^2 Pre-storm	R^2 Post-storm	R^2 DTM Post-storm
1	0.8542	0.4331	0.2327
2	0.8958	0.4349	0.4744
3	0.8375	0.9575	0.9297
4	0.8929	0.9614	0.5293
5	0.6446	0.7412	0.6866
6	0.7886	0.6608	0.8186
7	0.9066	0.7350	0.4737
9	0.9505	0.6361	0.9020
10	0.6511	0.2594	0.7799
11	0.6622	0.5210	0.5044
Average	0.8084	0.63404	0.63313

Analyzing the correlation results before Hurricane Matthew, almost all of them showed high R^2 values. These results may have been influenced since the DSM had the bathymetry data combined with the topography. The post-storm results, compared with the pre-storm results, were lower almost in all transects. Similarly, this could have been caused since our DSM did not have bathymetry data. The DTM R^2 results were quite similar with the DSM, except for a few transects. Overall, the average R^2 values from pre- and post storm were acceptable, and the difference between the used of DSM and DTM for the detection of morphological changes was almost negligible. The R^2 post-storm results could improve by implementing a hybrid model that includes bathymetry data and optimizing the DSM and DTM with more ground control points.

5.3.2.4 Sensitivity Analysis

For the vertical and longitudinal directions, the average and the standard deviation was calculated from the UAV and XBeach results; in addition to a statistical analysis including the MBE, MAE, RMSE, and R considering both data sets. These results were obtained considering the minimum (Table 5-22) and maximum (Table 5-23) D_{50} diameter, and were compared with the average (Table 5-24) D_{50} diameter used in this study.

Table 5-22. Statistical analysis for the erosion results using the minimum D_{50} (0.29 mm)

Vertical Direction:

	UAV	XBeach	UAV and XBeach
Average Erosion (m)	-0.737	-0.987	-0.862
Std. Dev (m)	0.702	0.173	

MBE (m)	MAE (m)	RMSE (m)	R
0.250	0.514	0.601	0.800

Longitudinal Direction:

	UAV	XBeach	UAV and XBeach
Average Erosion (m)	-6.332	-7.692	-7.012
Std. Dev (m)	1.410	1.974	

MBE (m)	MAE (m)	RMSE (m)	R
1.263	1.822	2.225	0.454

Table 5-23. Statistical analysis for the erosion results using the maximum D_{50} (2.28 mm)

Vertical Direction:

	UAV	XBeach	UAV and XBeach
Average Erosion (m)	-0.712	-0.541	-0.626
Std. Dev (m)	0.540	0.098	

MBE (m)	MAE (m)	RMSE (m)	R
-0.171	0.432	0.567	-0.196

Longitudinal Direction:

	UAV	XBeach	UAV and XBeach
Average Erosion (m)	-6.332	-5.846	-6.089
Std. Dev (m)	1.410	1.725	

MBE (m)	MAE (m)	RMSE (m)	R
-0.451	1.571	1.953	0.223

Table 5-24. Statistical analysis for the erosion results using the average D_{50} (0.97 mm)

Vertical Direction:

	UAV	XBeach	UAV and XBeach
Average Erosion (m)	-0.802	-0.693	-0.747
Std. Dev (m)	0.622	0.115	

MBE (m)	MAE (m)	RMSE (m)	R
-0.108	0.464	0.556	0.513

Longitudinal Direction:

	UAV	XBeach	UAV and XBeach
Average Erosion (m)	-6.332	-6.308	-6.320
Std. Dev (m)	1.410	1.797	

MBE (m)	MAE (m)	RMSE (m)	R
-0.023	1.589	1.748	0.377

The average erosion values obtained for the UAV changed due to the fact that with the variation of the diameter of the sediment, the model predicted values that were not previously considered, and that were within the study area.

For the vertical direction, based on the average erosion results, when the minimum D50 diameter was used, XBeach overestimated the erosion, compared to the other two diameters where it underestimated these values. The standard deviation results for the three diameters showed that the UAV values seemed to be more spread out compared to the XBeach values. When

determining the MAE, the maximum and average D_{50} diameter values (0.432 and 0.464 meters respectively) remained consistent; however, when using the minimum diameter, this error was greater (0.514 meters). When determining the MBE, the values for the minimum, maximum, and average diameter were 0.250, -0.108, and -0.171 meters, respectively. The positive error indicated that XBeach prediction results were larger in value than UAV observations, contrary to the negative error where XBeach prediction results were smaller in value than UAV observations. The RMSE values were consistent for the maximum and average diameter (0.567 and 0.556 meters respectively), and higher for the minimum diameter (0.601 meters). However, the coefficient of correlation value for the minimum diameter was higher (0.800) compared with the maximum and average diameters (-0.196 and 0.513 respectively).

For the longitudinal direction, based on the average erosion results, when the minimum D50 diameter was used, XBeach overestimated the erosion, compared to the other two diameters where it underestimated these values. The standard deviation results for the three diameters showed that the XBeach values seemed to be more spread out compared to the UAV values. When determining the MAE, the maximum and average D_{50} diameter values (1.571 and 1.589 meters respectively) remained consistent; however, when using the minimum diameter, this error was greater (1.822 meters). When determining the MBE, the values for the minimum, maximum, and average diameter were 1.263, -0.451, and -0.023 meters, respectively. The positive error indicated that XBeach prediction results were larger in value than UAV observations, contrary to the negative error where XBeach prediction results were smaller in value than UAV observations. The RMSE values were quite similar for the maximum and average diameter (1.953 and 1.748 meters respectively), and higher for the minimum diameter (2.225 meters).

92

However, the coefficient of correlation value for the minimum diameter was higher (0.454), compared with the maximum and average diameters (0.223 and 0.377 respectively).

Based on the results of this sensitivity analysis, using a small sediment diameter causes the model to overestimate erosion values. However, the use of an average or larger sediment diameter makes the results more consistent compared to those of UAV. A trend observed in this analysis is that the smaller the diameter, the easier it will be to transport the sediment and overestimate the erosion results.

CHAPTER 6 - CONCLUSIONS AND RECOMMENDATIONS

This study demonstrates the capacity of small UAVs for coastal monitoring and the application of the XBeach numerical model to determine morphological changes in coastal environments. In agreement with previous studies (Morelock 1984), this research study shows that erosion rates are not constants over time; there are accelerations, decelerations, and reversals of erosion to accretion. In general, both, XBeach model and UAV, showed the same trends but differences in the magnitude of erosion.

In this study the erosion rates were determined for the periods 1930-2004, 2004-10, 2010-16, 2016-17, 2017-18, and 1930-2018. Specifically, the erosion events after Hurricane María were determined and the results were -1.42 m/yr, -38.11 m/yr, and -3.82 m/yr for Jobos Beach at Isabela, Crash Boat Beach at Aguadilla, and Cofresí Beach at Rincón respectively. These results demonstrate the vulnerability of these beaches, which is why government attention is required.

XBeach numerical model simulations showed potential to determine morphological changes in the coastal zones. Additionally, the numerical model results demonstrate capabilities to simulate erosion and/or accretion events using real-time meteorological and oceanographic data. Both vertical and longitudinal results were consistent with UAV data. However, the results showed in this study were obtained using a model simplification by implementing uniform wave conditions; hence, a sensitivity analysis needs to be performed.

The UAV data was used to validate the XBeach simulation and the results shows potential to use UAV data in combination with bathymetry data as model input. The results from the validation showed that both methodologies coincide when determining erosion and/or accretion events.

However, the magnitude of the changes has to be adjusted as established in Tables 5-18 and 5-20.

In order to optimize the results, it is recommended to calibrate the way in which the shoreline is delimited using UAV images, optimize the modeling by considering variable wave conditions, and increasing the grid resolution. The implementation of a model that predicts the swell is recommended in combination with XBeach to capture accurately the morphological changes along the coasts. It is also recommended the systematic collection of UAV images that match with the tide pre-conditions.

To conclude, the explained methodology could be readily implemented in other areas of Puerto Rico where a rapid assessment is needed after any meteorological event. The results obtained from this analysis may be used as a tool to educate the population living near the coastal zone about the actual problems the coastal communities are suffering. It is recommended to outreach public awareness of coastal risk communities and to include transitioning monitoring for local emergency managers.

CHAPTER 7 - FUTURE WORK

As part of the future work, UAV coastal monitoring will continue to keep quantifying the erosion rates occurring in the coastal environments. Additionally, this work would be summarized in a publication to be submitted to the Natural Hazard and Earth System Sciences journal.

As a possibility, future work could consist in the implementation of a wave model such as SWAN combined with XBeach for the prediction of morphological changes and quantification of erosion rate in the coastal zones.

CHAPTER 8 - REFERENCES

Anderson, K., and Gaston, K. J. (2013). "Lightweight unnmaned aerial vehicles will revolutionize spatial ecology." *Frontiers in Ecology and the Environment*, (January 2014), 138–146.

Barreto-Orta, M. (1997). "Shoreline changes in Puerto Rico (1936-1993)." *ProQuest Dissertations and Thesis Global - University of Puerto Rico at Mayaguez.*

Boak, E. H., and Turner, I. L. (2005). "Shoreline Definition and Detection : A Review Shoreline Definition and Detection : A Review." *Journal of Coastal Research*, (214), 688–703.

Bolle, A., Mercelis, P., Roelvink, D., Haerens, P., and Trouw, K. (2011). "Application and validation of XBeach for three different field sites." *Coastal Engineering Proceedings*, 1(32), 40.

Car, M., Kaćunić, D. J., and Kovačević, M. (2016). "Application of unmanned aerial vehicle for landslide mapping." *Proceedings of the International Symposium on Engineering Geodesy-SIG*, 549–559.

Casella, E., Rovere, A., Pedroncini, A., Mucerino, L., Casella, M., Cusati, L. A., Vacchi, M., Ferrari, M., and Firpo, M. (2015). "Study of wave runup using numerical models and low-altitude aerial photogrammetry : A tool for coastal management." *Estuarine, Coastal and Shelf Science*, Elsevier Ltd, 149(August 2014), 160–167.

Casella, E., Rovere, A., Pedroncini, A., Stark, C. P., Casella, M., Ferrari, M., and Firpo, M. (2016). "Drones as tools for monitoring beach topography changes in the Ligurian Sea (NW Mediterranean) Drones as tools for monitoring beach topography changes in the Ligurian Sea (NW Mediterranean)." *Geo-Marine Letters*, 151–163.

Ciencia PR. (2015). "Preocupante la erosión y las construcciones en las costas del País." *Ciencia Puerto Rico*.

Clark, A. (2017). "Small unmanned aerial systems comparative analysis for the application to coastal erosion monitoring." *GeoResJ*, Elsevier Ltd, 13(Elsevier B.V.), 175–185.

Cook, K. L. (2017). "An evaluation of the effectiveness of low-cost UAVs and structure from motion for geomorphic change detection." *Geomorphology*, Elsevier B.V., 278, 195–208.

Córdova-López, L. F. (2014). "Evaluación del proceso de erosión en la playa de Varadero, Cuba." *Tecnología y Ciencia del Agua*, 1(1), 175–183.

Diaz, E. L., Jacobs, K. R., and Mentors, F. (2014). *Puerto Rico Coastal Zone Management Program. NOAA Coastal Services Center-Coastal Learning Services.*

Eling, C., Klingbeil, L., Wieland, M., Kuhlmann, H., Georeferencing, D., Filtering, E. K., and Operating, R. T. (2013). "A precise position and attitude determination system for lightweight unmanned aerial vehicles." *The International Archives of Photogrammetry, Remote Sensing and Spatial Information Sciences*, XL(September), 114–118.

Gonçalves, J. A., and Henriques, R. (2015). "UAV photogrammetry for topographic monitoring of coastal areas." *ISPRS Journal of Photogrammetry and Remote Sensing*, 104, 101–111.

Infante-Corona, J., Muñoz, J., Lakhankar, T., Romanov, P., and Khanbilvardi, R. (2015). "Evaluation of the Snow Thermal Model (SNTHERM) through Continuous in situ Observations of Snow's Physical Properties at the CREST-SAFE Field Experiment." *Geosciences*, 5(4), 310–333.

Islands of Puerto Rico. (n.d.). "Jobos Beach / Playa Jobos - Isabela Puerto Rico." <https://islandsofpuertorico.com/jobos-beach-isabela-puerto-rico/> (May 24, 2018).

Lomax, A. S., Corso, W., and Etro, J. F. (2005). "Employing Unmanned Aerial Vehicles (UAVs) as an Element of the Integrated Ocean Observing System." *OCEANS*, Proceeding, 184–190.

Long, N., Millescamps, B., Guillot, B., Pouget, F., and Bertin, X. (2016). "Monitoring the Topography of a Dynamic Tidal Inlet Using UAV Imagery." *Remote Sensing*, Multidisciplinary Digital Publishing Institute, 8(5), 387.

Mancini, F., Dubbini, M., Gattelli, M., Stecchi, F., Fabbri, S., and Gabbianelli, G. (2013). "Using Unmanned Aerial Vehicles (UAV) for High-Resolution Reconstruction of Topography: The Structure from Motion Approach on Coastal Environments." 6880–6898.

Matese, A., Toscano, P., Filippo Di Gennaro, S., Genesio, L., Vaccari, F. P., Primicerio, J., Belli, C., Zaldei, A., Bianconi, R., and Gioli, B. (2015). "Intercomparison of UAV, Aircraft and Satellite Remote Sensing Platforms for Precision Viticulture." *Remote Sensing Journal*, 2971–2990.

McCall, R. T., Van Thiel de Vries, J. S. M., Plant, N. G., Van Dongeren, A. R., Roelvink, J. A., Thompson, D. M., and Reniers, A. J. H. M. (2010). "Two-dimensional time dependent hurricane overwash and erosion modeling at Santa Rosa Island." *Coastal Engineering*, 57(7), 668–683.

Morelock, J. (1984). "Coastal Erosion in Puerto Rico." *Shore and Beach*, 18–27.

Morelock, J., and Barreto-Orta, M. (1999). *An Update of Coastal Erosion in Puerto Rico*. Department of Marine Sciences, University of Puerto Rico at Mayaguez.

NOAA. (2018). "Station Home Page - NOAA Tides & Currents." <https://tidesandcurrents.noaa.gov/stationhome.html?id=9759394> (May 24, 2018).

NOAA - Digital Coast. (2016). "Office for Coastal Management - Digital Coast Home." <https://coast.noaa.gov/digitalcoast/> (May 27, 2018).

El Nuevo Día. (2013). "Lenta muerte de las playas en Puerto Rico | El Nuevo Día." *El Nuevo Día*.

Puerto Rico Channel. (n.d.). "Crash Boat Beach, Aguadilla." <http://www.puertorico.com/beaches/crashboat/> (May 24, 2018).

Rodriguez, R. (2017). "USGS Fact Sheet: Sand and Gravel Resources of Puerto Rico." <https://pubs.usgs.gov/fs/sand-gravel/> (Feb. 14, 2018).

Roelvink, D., van Dongeren, A., McCall, R., Hoonhout, B., van Rooijen, A., van Geer, P., de Vet, L., Nederhoff, K., and Quataert, E. (2015). *XBeach Technical Reference: Kingsday Release*.

Sankey, T., Donager, J., Mcvay, J., and Sankey, J. B. (2017). "UAV lidar and hyperspectral fusion for forest monitoring in the southwestern USA." *Remote Sensing of Environment*, Elsevier Inc., 195, 30–43.

Scarelli, F. M., Sistilli, F., Fabbri, S., Cantelli, L., Barboza, E. G., and Gabbianelli, G. (2017). "Remote Sensing Applications : Society and Environment Seasonal dune and beach monitoring using photogrammetry from UAV surveys to apply in the ICZM on the Ravenna coast (Emilia-Romagna , Italy)." *Remote Sensing Applications: Society and Environment*, Elsevier B.V., 7(March), 27–39.

Scott, K. R., Canals, M., and Vélez, F. (2012). *Coastal erosion and beach morphology changes in Rincón, Puerto Rico*.

Thieler, B. E. R., Rodríguez, R. W., Himmelstoss, E. A., and Survey, U. S. G. (2007). "Historical Shoreline Changes at Rincón , Puerto Rico , 1936-2006." *Geological Survey (U.S)*.

Thieler, E. R., and Danforth, W. W. (1994). "Historical shoreline mapping (II): Application of the Digital Shoreline Mapping and Analysis Systems (DSMS/DSAS) to shoreline change mapping in Puerto Rico." *Journal of Coastal Research*, 10(3), 600–620.

Thieler, E. R., Himmelstoss, E. A., Zichichi, J. L., and Ergul, A. (2009). *Digital Shoreline Analysis System (DSAS) version 4.0 — An ArcGIS extension for calculating shoreline change*.

Turner, I. L., Harley, M. D., and Drummond, C. D. (2016). "UAVs for coastal surveying." *Coastal Engineering*, Elsevier B.V., 114, 19–24.

Unger, J., Reich, M., and Heipke, C. (2014). "UAV-based photogrammetry : monitoring of a building zone." *The International Archives of Photogrammetry, Remote Sensing and Spatial Information Sciences*, XL(June), 23–25.

Visockiene, J. S., Brucas, D., and Ragauskas, U. (2014). "Comparison of UAV images processing softwares." *Journal of Measurements in Engineering*, 111–121.

Willmott, C. J., and Matsuura, K. (2006). "On the use of dimensioned measures of error to evaluate the performance of spatial interpolators." *International Journal of Geographical Information Science*, Taylor & Francis , 20(1), 89–102.